Evaluation of co-culture sustainability and hydrogen production in an integrated fermentative microbial electrolysis cell

by

Nathan Wrana

A thesis submitted to the Faculty of Graduate Studies of
The University of Manitoba
In partial fulfillment of the requirements of the degree of

MASTER OF SCIENCE

Department of Biosystems Engineering
University of Manitoba
Winnipeg

UNIVERSITY
OF MANITOBA

I hereby declare that I am the sole author of this thesis. This is a true copy of the thesis, including any required final revisions, as accepted by my examiners. I understand that my thesis may be made electronically available to the public.

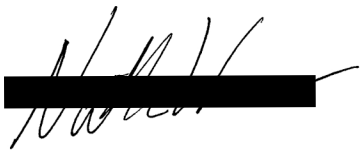

Nathan Wrana

Abstract

The relationship between the cellulolytic *Clostridium termitidis* and the electrogenic *Geobacter sulfurreducens* was evaluated in terms of co-culture sustainability and hydrogen (H_2) production. Batch co-culture experiments in triplicate balch tubes were conducted on a modified 1191 medium, using cellobiose as the sole carbon source and fumarate as a terminal electron acceptor. A carbon balance of 97.5 % and electron recovery of 113.8% was achieved. Despite high initial concentrations of acetate, no formate and very low H_2 concentrations were detected. This observation supports the hypothesis that a syntrophic association exists between both bacteria: i) mono-culture growth by *C. termitidis* on 2 g L^{-1} cellobiose generated 9.4 mM-H_2 and 8.3 mM-formate; ii) mono-cultures of *G. sulfurreducens* displayed preferential formate consumption (7.9 mmol g-dry $cell^{-1}$ h^{-1}) when grown on a synthetic cocktail of fermentation end-products; and iii) *G. sulfurreducens* expresses active respiratory hydrogenases capable of H_2 oxidation with concomitant fumarate reduction.

Co-culture growth characterization experiments were repeated in three microbial electrolysis cells (MECs) using modified 1191 medium and cellobiose as the sole carbon source. Initially, 9.7 mol-H_2 mol^{-1}-glucose was produced at a coulombic efficiency of 65.7 ± 0.8 %. A sustainable co-culture could not be maintained despite efforts to reduce reactor temperature (30^{o}C) and triple the medium's buffering capacity (100 mM). Strategies to achieve a sustainable co-culture are to: i) minimize the carbon flux through *C. termitidis* by using complex substrates, ii) maintain neutral operating conditions, and iii) introduce an acetogenic bacteria to control the flux of intermediates. Substrate preference by *G. sulfurreducens* was observed once again, suggesting online

measurements of formate could be a useful tool for indirectly monitoring co-culture health in a MEC.

Acknowledgements

There are many individuals I would like to thank for their continued aid and support throughout the scope of this project. First and foremost, I am extremely fortunate to have a committee as ambitious, intelligent, and balanced as I do. Dr. Levin, ever since you became my undergraduate thesis advisor, I have had the privilege of witnessing your vision and unrelenting drive develop this group into a leader in your field. The patience and trust you place in each one of your students is inspiring – you have made so much possible. Dr. Sparling, the depth of your knowledge never ceases to amaze me. You have continually challenged me, shaping me into the scientist I am today. Finally, Dr. Cicek, your practicality and relevancy have kept me grounded throughout this process. I have never met someone who can interpret a graph or ask a better question than you.

I would like to thank all of my friends and colleagues at the University of Manitoba, past and present, for their friendship, support, and advice. I would like to extend my gratitude to Dale Bourns and Robert Lavallee. Without your hard work, guidance, and trust in the workshop these reactors could never have been built. Thank you Debby Watson and Evelyn Fehr for dealing with my constant harassment, as well as Matt McDonald for his technical assistance.

Finally, I would like to thank my parents who have always been a source of inspiration and moral guidance. I sincerely appreciate everything you do for me. And thank you Amy. Not only do you possess an unrelenting patience, but you give me focus and purpose both in my studies and in my life.

This work was supported by funds provided by the Natural Sciences and Engineering Research Council of Canada's (NSERC) Hydrogen Canada (H_2CAN) Strategic Network.

Table of Contents

List of Figures

List of Tables

Chapter 1: Introduction

1.1 Hydrogen production: current status and drivers for the development of a renewable economy

A hydrogen (H_2) economy is well established, including the technology to produce it. Global H_2 consumption is estimated at 50 million metric tons at an overall growth rate between 5 and 10 % [1, 2]. The majority of H_2 produced is consumed as a reactant in hydrogenation processes, in either chemical manufacturing or petroleum processing industries [3]. According to Fig. 1.1a, approximately 50 % of all H_2 produced is used in the production of ammonia fertilizer. Petroleum refining or hydrocracking processes account for roughly 37 % while petroleum production processes total 8 % (*e.g.* methanol synthesis). Furthermore, H_2 is used as an oxygen (O_2) scavenger in the metals industry (during heat treatment processes), as a jet fuel, a coolant, and in the food industry (oil and fat hydrogenation processes). The high demand for H_2 makes it a valuable chemical, with

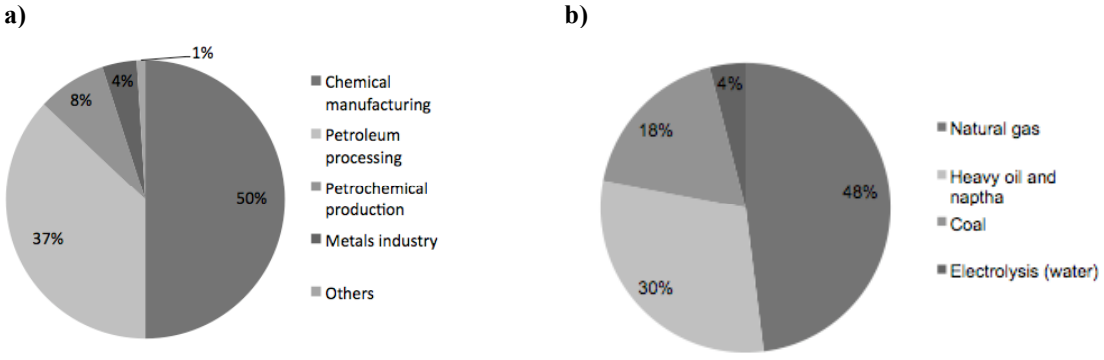

Figure 1.1 Summary of global H_2 production a) Major industrial applications and b) major energy sources for H_2 production are illustrated. Reproduced from [1, 3].

an average selling price of \$ 6 kg^{-1}. Comparing that against electricity, \$ 0.1 kWh, or natural gas, \$0.43 kg^{-1} – where, on a per mass basis, H_2 has an energy content 2.2 times greater than methane (CH_4) – clearly there is value in producing H_2 [1, 4].

Unfortunately, 96 % of global H_2 production is derived from fossil sources (Fig. 1.1b) [1, 2]. Nearly half of all H_2 is produced from natural gas streams, in particular steam methane reforming (SMR). Heavy oil, naphtha, and coal make up an additional 48 % of the market, while only 4 % of H_2 is generated from a renewable source via the electrolysis of water. Canada is one of the world's largest producers of H_2, generating 1.5 million metric tons annually in British-Columbia, Alberta, and Saskatchewan alone. Growth is expected to double in the next 20 years from oil sands developments in Alberta [5].

The dependency on fossil fuels places H_2 production in an economically vulnerable position, where pricing is influenced by a potentially unreliable and financially volatile oil market. A study by Agarwal (2007) [6] estimated that natural gas, oil, and coal reserves will last for 63, 41, and 218 years respectively, providing current production and consumption rates are maintained. With an industrializing and motorizing population base approaching 9 billion, consumption will only increase as crude oil reserves continue to shrink. Estimated oil demand is expected to double in the pre-industrialized countries of China and India. According to the International Energy Agency [7], by the year 2025, global oil demand will rise by 52 %, making an already stretched fossil fuel market in higher demand and even shorter supply. Clearly, there is strong incentive to reduce our dependency on hydrocarbon reforming and to develop renewable H_2 production strategies.

Many non-reforming approaches are capable of converting renewable energy sources into H_2 rich streams. For instance, solar, wind, and tidal energy can be used to generate electricity to drive the electrolysis of water [8]. The production of H_2 from water

can also be accomplished photosynthetically via direct photolysis by algae and bacteria [9, 10]. In the past 15 years, there has been a global interest in shifting the industry's dependence away from fossil sources to cellulosic biomass alternatives [11, 12]. Biomass is seen as an important contributor to the development of a sustainable H_2 society for several reasons [13]: i) it is a renewable feed that sequesters atmospheric carbon dioxide (CO_2); ii) having energy stored in chemical bonds makes it a versatile resource in which products other than H_2 can be extracted (*e.g.* gasoline, diesel, biofuels, value-added chemicals, biomaterials); and iii) a large variety of reserves which would otherwise be considered waste are available for processing, including agricultural and forestry residues and industrial, domestic, and fermentative wastewaters [14].

A novel process known as microbial electrohydrogenesis is capable of generating high yields of H_2 from cellulosic waste. Cellulolytic bacteria hydrolyze biomass into soluble fermentation end-products, which in turn are completely oxidized by electrogenic bacteria. The electrons and protons generated are chemically reduced within a microbial electrolysis cell (MEC). Thus, H_2 is produced both biologically via fermentation and chemically at the cathode of an electrochemical reactor. Organisms from the class Clostridia and δ-Proteobacteria are typically enriched in such systems. In particular, bacteria from the genus *Clostridium* and *Geobacter* dominate cellulolytic [15, 16] and electrogenic [17] environments respectively.

The engineering challenges associated with operation and scale-up are limited by our current knowledge of the microbial communities that develop at the anode. In particular, the relationship between fermentative and electrogenic bacteria is poorly understood. Although it is more than likely that the practical application of MEC technology will use

mixed consortia enriched from contaminated waste streams, it is critical to evaluate reactor performance using pure culture studies. Investigating the microbial relationships within a MEC will aid in determining optimized operating conditions leading to improved reactor design and increased H_2 production.

1.2 Hypotheses

Enhanced hydrogen production from renewable, cellulosic materials can be achieved by co-culturing the fermentative, cellulolytic *Clostridium termitidis* with the electrogenic *Geobacter sulfurreducens* in a MEC.

Characterizing mono- and co-culture growth in balch tube experiments and in MECs will further our understanding of the relationship that exists between fermentative and electrogenic bacteria, information that may be useful in formulating microbiological and engineering strategies for improved reactor design and consolidated operation.

1.3 Objectives

1. Design, fabricate, and test an autoclavable, anaerobic, single-chambered microbial electrolysis cell operating in fed-batch mode
2. Characterize mono- and co-culture growth of *C. termitidis* and *G. sulfurreducens* in triplicate balch tube experiments
3. Characterize mono- and co-culture growth of *C. termitidis* and *G. sulfurreducens* in triplicate MECs

Chapter 2: Literature Review

2.1 Cellulosic biomass

As much as 7.5 x 10^{10} tons of cellulose, the major component of plant biomass [8], is synthesized every year [18]. Found almost exclusively in plant cell walls, the high cellulose content typically ranges between 35 to 50 % of plant dry weight [19]. It is a linear, insoluble, polymer composed of the repeated union of β–D-glucopyranose[1] residues linked by β-1,4 glycosidic bonds [20, 21]. Unlike other glucan polymers (*e.g.* starch), the repeating unit of cellulose is not glucose but rather the soluble disaccharide cellobiose [22]. In cellulolytic bacteria (*e.g. Clostridium thermocellum, Clostridium cellulolyticum, Clostridium termitidis*), cellobiose hydrolysis can be phosphorylytically cleaved, yielding glucose in addition to glucose-1-phophsate (Fig. 2.1). The net effect of this process is reduced ATP requirements for the entry of glucose into glycolysis. This energy benefit is further exaggerated by the active transport of larger soluble oligosaccharides, where cleavage will also yield phosphorylated glucose residues. During bacterial growth studies, it is possible to circumvent the need of cellulose while justifying the use of cellobiose as a carbon source. Not only is metabolic behavior more easily studied using a soluble substrate, but it is assumed cellobiose is representative of growth on cellulose because cellobiose is the main product of cellulose hydrolysis [22].

[1] The cyclic form of glucose is also known as glucopyranose

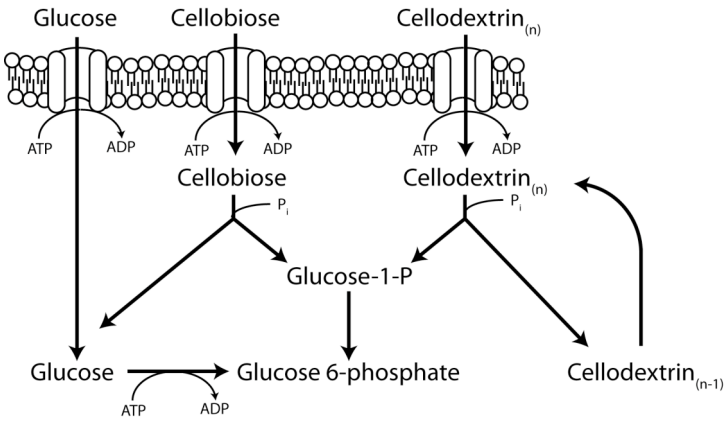

Figure 2.1 Carbohydrate uptake and phosphorylation by cellulolytic bacteria A net ATP benefit is possible by the active transport of larger oligosaccharides into the cell [image courtesy of Carlo Carere].

Cellulose possesses a relatively unusual crystalline structure. Individual glucan chains, known as cellodextrins, exhibit a high degree of polymerization (DP), which can exceed lengths of over 25,000 glucan residues [22]. The cellodextrins are stiffened by both intrachain and interchain hydrogen bonds and form adjacent overlying sheets held together by weak intersheet van der Waals forces. These factors combined bring structural order to the crystalline nature of cellulose, creating tightly packed, insoluble regions that prevent penetration and increase resistance to most forms of degradation [19]. It is for this reason why there is a tendency for cellulose to accumulate within the environment. Yet despite its crystalline structure, cellulose rarely exists in this pure state. Instead, natural cellulosic substrates are heterogeneous and are composed of amorphous regions containing voids and irregularities. Cellulose fibers are embedded in a complex, intertwined matrix of other structural biopolymers, primarily xylan or other hemicelluloses and lignin, which account for 20 to 35 and 5 to 30 % of plant dry weight, respectively [19].

The prominence of cellulose in the environment strongly reflects the ecological importance of organisms to utilize this biopolymer as a carbon source. Although the

majority of cellulose is degraded under aerobic conditions, up to 10 % of cellulose is metabolized anaerobically by a range of physiologically diverse bacteria. In particular, a wide array of metabolic end-products can be produced through dark fermentation, including the generation of bioH_2. There is enormous potential to capture H_2 from cellulosic materials through biological means. Cellulose degradation via dark fermentation is of widely recognized importance in both a technological and ecological context, and has the most immediate potential for sustainable bioH_2 production [23].

2.2 Dark fermentation and the theoretical limitations of hydrogen production

There are many microorganisms capable of both cellulose hydrolysis and H_2 production [24]. Among this group of cellulolytic microorganisms, bacteria of the class Clostridia and the genus *Clostridium* are not only well studied and characterized but are often found dominant in cellulolytic, H_2-producing reactor systems [15, 16]. Soluble cellodextrins and cellobiose released from cellulose degradation enter the cell and are metabolized via fermentation, where energy is gained through substrate-level phosphorylation (SLP). The glucan polymers are hydrolyzed into glucose-1-phosphate (G-1-P) and converted to glucose-6-phosphate, entering the Embden-Meyerhof (glycolysis) pathway for sugar catabolism and generating pyruvate as its end metabolite. Hydrogen is produced from the decarboxylation of pyruvate to acetyl-CoA, reducing ferredoxin (Fe_{red}) in the process. Transferring electrons to a dehydrogenase re-oxidizes Fe_{red} while reducing protons to form H_2. Unfortunately, H_2 is not the only product synthesized during fermentation. Pyruvate catabolism consists of numerous metabolic pathways to satisfy metabolic energy requirements with the generation of ATP as well as regenerating the reducing power of the cell by re-oxidizing reduced electron carriers (*e.g.*

NADH, NADH(P), Fe_{red}). The result is a branched metabolism and the production of other end-products including organic acids (formate, lactate), fatty acids (acetate, butyrate), alcohols (ethanol), and biogas (H_2, CO_2).

The complete oxidation of glucose in the absence of oxygen[2] can be written as:

$$\text{Glucose} + 12\ H_2O \rightarrow 6\ HCO_3^- + 6\ H^+ + 12\ H_2 \qquad (\Delta G^{\circ\prime} + 3.2\ \text{kJ mol}^{-1})$$

Despite a stoichiometric potential of 12 mol-H_2 mol^{-1}-glucose, the maximum amount of H_2 that can be produced by fermentation is 4 mol H_2 mol^{-1}-glucose, assuming only acetate is produced:

$$\text{Glucose} + 4\ H_2O \rightarrow 2\ \text{Acetate}^- + 2\ HCO_3^- + 4\ H^+ + 4\ H_2 \qquad (\Delta G^{\circ\prime}\ -206.3\ \text{kJ mol}^{-1})$$

In practice, H_2 yields are even lower, primarily due to electron assimilation into biomass, metabolic shifts to more reduced products, or H_2 re-consumption by uptake hydrogenases. Actual numbers are close to or lower than 2 mol H_2 mol^{-1}-glucose [25, 26], making practical H_2 production from biomass too small for dark fermentation to be considered economically competitive with other H_2 producing technologies [27]. Further H_2 can be extracted from the reduced metabolic end-products but an additional investment of energy would be required to overcome these thermodynamically unfavorable reactions. For example, the complete degradation of acetate requires +104.6 kJ mol^{-1} under standard temperature and pressure conditions (STP) (25^{o}C, 1 M aqueous species, 1 bar), adjusted to pH 7:

$$\text{Acetate}^- + 4\ H_2O \rightarrow 2\ HCO_3^- + H^+ + 4\ H_2 \qquad (\Delta G^{\circ\prime}+104.6\ \text{kJ mol}^{-1})$$

[2] Gibbs free energy calculations do not include the formation or consumption of ATP.

Coupling microbial electrohydrogenesis with dark fermentation may be the solution necessary to achieve high yields of H_2 from cellulosic biomass.

2.3 Enhanced hydrogen production by microbial electrohydrogenesis

Electrohydrogenesis is a novel process capable of high H_2 production from organic waste streams (Fig. 2.2). Microbial electrolysis cells are bio-electrochemical reactors that microbially oxidize organic material at an anode, producing CO_2, electrons, and protons. Electrons are shuttled from one electrode to the other through an external electric circuit while protons diffuse through the electrolyte to the cathode. Electrons and protons are chemically reduced at the cathode, in the presence of a catalyst, to form H_2. Current production is very small and must be calculated according to Ohm's law by measuring the voltage drop (V_{drop}) across an external resistor (R_{ext}).

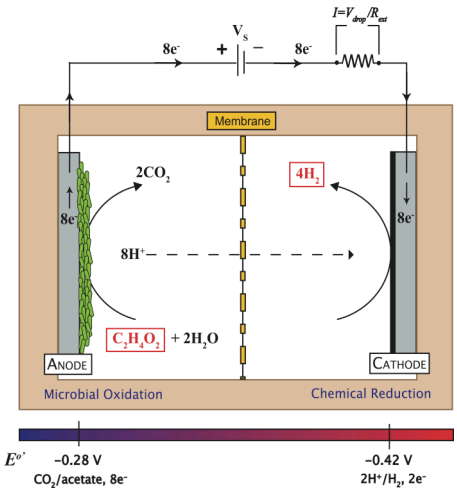

Figure 2.2 Principles of operation of a MEC Microbial oxidation of organic material at the anode, *e.g.* acetate oxidation, liberates electrons (e^-) and protons (H^+), which undergo chemical reduction at the cathode to form H_2. The reduction potential at the anode is higher than at the cathode and thus a small voltage must be supplied to drive this non-spontaneous reaction.

This is not a spontaneous reaction. The standard reduction potential, $E^{o\prime}$, for H_2 production is lower than the reduction potential at the anode. In practice, this potential

difference is even greater due to ohmic resistance through the system and overpotentials at the electrode-electrolyte interface. Consequently, energy from an external power source must be supplied to the cell in order to drive electrons from the anode to the cathode. Although not required, a membrane is typically used to separate the anode and cathode reactions while facilitating proton transfer.

The number of studies investigating H_2 generation by microbial electrohydrogenesis is rapidly increasing. High H_2 yields and recovery efficiencies can be achieved using energy sources that were once considered waste, such as fermentation end products and wastewater streams. Several bench-scale reactors have been summarized in Table 2.1 to demonstrate the technology's rapid progression from proof-of-concept design to its current status. The performance of each reactor was compared in terms of H_2 yield, volumetric H_2 production rate, and coulombic efficiency[3]. For the purpose of consistency, all papers selected in this evaluation were inoculated with mixed cultures and used acetate as the sole carbon source.

It was mentioned in the introduction that even though over 95 % of current H_2 producing technologies depend on fossil sources, many non-reforming approaches also exist which convert alternative resources such as biomass and water into H_2 rich streams [9]. A brief description of the most popular H_2-from-biomass and H_2-from-water technologies is presented in Table 2.2. The major advantages and disadvantages of each process are described, and H_2 production rates and efficiencies are evaluated with respect to microbial electrohydrogenesis. All systems are compared against the industry standard, H_2 production using SMR.

[3] Coulombic efficiency is defined as the fraction of electrons recovered as current versus the total number of electrons available in the substrate

Table 2.1 Overview of various MEC architectures and system performances reported in literature All studies used mixed consortiums as inoculums and acetate as the sole substrate. Overall H_2 production (Y_{H2}), volumetric H_2 production rates, and coulombic efficiency (C_E), measured at specific applied voltages (E_{ap}), were compared to reactor volume and electrode and membrane material and size.

Reference	Operation	Applied voltage E_{ap} (V)	Overall H_2 yield Y_{H2} (%)	Vol. H_2 production rate (m^3-H_2 m^{-3} d^{-1})	Coulombic efficiency C_E (%)	Total liquid vol. (L)	Membrane		Anode		Cathode		Electrode spacing (cm)
							Material	Area (cm^2)	Material	Area (cm^2)	Material	Area (cm^2)	
[28] [Bottle]	B	0.25	54[a]	0.005	60[a]	0.4	CEM (Nafion 117)	3.5	C-cloth (plain)	12	C-paper (0.5 mg Pt/cm^2)	12	15
[29]	B	0.5	53	0.02	92	6.6	CEM (Nafion 117)	256	G-felt (disc)	452 (400)[b]	Ti-mesh (5 mg Pt/cm^2)	452 (400)[b]	Direct contact w/ CEM
[30]	B	1.0	23	0.31 0.33	23	3.3	AEM (Fumasep FAB) CEM (Nafion 117)	256	G-felt (disc)	400	MEA Ti-mesh (5 mg Pt/cm^2)	400	Direct contact w/ membrane
[31]	B	0.6	88[c]	1.1	88[a]	.04[c]	AEM (AMI-7001)	n/a	G-granules	528	C-cloth (0.5 mg Pt/cm^2)	1	4
[32]	B	0.6	88[c]	3.12	92[c]	0.028	No membrane		G-brush (NH_3)	2,200	C-cloth (0.5 mg Pt/cm^2)	7	n/a
[33] †	C	1.0	98	6.3	98	0.1	No membrane (J-cloth)		C-felt	50	GDE (E-tek) (0.5 mg Pt/cm^2)	n/a	0.03

n/a not available
$Y_{H2,th}$ is calculated based on the number of moles H_2 produced versus theoretical amount of H_2 that can be extracted form substrate (*i.e.* 4 mol-H_2 mol^{-1}-acetate)
B batch, *C* continuous, *CEM* cation exchange membrane, *AEM* anion exchange membrane, *C* carbon, *G* graphite, *Ti* titanium, *MEA* membrane electrode assembly, *GDE* gas diffusion electrode
† equivalent acetate loading rate of 4 g L^{-1} d^{-1}
[a] referenced from Logan [26]
[b] surface area of electrode submerged in electrolyte
[c] referenced from Logan *et al.* [34]

Table 2.2 Comparison of H_2 production technologies Hydrogen production technologies are evaluated based on maturity, capacity, and efficiency. Only processes relevant to microbial electrohydrogenesis and renewables (biomass and water sources) were selected. Steam methane reforming was included in this analysis because it is the largest net producer of H_2 (adapted from [9, 10])

Technology	Description	Advantages	Disadvantages	Maturity	H_2 production	Efficiency	Reference
Microbial electrohydrogenesis	electrochemical oxidation of organic material (microbial catalysis) and reduction of H^+ and e^- to from H_2 (chemical, biological catalysis)	organic waste materials can be used as energy sources near complete substrate utilization (>90%) very high H_2 recovery efficiency (>93%) low operating temperatures and pressures	requires additional energy input (~0.6 V) methanogenic competition in mixed cultures (H_2 consumption for CH_4 production) high internal energy losses requires anodic anaerobic conditions technology still in its infancy (more research needed in catalyst development, membrane design, scale-up testing)	L	6.3 m^3-H_2 m^{-3} d^{-1}	81%[a]	[33]
Hydrocarbon reforming							
Steam reforming (methane)	steam at high temperatures reacts with CH_4 to produce CO and H_2. WGS reaction further converts CO into H_2 and CO_2	extensive industrial use no O_2 required High H_2/CO_2 ratio (3:1)	highest CO and CO_2 emissions vs. other fossil fuel H_2 producing technologies operating near theoretical limits – little room for improvement	C	1.5 million Nm^3 d^{-1}	70-85%[b]	[35]
Hydrogen from biomass							
Biomass gasification	chemical conversion of biomass at high temperature and controlled O_2 (endothermic, partial oxidation reaction) into a producer gas or syngas (H_2, CH_4, CO, CO_2, N_2, NH_3).	extensive industrial use fuel flexibility simplicity syngas can be used as feed for steam reforming and WGS reaction to increase H_2 yields	significant accumulation of tar low thermal efficiency and energy density H_2 separation from syngas required commercial systems requires large quantities of biomass – high transportation costs	C	40,482 Nm^3-H_2 d^{-1}[†]	35-50%[b]	[36, 37]
Photolysis	**Direct** - photosynthetic production of H_2 from H_2O by algae and bacteria **Indirect** - production of H_2 from carbohydrates produced by photosynthesis (photoheterotrophs)	water is primary feed for direct photolysis ability to metabolically engineer designer strains use sunlight as energy source simple nutritional requirements	low light utilization efficiency (5-15%) co-production of O_2 inhibits H_2 production	L	0.04 m^3-H_2 m^{-3} d^{-1} 0.19 m^3-H_2 m^{-3} d^{-1}	0.5%[c]	[9, 10]
Dark fermentation	fermentation of carbohydrate rich substrates by anaerobic bacteria (sometimes algae). Typical	ability to metabolize soluble and insoluble biomass ability to metabolically engineer strains	separation step required to produce high quality H_2 H_2 competition with reduced	L	4.4 – 65.1 m^3-H_2 m^{-3} d^{-1}	60-80%[d]	[9, 10]

	fermentation end-products include mixed gas (H_2, CO_2, CH_4, H_2S), organic acids, alcohol (ethanol, butanol)	for enhanced H_2 production low temperature demand	fermentation end-products strongly depends on environmental growth conditions process inhibited by O_2				
Photo fermentation	light energy and reduced compounds (organic acids) are catalyzed by a nitrogenase to form H_2 under N_2-deficient conditions	ability to use reduced organic compounds as a carbon source can be grown using a variety of processes (batch, continuous, porous glass, activated glass, polyurethane foam) process not inhibited by O_2	H_2 consumption by uptake hydrogenases slow nitrogenase enzyme activity not efficient solar collectors (current collection efficiency, 1.9%)	L	0.09 m^3-H_2 m^{-3} d^{-1}	0.1%[e]	[9, 10]
Biological water-gas-shift (WGS)	microbial oxidation of CO to CO_2, following the WGS reaction	low temperature and pressure reaction (enzymatic catalysis) thermodynamics favor high conversion of CO to CO_2 and H_2	requires a CO source requires darkness (photoheterotrophic)	L	51.7 m^3-H_2 m^{-3} d^{-1}	n/a	[9, 10]
Hydrogen from water							
Alkaline electrolyzer	H_2O is introduced at the cathode and is separated into H_2 and OH^-. The OH^- travels through the alkaline electrolyte (30 wt% KOH or NaOH), forming O_2 at the anode.	mature technology low operating temperature modest current density (100-300 mA cm^{-1})	expensive Pt catalysts required electrolyte must be replenished H_2 must be separated from electrolyte	C	11,640 Nm^3-H_2 d^{-1}[††]	50-60%[e]	[38, 39]
PEM electrolyzer	similar to electrohydrogenesis. H_2O is split into H^+ and O_2 at the anode. H^+ combine at the cathode to produce H_2	low operating temperature high current density (>1600 mA cm^{-1}) no H_2 separation unit required	stringent regulation of fuel quality (CO and H_2S poisoning)	N	24 Nm^3-H_2 d^{-1}[†††]	55-70%[e]	[40]

n/a = not available
C = Commercial; N = Near term; L = Long term
Nm^3 = cubic meter of gas volume at normal (*i.e.* atmospheric) pressure conditions
[†] MTCI (Manufacturing and Technology Conversion International) gasifier; type: BFB (bubbling fluidized bed); feedstock: pulp sludge
[††] Norsk Hydro Electrolyser – Atmospheric Type No.5040.
[†††] HOGEN RE PEM electrolyzer by Proton EnergySystems
[a] Energy-conversion efficiency (ECE) includes applied voltage but not energy in substrate (see [41]). Does not include H_2 purification.
[b] Thermal efficiency based on higher heating values
[c] Does not include H_2 purification
[d] Theoretical maximum, 4 mol-H_2 mol^{-1} glucose
[e] lower heating value of generated H_2 divided by the electrical energy to the electrolysis cell

From Table 2.2, it becomes apparent that even though microbial electrohydrogenesis is competitive with many H_2-from-biomass processes, it is still a technology in its infancy. To be considered a mature process, H_2 production rates and volumetric throughput must be comparable with SMR, biomass gasification, and alkaline electrolyzers. Target objectives have been proposed [4, 42]. As an example, for MECs to be competitive with high performance wastewater treatment systems[4], volumetric production rates must be greater than 10 m^3-H_2 m^{-3} d^{-1}, operating at 90% H_2 efficiency in a reactor scaled-up to 10^4 – 10^6 L in size. Despite bench-scale reactors operating near some of these goals, the major hurdle facing microbial electrohydrogenesis is scale-up: the ability to maintain this performance in reactor volume's six orders of magnitude greater, and doing so at a competitive price.

The purpose for the remainder of this chapter is twofold: i) to explain the fundamental principles of microbial electrohydrogenesis in an attempt to identify major bottlenecks within this process and ii) to discuss strategies to overcome the technical limitations that currently impede MEC technology. Investigation into the microbial communities that develop at the anode and the various mechanisms of electron transfer responsible for cell growth are examined. The thermodynamics of electrode reactions and electrode potentials are derived to determine theoretical operating conditions. Finally, energy losses associated with internal resistance and current flow are examined to explain deviations from ideal behavior. First, however, the history of MEC technology and its evolution from bio-electrochemical systems (BES) is explored.

[4] Target based on wastewater systems from BIOPAQ (Netherlands): high rate aerobic systems (up to 5 kg-COD m^{-3} day^{-1}) and high rate anaerobic systems (>10 kg-COD m^{-3} day^{-1})

2.4 History of the MEC

The first connection between electricity and biology was made in 1791 by Luigi Galvani, who discovered that severed frog's legs contract every time the muscle and nerve endings are connected to a static electricity generator [43, 44]. Around the same time, the concept of the fuel cell was developed by W.R. Grove who successfully produced an electric current and water by combining H_2 with O_2 [45]. Surprisingly, the first correlation between a half cell and microorganisms was not made until 1911 when M.C. Potter observed small amounts of electricity could be derived from microbial communities, introducing the possibility that bacteria were capable of generating an electric current [43, 46]. This discovery led to the BES in which anodic and/or cathodic reactions are biologically catalyzed by microorganisms. When electricity is produced in a BES, the term microbial fuel cell (MFC) is used. However, the term MEC is employed when electricity is consumed to drive electrochemical reactions [42]. In the context of this thesis, BESs apply specifically to microbial catalysis and not isolated enzymatic catalysis when assisting redox reactions in electrochemical cells [43, 47, 48].

Electricity production has been and remains the principle driving force behind the development of BES technology. In 1931, Cohen conducted the first bacteria-electrode interaction studies by examining overall potentiometric intensities of chemical reactions during bacterial growth [49, 50]. He demonstrated bacterial cultures are electrical half-cells that can perform work. With the introduction of artificial electron mediators (potassium ferricyanide or benzoquinone), Cohen was able to build the first bacterial battery, producing a voltage of 35 V when six cells were connected in electrical series. During the late 1950s and throughout the1960s, interest in converting organic material

into electrical energy surfaced. Initiated by the US space program, MFCs were seen as potential waste disposal units that could generate power during space missions [43, 51]. Despite an improved understanding of the electrical connections between electrodes and microorganisms as well as the introduction of potentially new applications, it was determined that current could not be produced at a consistent rate or in quantities large enough to be a viable source of electrical energy [47, 50 - 53].

A revived interest in electricity production from microbes came in the 1990's. Apart from the search for new, environmentally responsible sources of energy, studies showed increases in power densities using exogenous chemical mediators to deliver electrons to acceptors outside of the cell [54]. The breakthrough came with the discovery of the electricigen, bacteria capable of direct extracellular electron transfer to fuel cell anodes through the complete oxidation of organic compounds [17, 53]. It has been known for almost 100 years that electrode-reducing microorganisms can transfer electrons via direct contact with the anode or through the synthesis of chemical mediators, both exogenous and endogenous. However, it was observed for the first time that organic compounds were completely oxidized to CO_2 with all available electrons converted to current [55].

2.5 Electrogenic bacteria

Taxonomic profiles of electrode-reducing microbial communities from numerous MFC systems have been reported [42, 56 - 59]. The bacterial communities that develop show great diversity and typically depend on the enrichment conditions used to colonize the electrode surface [60]. However, amongst this group of electrode-respiring microorganisms, bacteria from the phylum Proteobacteria dominate anode communities. According to an eight system comparative study conducted by Aelterman *et al.* [59], 64%

of the anode population belonged to the class of α-, β-, γ-, or δ-Proteobacteria, the most studied of these belonging to the families of *Shewanella* and *Geobacteraceae* [17]. The complete genome of *Shewanella oneidensis* was sequenced in 2002 [61] and subsequently that of *Geobacter sulfurreducens* in 2003 [62] (Fig. 2.3). Both organisms will serve as excellent models to elucidate the mechanisms of electron transfer between microorganism and electrode.

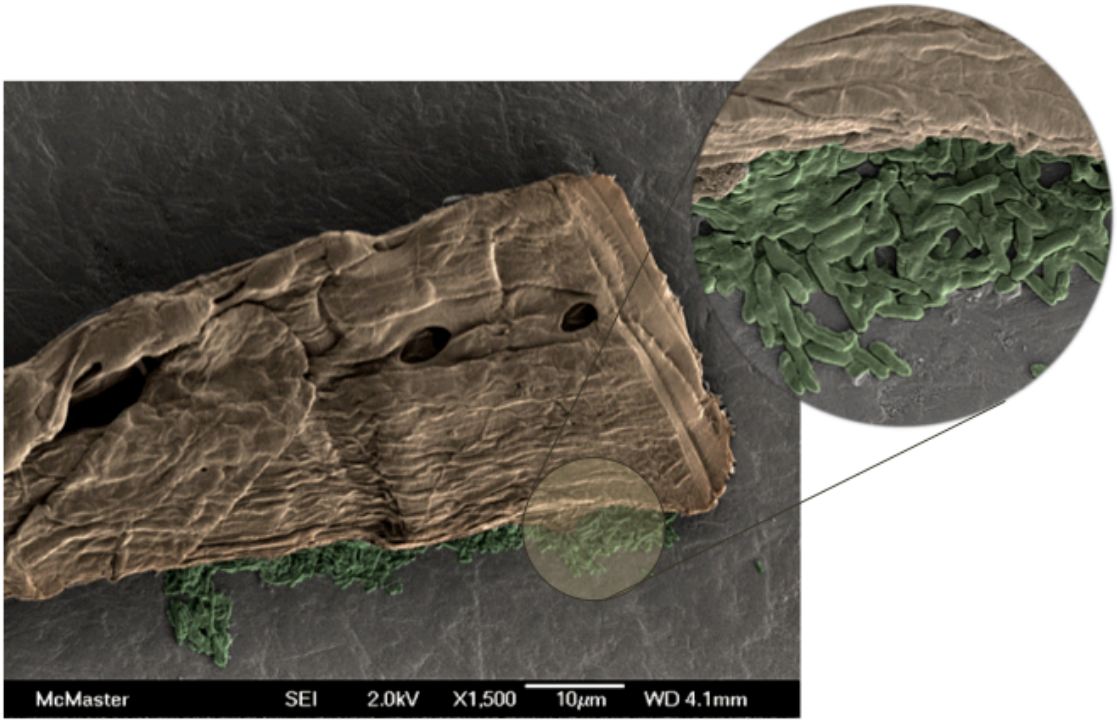

Figure 2.3 Scanning electron microscopy of the electrogenic bacterium *G. sulfurreducens* Gram-negative cells (green), approximately 2 nm in length, group along a gold plate (brown), illustrating the organism's ability to develop thick biofilms [Image taken by J. Paige Byers, Brockhouse Institute for Materials Research and Canadian Centre for Electron Microscopy, McMaster University, as part of a collaboration between Dr. Gianluigi Botton at McMaster University and Dr. David Levin, Department of Biosystems Engineering, University of Manitoba, funded by the NSERC Hydrogen Canada (H2CAN) Network.].

2.5.1 Mechanisms for microbe-electrode electron transfer

Understanding the principles of electron transfer between a microorganism and an electrode are essential in optimizing the current generated by any BES. Closer

investigation into these mechanisms could not only influence material selection used to improve the electrical connection between the bacteria and the electrode but also manipulate the surface design of the electrode to facilitate electron delivery [53]. Although the exact mechanisms for electron transfer are not completely understood, three methods have been proposed (Fig. 2.4): i) long-range electron transfer via electron shuttles, ii) direct electron transfer via outer-surface *c*-type cytochromes, and iii) long-range electron transfer via conductive pili or "microbial nanowires".

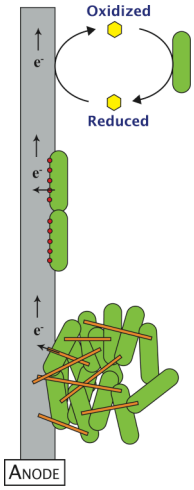

Figure 2.4 Proposed mechanisms for electron transfer to the anode of a MEC i) Long-range electron transfer via electron shuttles (yellow hexagon), ii) direct electron transfer via outer-surface *c*-type cytochromes (red circles), and iii) long-range electron transfer via conductive pili or "microbial nanowires" (orange rods).

Electron shuttles: Certain microorganisms produce soluble exogenous mediators that shuttle electrons from cells to insoluble compounds via diffusion. This phenomenon was first identified in mutant species of *Shewanella putrifaciens* [63] and later demonstrated in MFCs inoculated with *S. oneidensis* MR-1 [64]. Results showed that as many as half of the *S. oneidensis* cells were planktonic, suggesting substrate oxidation and concomitant current generation were coupled to long-range electron shuttles. Various

techniques used to detect redox-active molecules eventually identified riboflavin secretion as the mechanism for extracellular electron transfer in *Shewanella sp.* [60, 65, 66]. This mechanism for electron transfer has been observed in other bacteria, such as *Geothrix fermentans* [67]. Unfortunately, despite the advantages of long-distance interaction with an electrode, electron shuttles are energetically taxing and may not be the most desirable system for the bacterium [53, 68].

Direct contact via outer membrane c-type cytochromes: In contrast to synthesized shuttles that indirectly transfer electrons to an electrode, direct contact between the cell and anode is also possible through outer membrane *c*-type cytochromes. In the same study conducted by Lanthier *et al.* [64], the other half of *S. oneidensis* cells that were not planktonic were attached to the surface of the anode, suggesting multiple strategies for electron transfer exist. In order to differentiate between direct and indirect mineral reduction pathways, further investigation was required. Nanoporous glass beads deposited with Fe(III) (hydr)oxide were used to measure iron reduction by *S. oneidensis* MR-1 both indirectly and as a biofilm [69]. Results from strains with mutations in *cyma* and *omcB* identified a potential reduction process in which cytoplasmic *c*-type cytochrome CymA is required for both direct and indirect mineral reduction whereas outer membrane *c*-type cytochrome OmcB is not necessary for indirect iron reduction [69]. It has been proposed that CymA functions as the terminal electron acceptor in the electron transport chain of *S. oneidensis* MR-1 whereas OmcB acts as a direct electrical contact between the microbe and the electrode surface [17].

Gene deletion studies in *G. sulfurreducens* further highlight the importance outer membrane *c*-type cytochromes have as direct electrical contacts between microbe and

electrode. Two genes that encode outer membrane cytochromes, *omcS* and *omcE*, were targeted based on high transcript levels during growth on an electrode as the sole electron acceptor [70]. Deletion of *omcS* significantly reduced current production, which was restored after re-expression of the gene *in trans* on a plasmid. However, current inhibition was only temporary following the deletion of *omcE*. Over time, *G. sulfurreducens* found alternative routes to transfer electrons to the anode surface [53]. Results from this study outline the significance of outer membrane *c*-type cytochromes in direct electron transfer to an electrode. However, some organisms capable of reducing Fe(III) oxides lack *c*-cytochromes [71]. In addition, electron transport proteins attached directly to the outer membrane of the cell cannot explain how thick biofilms up to 75 μm [72] develop along anode surfaces reported in many MFC studies [73 - 75]. Further investigation using *G. sulfurreducens* led to the discovery of electrically conductive pili known as "nanowires" [76].

Electron transfer via microbial nanowires: According to Reguera (2009) [77], the nanowires of *G. sulfurreducens* are classified as type IV pili, protein filaments composed of the repeated single structural subunit, pilin or PilA. Typically, type IV pili aid in cell motility or adhesion to solid surfaces and are generally required by many Gram-negative organisms for biofilm establishment and maturation [78]. Unlike other pili, the microbial nanowires of *G. sulfurreducens* behave differently. Functionally, they act as electrical conductive conduits that enable microbial cell-cell communication and metal reduction. Structurally, the nanowires are much smaller in size, ranging from 4-5 nm in diameter[5]

[5] 10,000 times finer than a human hair

and 20 μm in length[6]. Genomically, nanowire pilin come from an independent line of descent following the pilin subunits from other members of the family *Geobacteraceae* (*e.g. Geobacter metallreducens*) [76, 77]. Additionally, the conservation of the N-terminal domain phylogenetically distances itself from other bacterial pilins, including the type IV pilin of *S. oneidensis* [76, 77]. Microbial nanowires are responsible for maximizing biofilm health by coordinating a cooperative electronic community, aggregating and interconnecting cells into a network capable of effectively distributing and dissipating electrons. They are responsible for high current and power production in MFCs, enabling active participation from cells located not only on the surface of the electrode but also at the outer boundaries of the biofilm.

A study by Reguera *et al.* [76] investigated the relationship between the nanowires of *G. sulfurreducens* and soluble and insoluble electron acceptors. Deletion of the *pilA* gene inhibited the production of pili and the reduction of insoluble Fe(III) oxides. The mutant was still able to reduce the soluble electron acceptors fumarate and Fe(III) citrate. Introducing a copy of the *pilA* gene *in trans* restored pili production and the ability to reduce Fe(III) oxides. Further studies revealed that PilA may have a structural role in biofilm formation [79]. However, it was observed that *pilA*-deficient mutants of *G. sulfurreducens* still formed biofilms along the surface of a graphite anode that was not connected in electrical series to a cathode, using fumarate as the terminal electron acceptor [53]. These findings suggest that although nanowires may not be necessary for biofilm growth, they are required for high-current production in BESs.

[6] capable of extending 10 times the length of the cell

2.6 Bio-electrochemical principles and challenges

2.6.1 Introduction

As previously mentioned, an electrolysis cell is an electrochemical system composed of two electrodes connected in electrical series and separated by an ionic conductor, or electrolyte. Unlike a galvanic cell that produces energy from spontaneous chemical reactions, electrolysis requires an input of energy to drive chemical changes that would otherwise not occur. When a current is added to the cell, charge is transferred by two separate means: electrons are carried externally by electrical conduction and ions flow internally through the electrolyte by ionic conduction. The interface where these two chemical phases meet is particularly important because this is the site of charge transfer between electrode and electrolyte: the reactions that occur here determine the operation and performance of the electrolysis cell. Thus, understanding the principles of electrode reactions with respect to microbial electrohydrogenesis is required in order to calculate theoretical limitations and explain deviations from ideal behavior.

The energy losses measured within a MEC determine the amount of potential that must be supplied to the reactor to generate H_2. However, total resistance within an electrochemical system is complicated and depends on the interrelation between three phenomena – thermodynamics, kinetics, and transport. The thermodynamic properties of the electrode and electrolyte determine the driving force for chemical reactions occurring at its interface. Kinetic parameters determine the rate at which these reactions will occur, while the transport of reactants to the interface and the continuous flow of charge through the cell is governed by principles of mass and charge transfer. Additionally, BESs must

consider any biological losses associated with microbial activity, which determine the extent of electron generation and transfer to the anode.

In this section, the thermodynamics of electrode reactions in terms of the electrochemical potential will be reviewed. The rates of these reactions in terms of current densities, j (A m^{-2}), will be discussed, introducing several models typically used to determine the kinetic parameters for microbial systems. Finally, mechanisms for the transport of charge and mass will be examined with an emphasis on the technical challenges that MEC technology currently faces. This section is intended to be an introduction to electrochemistry and its application to microbial electrohydrogenesis. For a closer analysis on electrochemical principles and methods, many excellent textbooks are available [80 - 82].

2.6.2 Thermodynamic evaluation in terms of electrochemical potential

Fundamentals: The chemical potential, μ, is a thermodynamic quantity used to describe the energy level of a chemical species. It is a function of temperature, pressure, and concentration. Analogous to a ball rolling down a hill due to gravitational potential, a species will always move from a higher chemical potential to a lower chemical potential. When the species is charged, the electrical state must also be considered. In the presence of an electric field, the contribution of the electrostatic potential, ϕ, is very strong and is evaluated separately from the internal chemical potential components of that species. Thus, the electrochemical potential, $\overline{\mu}_i$, is the sum of the contributions from both the chemical potential and electrostatic potential of species i:

$$\overline{\mu}_i = \mu_i + z_i F \phi \qquad \ldots \qquad (2.1)$$

where z is the charge of species i and F is Faraday's constant, 96,485 C mol^{-1} [7].

The electrode-electrolyte interface of an electrochemical cell is a multi-component, open system in which mass (*i.e.* the electron) of each species is free to move between the liquid, α, and solid, β, phases. According to Gibbs, once a state of equilibrium is achieved, the electrochemical potential of each species will be the same in both phases:

$$\overline{\mu}_i^{\alpha} = \overline{\mu}_i^{\beta} \qquad \ldots \qquad (2.2)$$

By introducing the phase equilibrium constraint (Eq. 2.2) to a multi-component, open system in phase equilibrium, the electrochemical potential can now be related in terms of its natural variables temperature, T, pressure, P, and mole number, n. This is accomplished using the fundamental thermodynamic differential equation Gibbs energy, G:

$$dG = -SdT + VdP + \sum_i \overline{\mu}_i dn_i \qquad \ldots \qquad (2.3)$$

where S is the entropy of the system. What makes Eq. 2.3 so important is that once a thermodynamic function is described in terms of its natural variables, all thermodynamic properties of that system can be determined [83]. Assuming isothermal and isobaric reaction conditions typical of MECs, the Gibbs equation varies only with composition. Upon integration, the energy change for a chemical reaction is given by a change in Gibbs free energy for each half-reaction:

[7] It is easily shown that if the species is uncharged, $z_i = 0$, the electrochemical potential equals the chemical potential, $\overline{\mu}_i = \mu_i$.

$$\Delta G = \left(\sum_i \overline{\mu}_i n_i \right)_{\text{Products}} - \left(\sum_i \overline{\mu}_i n_i \right)_{\text{Reactants}} \quad \ldots \quad (2.4)$$

Gibbs free energy is a convenient measure for describing the spontaneity of a process and can be viewed as the tendency for a reaction to reach equilibrium. If ΔG is negative, the electrochemical potential for the reactants is at a higher energy level and electrons will spontaneously flow to products. If ΔG is positive, the electrochemical potential is lower for reactants and additional energy must be supplied to drive electrons to products. When ΔG is zero, the system is said to be in equilibrium.

It may be more convenient to measure the electromotive force, E_{emf}, of a MEC rather than calculate the Gibbs free energy. An electromotive force is a measure of the work, W, required to produce an electrical potential difference between two electrodes:

$$W = E_{emf} Q = E_{emf} nF \quad \ldots \quad (2.5)$$

where Q is the charge and n is the molar number of electrons transferred in the reaction. The E_{emf} of a MEC is the minimum amount of energy required to drive electrons from the anode to the cathode but can only be determined after chemical equilibrium of each half-cell is achieved. Allowing current to flow through an electrode gives rise to polarization effects, or departures from the equilibrium potential. When the rate of forward reactions equals the rate of backwards reactions, no net current is flowing allowing the true difference in equilibrium potentials of each electrode half-reaction to be compared. This is also termed the open-circuit potential (OCP) because the voltage is measured between two open terminal electrodes. Under equilibrium conditions, the amount of reversible work to establish a potential difference is equal to the Gibbs free energy:

$$E_{emf} = -\frac{\Delta G}{nF} \quad \ldots \quad (2.6)$$

The evolution of H_2 is a thermodynamically unfavorable reaction. For typical MECs, the cell E_{emf} is negative making the ΔG positive. These calculations provide the minimum requirements to drive H_2 production but more energy is required due to various potential losses throughout the system (described in detail below).

Electrode Potentials: Any electrochemical cell can be viewed as a controlled redox reaction, where oxidation and reduction are spatially separated into half-reactions located at the anode and cathode respectively. The minimum cell potential to drive microbial electrohydrogenesis, expressed as an electromotive force, can be determined by evaluating each electrode separately:

$$E_{emf} = E_c - E_a \quad \ldots \quad (2.7)$$

The Nernst equation is used to determine the equilibrium potential for each half-reaction:

$$E_{electrode} = E^o_{electrode} - \frac{RT}{nF}\ln(\Pi) \quad \ldots \quad (2.8)$$

where R is the universal gas constant, 8.31447 J mol^{-1} K^{-1}, and T is the absolute temperature. According to IUPAC convention, all reactions are reported as a reduction potential: $oxidized + e^- \rightarrow reduced$. Therefore, the reaction quotient, Π, is the ratio of products divided by reactants expressed as activities. To simplify this treatment, dilute solution conditions are assumed and the Nernst equation can be expressed directly in

terms of concentrations (*i.e.* activity coefficients are assumed to be unity). The reaction quotient becomes:

$$\Pi = \frac{[reduced]^p}{[oxidized]^r} \quad \ldots \quad (2.9)$$

where r and p are the stoichiometric coefficients for reactants and products, respectively.

The standard potential, $E^o_{electrode}$, is the equilibrium reduction potential under standard temperature and pressure (STP) conditions (298.15 K, 1 M for all species, 1 bar). All standard potentials are reported relative to a stable, well-defined reference electrode, which is typically the standard hydrogen electrode (SHE) or normal hydrogen electrode (NHE) (assigned a value of 0.000 V under STP conditions). Other standard reference electrodes are used, which include the saturated calomel electrode (SCE) and saturated Ag/AgCl electrode with potentials of +0.242 V and +0.197 V versus NHE respectively [80].

Typically when calculating the thermodynamics of biological reactions, neutral conditions are assumed [84]. Microbial electrohydrogenesis is no exception and the NHE is adjusted to a pH of 7.0. However, caution is advised and thermodynamic calculations should be adjusted according to actual operating pH values. The corrected NHE potential for the reduction of H_2 can be calculated using Eq. 2.8:

$$2H^+ + 2e^- \rightarrow H_2 \quad \ldots \quad (2.10)$$

$$E^{o/}_{(H_2/H^+)} = E^o - \frac{RT}{nF}\ln\frac{H_2}{[H^+]^2}$$

$$E^{o/}_{(H_2/H^+)} = 0 + \frac{(8.31 \cdot 298.15)}{(2 \cdot 9.65 \cdot 10^4)} \ln \frac{1}{(10^{-7})^2} = -0.414\ V\ (\text{vs. NHE})$$

Depending on the substrate consumed at the anode by the bacteria and the operating conditions of the MEC, the theoretical total cell potential will vary. Standard and actual potentials of the typical electrode reactions found in MECs are summarized in Table 2.3. For clarity purposes, all anode reactions are written as oxidation potentials to indicate electron loss. Additionally, many excellent review papers and textbooks compare the standard potentials of the reactions typically found in BESs [26, 81, 82, 84 - 86].

Table 2.3 Reduction half-reactions and reduction potentials for common reactions in MEC studies

	Half-reaction	E^o (V vs NHE)	E (V vs NHE)	Reference
Anode reactions				
Acetate†	$8C_2H_3O_2^- + 3H_2O \rightarrow 8CO_2 + 8HCO_3^- + 8H^+ + 8e^-$	0.130	-0.284	[26, 87]
Propionate†	$C_3H_5O_2^- + 5H_2O \rightarrow 2CO_2 + HCO_3^- + 14H^+ + 14e^-$	0.128	-0.286	[87]
Butyrate†	$20C_4H_7O_2^- + 7H_2O \rightarrow 3CO_2 + 20HCO_3^- + 20H^+ + 20e^-$	0.127	-0.287	[87]
Glucose	$C_6H_{12}O_6 + 12H_2O \rightarrow 6HCO_3^- + 30H^+ + 24e^-$	0.104	-0.289	[86]
Ethanol†	$C_2H_6O + 3H_2O \rightarrow 2CO_2 + 12H^+ + 12e^-$	0.090	-0.324	[87]
Cathode reactions				
H_2	$2H^+ + 2e^- \rightarrow H_2$	0.000	-0.414	[26, 86]
Methane	$HCO_3^- + 9H^+ + 8e^- \rightarrow CH_4 + 3H_2O$	0.227	-0.248	[86]
H_2O_2	$O_2 + 2H^+ + 2e^- \rightarrow H_2O_2$	0.695	0.328	[26]
N_2	$2NO_3^- + 12H^+ + 10e^- \rightarrow N_2 + 6H_2O$	1.246	0.734	[86]
H_2O	$O_2 + 4H^+ + 4e^- \rightarrow 2H_2O$	1.229	0.805	[26, 86]

The third column represents reduction potentials under STP conditions (T = 298.15 K, P = 1 bar, [] = 1 M).
The fourth column represents actual experimental conditions:
$T = 298.15\ K$
$[H^+] = 10^{-7}\ M$
$[H_2O] = 1\ M$
$[HCO_3^-], [NO_3^-], glucose = 0.05\ M$
$[H_2O_2] = 0.5\ M$
$pCO_2 = 1\ bar$
$pO_2 = 0.2\ bar$
All other product concentrations = 1 M
† $[HCO_3^-] = 1\ M$

2.6.3 Total energy losses

As mentioned above, the driving force required for an electrochemical reaction to occur is the difference in potential energy between the anode and the cathode. This was quantified as a voltage, E_{emf}, or OCP, and is the minimum amount of energy required to drive an electrolytic process. However, this value represents a theoretical limit based on thermodynamic relationships whereas in practice, voltage requirements are considerably higher. The additional amount of energy required to generate H_2 in a MEC can be treated as a series of resistances. It is the sum of the overpotentials at the anode, η_a, and the cathode, η_c, as well as ohmic losses, IR_Ω, within the system:

$$E_{cell} = E_{emf} + (\sum \eta_a + \sum \eta_c + I \sum R_\Omega) \quad \ldots \quad (2.11)$$

It was already mentioned that when a current runs through an electrochemical cell, a departure from equilibrium conditions is observed. This phenomenon is known as polarization. The magnitude of this potential drop is caused by a resistance to the passage of current and is appropriately termed overpotential, η. The extent of polarization at any one of the two electrodes depends on the current density and the nature of the reaction but is independent of the other electrode and the processes occurring there [82]. Therefore, each electrode can be studied individually when treating this phenomenon. A more thorough investigation into the variables that influence overpotentials and their effect on the reaction rates at the electrode-solution interface is discussed below.

It should be noted that the contribution of overpotentials and ohmic resistances to total energy loss is represented by polarization curves. By plotting the potential as a

function of current density, deviations from OCP conditions, and thus overall MEC performance, can be observed [42, 80, 81].

2.6.4 Ohmic losses

Ohmic voltage losses are determined by resistance to electron flow through electrical conductors (*i.e.* electrodes and external circuitry) and resistance to ion flow through ionic conductors (*i.e.* electrolyte and proton exchange membrane) [42, 85]. According to Ohm's Law[8], ohmic resistances are independent of current. However, because the voltage input for H_2 production is constant in a MEC, both the current density and total ohmic resistance depend on each other [88]. To compare different MEC architectures, resistances should be calculated using current density (A m^{-2}) rather than current. Additionally, current density should be expressed as a function of the projected anode surface area to normalize against biofilm growth [88].

Sleutels *et al.* [88] conducted ion transport resistance studies in a MEC using anion and cation exchange membranes (AEM, CEM). Resistance to the transport of ions through the AEM configuration was much lower both at the beginning of the experiment and end of the experiment (12 and 8 mΩ m^2 respectively) compared to the CEM configuration (48 and 128 mΩ m^2). In addition to transport losses across the membrane, the total resistance based on electrode and electrolyte conductivity was estimated [88, 89]. At the end of the experiment, the total resistance using the AEM configuration was significantly lower than the CEM, at 192 and 435 mΩ m^2 respectively. As a result, using an AEM produced higher rates of H_2 (2.1 m^{3}-H_2 m^{-3} d^{-1} at a current density of 5.3 A m^{-2}) compared to the CEM configuration (0.4 m^{3}-H_2 m^{-3} d^{-1} at a current density of 2.3 A m^{-2})

[8] Ohm's Law states that cell potential is a function of the current flow and cell resistance: $E = IR$

[88]. These findings are consistent with other published work comparing AEM and CEM configurations [29 - 31].

In addition to transport losses, potential losses associated with pH gradients across the membrane have also been observed [29, 88]. The concentration of ions will be different inside the membrane than outside in solution because membranes carry a charge. This ion gradient can be expressed as a Donnan equilibrium [90]. Measured potential losses due to changes in ion concentration between CEM and AEM configurations is significant, at 0.16 and 0.10 V (vs. NHE), respectively [88]. A closer examination into the design of membranes is given in subsequent sections (see Future outlook for MEC technology).

Besides membrane selection, reducing electrode spacing, increasing electrolyte conductivity, and selecting electrode materials with low resistivity are options necessary to manage voltage losses and increase system performance.

2.6.5 Overpotentials at the cathode

The reaction at the cathode in a MEC is known as the hydrogen evolution reaction (HER) and is driven by the reduction of protons to H_2 (Eq. 2.10). The HER reaction has been heavily studied under extreme conditions of low pH or high alkalinity [91], but with the introduction of microorganisms at the anode (and possibly the cathode), neutral operating conditions (pH 7, mesophilic temperatures) is required. Two overpotentials account for the majority of energy lost at the cathode: charge-transfer losses, η_{ct}, and mass-transfer losses, η_{mt}:

$$\sum \eta_C = \eta_{ct} + \eta_{mt} \quad \ldots \quad (2.12)$$

A third overpotential may also exist, termed a reaction overpotential, η_{rxn}. These losses are associated with chemical reactions preceding the transfer of electrons, which include protonation or dimerization effects [80]. With respect to microbial electrohydrogenesis, the energy losses associated with η_{rxn} are very small when compared with η_{ct} and η_{mt} and are therefore ignored [42, 85, 91].

Charge-transfer (activation) overpotential: Slow kinetics related to the sluggish transfer of electrons at the electrode surface results in charge-transfer or activation losses. Factors that determine the nature of this reaction include electrode material, electrode surface area, nature of the electron transfer reaction, and operating temperature [91]. Assuming that the reaction is reversible, current can be related to the activation overpotential using the Butler-Volmer equation [80, 81]. The general form of this equation is given by:

$$j = -j_o\left[\exp\left(\frac{\alpha_a F}{RT}\eta_{ct}\right) - \exp\left(\frac{\alpha_c F}{RT}\eta_{ct}\right)\right] \quad \ldots \quad (2.13)$$

where j_o is the exchange current density (A m^{-2}), analogous to the rate constant in chemical kinetics, and α is the apparent transfer coefficient, relating potential to reaction direction (*i.e.* determines whether a reaction is an anodic or cathodic current[9]). For H_2 evolution, and thus a cathodic current, the first term in Eq. 2.13 is negligible and can be removed. Assuming no concentration polarization [42], large activation overpotentials

[9] An anodic current results in the flow of electrons from species in solution to the electrode, whereas the opposite is true for a cathodic current, where electrons flow from the electrode back into solution.

are linearly correlated to the logarithmic value of the reaction current density, and a Tafel plot can be created:

$$\eta_{ct} = \frac{RT}{\alpha_C F} \ln\left(\frac{j}{j_o}\right) \quad \ldots \quad (2.14)$$

Tafel plots show that activation polarization rates decrease as current densities increase, meaning associated potential losses are most prominent under low current conditions, between 0 and 1 mA cm^{-2} [92]. This result has serious implications since MECs operate under low current conditions. One strategy to minimize the impact of activation losses is to increase the specific surface area of the cathode in the order of 10^6 m^2 m^{-3} [93]. Increasing the surface area decreases the current density and thus the activation losses. Other strategies aim to improve catalyst reaction kinetics by testing new catalysts, increasing operating temperatures, or increasing catalyst loading to effectively boost the number of reactive sites [26, 42, 85].

Microbial electrolysis cells have typically used platinum (Pt) to overcome the slow reaction kinetics of the HER on carbon-based [28, 31, 32, 94, 95] and titanium (Ti)-based [29, 30] cathodes. The highest H_2 volumetric production rate in a MEC was achieved using a 0.5 mg cm^{-2} Pt catalyst loaded on a gas diffusion electrode (6.3 m^3-H_2 m^{-3} d^{-1} at an applied voltage of 1.0 V) [33]. Low overpotentials for Pt catalyzed HERs (-0.05 V at 15 A m^{-2}) have also been reported under optimized mass transport conditions [91]. However, Pt is very costly and not a practical solution for MEC scale-up.

Stainless steel (SS), nickel (Ni), and Ni alloys have been used to catalyze the HER in water electrolysis [96]. They have shown good performance but at high alkalinity and high temperatures (450-700 ^oC) [97]. The potential of using these metals as a replacement

for Pt has been investigated in several MECs. Stainless steel brushes produced H_2 at a rate of 1.7 m^3-H_2 m^{-3} d^{-1} at an applied voltage of 0.6 V [98]. Increasing the surface area of the cathode decreased activation overpotentials by 10.5 % (η_{ct} with 50 % bristle loading versus η_{ct} with brush core only). At an applied voltage of 0.9 V, metal sheets composed of SS alloy A286 produced H_2 at twice the rate than Ni 625 (1.5 versus 0.8 m^3-H_2 m^{-3} d^{-1} respectively) [99]. The use of Ni 210 catalyst powder rather than a solid Ni plate increased H_2 production rates to 1.3 m^3-H_2 m^{-3} d^{-1}, despite operating at a lower applied voltage of 0.6 V [97]. The use of SS and Ni to replace platinum catalyzed cathodes shows promise, however long-term corrosion testing and its impact on current density and H_2 evolution is required.

The use of a microbial biofilm to produced H_2 at the cathode has been successfully reported [100, 101]. To achieve a functional biocathode, the group exploited the principal that hydrogenases are reversible. A three-step process was exercised which: i) developed a healthy, acetate-fed bioanode, ii) adapted the bioanode for H_2 oxidation by feeding the chamber with H_2 only, and iii) reversed the polarity of the cell to naturally select for an H_2-producing, electrochemically active community at the cathode. Initial experiments produced H_2 at a rate of 0.63 m^3-H_2 m^{-3} d^{-1} (current density of 1.2 A m^{-2} and cathode potential of -0.7 V) [100]. Jeremiasse *et al.* [101] demonstrated for the first time that an MEC with both a bioanode and biocathode can produce H_2. Two MECs were operated at an applied voltage of 0.5 V. Both MECs had cathode potential of -0.7 V, however the current density of 1.9 A m^{-2} for MEC 1 was less than the 3.3 A m^{-2} generated in MEC 2. The overpotential at the cathode for both experiments, based on a theoretical potential of -0.42 V for the HER at pH 7 was -0.28 V. For biocathodes to be a

viable option, the overpotential must be reduced to -0.1 V and the current density increased to 10 A m^{-2} [4, 101].

The number of available reaction sites and total surface area of an electrode heavily influence the rate of a reaction. However, the rate of mass transport to that surface will also play a significant role in the overall reaction rate. The different modes of mass transport must be discussed.

Mass-transfer (concentration) overpotential: Poor transfer of material in and out of the electrode-electrolyte interface is important in predicting current flow because the rate of the reaction will depend on the concentration of reactants and products. Poor mass-transfer develops chemical and potential gradients between the bulk solution and the interface, creating overpotentials at the electrode. Three modes of mass transport can influence an electrolysis reaction: i) migration (electrical potential gradient), ii) convection (bulk fluid movement, and iii) diffusion (chemical potential gradient).

Migration. Electrolysis places a positive charge on the anode and a negative charge on the cathode, creating an electric field and a driving force for ions in solution. Assuming no concentration effects, anions and cations will move in opposite directions creating a build-up of charge at the electrode interface. Migration is essentially an electrostatic effect where any charged species near the interface will be attracted or repelled by electrostatic forces. However, due to the complexity of real solutions, such as diffuse layer interactions and solvation effects, migratory flux in MECs has never been reported.

Convection. Material can be transported to the interface by the bulk movement of the solution. Convection can be caused naturally by the formation of density gradients or

thermal differences or may be forced by mechanical stirring or pressure gradients. Natural convection in electrolysis is discouraged because of its unpredictability. Although mixing a solution cannot cause a current, it can have a large impact on the concentration profile of ions and may be an effective means of bringing reactants to or removing products from an electrode surface.

To enhance the mass transport of substrate, protons, and buffer at the anode, a forced flow was introduced both through and perpendicular to a porous carbon felt anode [102]. At an applied voltage of 1 V, a high current density of 16.4 A m^{-2} (1 mm thick electrode) was achieved at a H_2 production rate of 5.6 m^3-H_2 m^{-3} d^{-1}. However, these results represent a combination of strategies that also included a higher buffer concentration. The contribution of forced flow to improve current density and H_2 production was not reported.

Diffusion (concentration). During current flow, the surface concentrations of the substances involved in the reaction change relative to the bulk concentrations in solution. Concentration polarization is observed when the supply or elimination of reactants and products is limited. Migration of ions to the electrode, diffusion gradients resulting from improper mixing, or unbalanced ratios of oxidized to reduced species at the electrode surface are all contributing factors that will result in a potential shift away from the electrode's equilibrium position [42, 85]. Concentration polarization is the most significant mass-transport process in MEC cathode reactions [42, 86, 91].

Jeremiasse *et al.* [91] investigated the use of biocompatible buffers to lower the concentration polarization for the HER at Pt-cathodes (0.5 mg cm^{-2} Pt/Ir mixed metal oxide coated Ti). It was shown that the overpotential at the cathode was strongly

dependent on the pH. At 50 mM and 15 A m^{-2}, the use of phosphate and ammonia led to the lowest overpotentials of -0.05 V at a pH of 6.2 and 9.0 respectively. Under the same experimental conditions, Tris, Hepes, and carbonate each had overpotentials of -0.07 (pH 7.8), -0.08 (pH 7.2), and -0.09 V (pH 9.3) respectively. Increasing the buffer concentration, increasing the linear flow speed, and decreasing the current density further reduced the concentration overpotential to a minimum, under conditions where pH approached the buffer dissociation constant (pKa). Higher current densities were reported by other groups by increasing the buffering capacity of the electrolyte [102]. A higher phosphate concentration in the anode chamber increased H^+ away from the biofilm and lowered the ionic resistance of the electrolyte.

Sleutels *et al.* [88] developed a method to compare the performance of different systems based on resistance rather than potential. Expressing the sum of potential losses as partial resistances normalizes energy losses with respect to current density since the cell voltage of an MEC remains constant. The cathode potential loss with a CEM configuration (0.15 V at a current density of 2.3 A m^{-2}) was smaller than the AEM configuration (0.17 V at a current density of 5.3 A m^{-2}). However, when current density is taken into account, the CEM cathode resistance is much large than the AEM configuration, at 65 and 32 mΩ m^2 respectively [88].

2.6.6 Overpotentials at the anode – a kinetics perspective

The reaction at the anode is catalyzed microbially. A carbon source is oxidized by anode-respiring bacteria (ARB), which in turn produce electrons (transferred to the electrode), protons (migrate and diffuse to the cathode), CO_2, and biomass. Clearly, the same potential losses that exist at the cathode are also present at the anode. However, in

addition to charge-transfer and mass-transfer overpotentials, the anode is the site for metabolic losses associated with biofilm growth, η_{ARB}:

$$\sum \eta_a = \eta_{ct} + \eta_{mt} + \eta_{ARB} \quad \ldots \quad (2.15)$$

The reported OCP for acetate oxidation in an MEC (-0.200 V vs NHE) is close to the theoretical value (-0.284 vs NHE) [30]. Typically, overpotentials are much smaller at the anode than at the cathode, ranging from 0.12 to 0.15 V (vs NHE) [30, 88]. However, these values represent total energy losses. To quantify specific overpotentials within an ARB community, electron flux from the electron donor (substrate) to the electrode surface must be fully understood.

Lee *et al.* [103] have proposed a three-stage conceptual model that relates substrate potential to anode potential: i) the substrate is oxidized and cellular electron carriers are reduced, ii) electrons travel down the potential gradient to outer-membrane, terminal cellular electron acceptors, and iii) electrons are passed to the anode via an extracellular electron-transfer mechanism. In order to achieve high yields of H_2, the ARB community must be able to produce high current densities at the lowest possible potential (*i.e.* as close to the potential of the substrate) [103]. Steps i) and ii) represent the intracellular potential drop. This is the only process where ARB can gain energy because it is assumed that potential losses related to extracellular activity, step iii), are mainly dissipated as heat given electron transfer occurs outside of the cell [60, 104]. Therefore, in order to maximize cell growth, and thus current densities, it is necessary to keep extracellular potential losses to a minimum.

The Monod equation is typically used to model bacterial growth kinetics, particularly rates of substrate utilization (*i.e.* substrate oxidation and cellular electron carrier reduction) [105, 106]. According to Torres *et al.* [87], under substrate limiting conditions, substrate flux within a biofilm can be expressed as:

$$j = j_{\max} \frac{S}{K_s + S} \quad \ldots \quad (2.16)$$

where j_{max} is the maximum biofilm current density (A m^{-2}) (j_{max} is a function of the maximum rate of substrate utilization, biofilm density, biofilm thickness, and fraction of electrons used for cell synthesis; see [87]), S is the substrate concentration (g m^{-3}), and K_s is the half-saturation coefficient (g m^{-3}) which corresponds to the concentration at which j_{max} is one-half of its maximum.

Monod-type growth was observed and kinetic parameters were determined for *G. sulfurreducens* using acetate (5.5 mM) as the limiting substrate and fumarate (30 mM) and Fe(III) (60 mM) as soluble electron acceptors [107]. High rates of acetate consumption coupled with low K_s values were observed, making *G. sulfurreducens* an ideal candidate for MECs due to high substrate oxidation rates at low substrate concentrations [108].

The Monod equation can be used only when the electron acceptor concentration is known. Unfortunately, the terminal electron acceptor for ARB is a solid anode lacking a defined concentration [109]. In order to describe the biofilm's response to changes in anode potentials, the Nernst-Monod equation was developed [110]:

$$j = j_{\max}\left[\frac{1}{1+\exp\left(-\frac{F}{RT}\eta_{ARB}\right)}\right] \quad \ldots \quad (2.17)$$

where $\eta_{ARB} = E_a - E_{KA}$. E_{KA} is an electrochemical parameter, which is a measure of potential when $j = 1/2 j_{max}$. E_{KA} is analogous to K_s and is indicative of an ARBs desire to transfer electrons to the anode - the more negative E_{KA} is, the greater the affinity to transfer electrons [108]. Combining Eq. 16 with Eq. 17 introduces both the biological and electrochemical factors required to describe the current density of an ARB community as a function of the potential at the anode [103]:

$$j = j_{\max}\frac{S}{K_S + S}\left\{\frac{1}{1+\exp\left[-\frac{F}{RT}(E_a - E_{KA})\right]}\right\} \quad \ldots \quad (2.18)$$

Under substrate limiting conditions, biological parameters such as K_S and substrate utilization rates play an important role and must be determined experimentally. Under substrate excess conditions ($S >> K_s$), the rate of substrate utilization will approach unity (*i.e.* $S/K_s+S = 1$) and intracellular ARB kinetics will be a function of the anode potential only. It should be noted that although anode potential has the greatest impact on current flux through the ARB [108], biofilm kinetics should also consider substrate gradients that develop within the biofilms [74].

The effects of anode potential on the kinetic parameters of the Nernst-Monod equation were evaluated for an ARB community [108]. A very negative E_{KA} of -0.448 V (vs Ag/AgCl) was reported, indicating fast biofilm growth and high current flux to the

anode close to saturation levels (where j_{max} = 9.25 A/m^2). At a poised anode potential of -0.400 V (vs Ag/AgCl), η_{ARB} was calculated to be 0.048 V. Thus having E_{KA} values lower than the potential of the anode is the most effective strategy for ARBs to achieve high current densities in MECs.

2.7 Future outlook for MEC technology

For microbial electrohydrogenesis to become an economically competitive technology, high H_2 production rates must be achieved at low applied voltages. This can only be accomplished if current flux to the anode in maximized while total energy losses is minimized. Several strategies are discussed.

2.7.1 Positive energy balance

For microbial electrohydrogenesis to have a net positive energy balance, the summation of all energy losses associated throughout all aspects of the system must be lower than the energy produced from the generation of H_2. A number of studies have characterized total energy losses within MECs. In order to have a more tangible understanding of overpotentials at the anode and cathode, ohmic resistance, and theoretical requirements to total system loss, two studies were compared (Fig. 2.5).

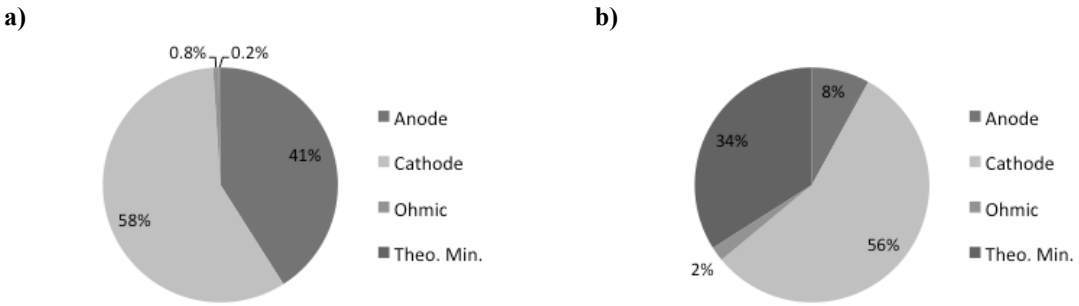

Figure 2.5 Comparison of total energy losses within a MEC The contribution of overpotentials at the anode and cathode, ohmic losses, and theoretical requirements were compared. a) Rozendal *et al.* [29] used a dual chamber MEC at an applied voltage of 0.5V. b) Lee and Rittmann [41] used a single chamber MEC at an applied voltage of 1.1 V. Both reactors were operated in batch mode and used acetate as the sole carbon source (figures adapted from [29] and [41] respectively).

By examining the figures adapted from Rozendal *et al.* [29] (Fig. 2.5a) and Lee and Rittmann [41] (Fig. 2.5b), two themes immerge: i) the use of a membrane drastically increases ohmic resistance, in this case by more than 50%, and ii) the majority of energy lost is from electrode overpotentials, particularly at the cathode. Despite operating at different applied voltages (0.5 and 1.1 V), the percent of energy consumed from anode and cathode losses was similar. In a later study, it was recommended that the operating voltage for any MEC should be 0.6 V or lower in order to achieve a positive net energy benefit from the process, assuming a cathodic energy recovery of at least 80% [41].

2.7.2 Membrane design

The decision to include a membrane into the design of a MEC has serious implications. The most obvious advantage of a membrane is that it acts as a barrier, separating the anode chamber from the cathode chamber. This produces a clean H_2 stream, preventing mixing with CO_2 and other metabolic gases (CH_4, H_2S) that may be produced at the anode during mixed culture experiments. Additionally, greater coulombic

efficiencies and higher cathodic recoveries can be achieved since proton transfer is facilitated through the electrolyte [29, 86, 88].

Unfortunately, improved reactor performance comes at a cost. Not only will resistance within the membrane increase total ohmic energy losses by as much as 50% [41, 111], but a significant pH gradient will also develop across the membrane. One way to describe proton consumption at the cathode is the formation of hydroxyl ions (OH^-)[10]. According to Rozendal (2007) [4], as [OH^-] increases with time, an uneven distribution of charge is created. As the membrane attempts to maintain electroneutrality, ionic species are transported between the two chambers. Unfortunately, under neutral conditions (pH 7), typical MEC membranes predominantly transport ionic species other than OH^-. A concentration gradient develops, inducing the diffusion of charged species in the opposite direction. This pH gradient will continue to build until the migration of cations and anions in one direction equals the diffusion of ionic species in the opposite direction. The result of this phenomenon is severe, with experiments showing cathode pH greater than 12. In terms of energy loss, every additional increment in pH unit results in an ohmic loss of approximately 0.059 V, requiring an additional energy input of 0.13 kWh m^{-3}-H_2 [4]. This explanation is general and applies to all semi-permeable membranes. Actual pH increases in the cathode chamber will depend on the type of membrane being used. For example, the cathode pH is lower for MECs using AEMs rather than CEMs based on their different affinities for hydroxyl ions [4]. This statement is in agreement with experimental results [30].

[10] based on the equilibrium of H^+ and OH^- through the water dissociation constant ($K_w=[H^+][OH^-]\approx10^{-14}$)

One way to lower pH gradients and energy losses is to remove the membrane from the design. By doing so, single-chambered MECs have achieved the highest volumetric H_2 production rates at 3.12 m^3-H_2 m^{-3} d^{-1} [32] and 6.3 m^3-H_2 m^{-3} d^{-1} [33]. Additionally, membrane-less operation simplifies the MEC design, lowering construction costs. Unfortunately, several major drawbacks do exist. First, H_2 is no longer a pure product. As mentioned above, additional purification steps are required to remove metabolic gases being produced at the anode by electrochemically active bacteria (mainly CO_2). Secondly, membrane-less operation results in the microbial consumption of H_2 via methanogens, homoacetogens, or H_2 scavengers able to convert H_2 back into current (H_2 recycling) [103].

A number of studies have reported CH_4 production by hydrogenotrophic and acetoclastic methanogens, not only at the anode but also at the cathode [109, 111 - 114]. One study by Clauwaert and Verstraete [111] reported that CH_4 was the main energetic product (78% of total gas) despite continuous operation and slightly acidic conditions (pH 6.1–6.2). Another study by Lee and Rittmann [109] not only observed CH_4 production (6.9% of total gas) but also determined H_2 recycling accounted for 62–76% of the total current generation. Controlling methanogenesis and preventing H_2 recycling present significant challenges for the practical application of membrane-less MECs.

2.7.3 Reducing electrode overpotentials

Designer consortiums – anode: Greater current densities can be achieved by packaging electricigens as designer consortiums. Designing experiments that force bacteria to produce current is a promising approach since no previous evolutionary selection pressure on microorganisms has existed [53]. This strategy was successful in selecting a

variant of *G. sulfurreducens* with an enhanced capacity for current production [115]. *Geobacter sulfurreducens* strain KN400 was recovered from a biofilm after 5 months of growth in a MFC. Although further functional analysis is required, phenotypic changes to the outer surface of the cell were observed, resulting in a greater abundance of conductive pili with a lower internal resistance and greater tendency to form biofilms.

Improved catalysts – cathode: A qualitative summary of the most commonly used cathode catalysts is presented in Table 2.4 (for a quantitative comparison, see section on charge-transfer (activation) overpotentials). Replacing Pt with inexpensive cathode materials or even the use of biocathodes to catalyze the HER is necessary if MEC scale-up is to be economically feasible. Pilot plant testing has begun at the Napa Wine Company in Oakville, CA, USA, using SS cathodes [116]. Although promising, reaction kinetics must be improved and the long-term mechanical stability requires further testing [99].

Table 2.4 Comparison of cathode catalysts used in MECs Advantages and disadvantages are discussed to qualitatively compare commonly used catalysts.

Material	Advantages	Disadvantages	Reference Experiments
Platinum (Pt)	low overpotentials for HER (0.05 V) high volumetric H_2 production rates (6.3 m^3-H_2 m^{-3} d^{-1})	very costly – not feasible for scale-up: Pt = \$630 m^{-2}	see Table 1
Stainless Steel (SS 305) & Nickel Alloys (Ni 625)	have been used to catalyze HER in water electrolysis bench scale performance similar to Pt economical: SS = \$63 m^{-2}; Ni = \$370 m^{-2}	long term corrosion / performance testing required	[99]
Biological	no metal catalyst required robust biofilm	high overpotentials (0.28 V) further testing required	[101]

Chapter 3: Hydrogen production and growth characterization by *Clostridium termitidis* strain CT1112 and *Geobacter sulfurreducens* strain PCA in mono- and co-culture batch experiments

3.1 Summary

The production of H_2 from the fermentation of cellulosic materials can be optimized with the integration of a MEC. Mono- and co-cultures of *C. termitidis* (a fermentative organism) and *G. sulfurreducens* (an electrogenic organism) were studied in batch to characterize growth, end-product synthesis, and substrate consumption. The culture medium was modified to support both organisms, significantly influencing the end-product profile of *C. termitidis* on cellobiose. Slower specific growth and a shift in carbon and electron flow away from CO_2 and H_2 production towards formate synthesis was observed. Mono-culture growth of G. *sulfurreducens* indicated formate preference above all other substrates when cultured in a synthetic cocktail of fermentation end-products. Despite high initial concentrations of acetate, a syntrophic association was observed during co-culture growth of *C. termitidis* and *G. sulfurreducens*, resulting in no net H_2 or formate production. A variety of microbial quantification tools (OD, protein, and qPCR) were used to track population growth and dynamics in mixed cultures. Accumulation of fermentation end-products and H_2 re-consumption have been identified as key challenges preventing a sustainable fermentative / electrogenic co-culture. These problems are verified in single-chambered MECs in the next part of this study (Chapter 4) and strategies to achieve successful co-cultures for enhanced H_2 production are discussed.

3.2 Introduction

Despite many bacteria demonstrating electrochemical activity that could potentially serve as electron donors in a MEC, none so far have cellulolytic capabilities [117 - 119]. Electricigens are particularly important organisms. Not only can they completely oxidize organic material, including most fermentation end-products, but the formation of conductive nanowires, and subsequent biofilm development, enables fast electron transfer to an insoluble electrode at high current densities. Co-culturing cellulolytic, fermentative bacteria with electricigens can provide the support required to maximize H_2 yields from cellulosic waste. Not only has this method been proven to generate electricity in microbial fuel cells [120], but microbial consortia may also offer a thermodynamic advantage. First proposed by McInerney and Beaty [121] and explored by Lovley [119, 122], it is hypothesized that the energy released per electron transferred is more important than the amount of energy available per mole of glucose. Coupling the fermentation of glucose with the oxidation of its end-products will offer a greater potential energy yield (per electron transferred) than the complete anaerobic oxidation of glucose to CO_2 alone.

Clostridium termitidis is a gram positive, mesophilic, obligate anaerobe capable of fermenting cellulosic substrates into organic acids (lactate, formate, pyruvate), fatty acids (acetate), alcohols (ethanol), and biogas (H_2, CO_2). What makes *C. termitidis* such an appealing organism is its promising cellulolytic capabilities, high rates of H_2 production, and diverse range of end-products [123]. *Geobacter sulfurreducens* is an electrochemically active, gram-negative, mesophilic, facultative anaerobe known to completely oxidize formate, acetate, lactate, pyruvate, and H_2 [124, 125]. Not only is *G.*

sulfurreducens capable of generating high electron fluxes to anodes, but it also serves as an excellent model in characterization studies – it is an organism that is well-studied and whose genome has been completely sequenced [62]. Based on a syntrophic exchange of metabolites, it is anticipated that co-culturing both bacteria will create a system where maximum H_2 production from cellulosic waste can be achieved.

In part one of this study, we characterized mono- and co-culture growth of fermentative and electrogenic bacteria in batch experiments in an attempt to evaluate changes in microbial performance with respect to changes in environmental conditions. Three sets of experiments were conducted using *C. termitidis* and *G. sulfurreducens* grown in a modified 1191 media designed to support growth of both organisms: i) a pure culture of *C. termitidis* was grown solely on cellobiose to develop an end-product profile that could be used as possible substrates by *G. sulfurreducens*; ii) a pure culture of *G. sulfurreducens* was grown on a synthetic cocktail of substrates as determined by the fermentation end-products of *C. termitidis* at end-point concentrations with fumarate as a terminal electron acceptor; and iii) a co-culture of *C. termitidis* and *G. sulfurreducens* was grown together using cellobiose as the sole carbon source with fumarate as the terminal electron acceptor.

Part two of this study (Chapter 4) reproduces pure culture and co-culture experiments in single-chambered MECs. It is hoped that the results generated will help engineers and microbiologists design a better system that will improve the way microbial consortia are studied, and ultimately manipulated, for enhanced H_2 generation via microbial electrohydrogenesis.

3.3 Materials and Methods

3.3.1 Microbial source and media

Pure cultures of *C. termitidis* CT1112 and *G. sulfurreducens* PCA were obtained from the American Type Culture Collection (ATCC). Fresh stock was maintained by transferring 10 % (v/v) inocula into fresh media, grown at 35^{o}C. Cultures of *C. termitidis* were given 2 g L^{-1} cellobiose as the sole carbon source while *G. sulfurreducens* was fed acetate (50 mM) as a carbon source and fumarate (50 mM) as a terminal electron acceptor.

All chemicals and reagents for media and substrates were obtained from Fisher Scientific with the exception of cellobiose and $MgCl_2 \cdot 6H_2O$ (Sigma-Aldrich), and yeast extract (VWR, bacteriological grade). In order to satisfy growth requirements for both organisms, ATCC 1191 medium [123, 126] was combined with ATCC 1957 medium and a media designed by Ren *et al*. [120] previously used in co-culture experiments. This modified complex medium contained (per liter milliQ water): NaH_2PO_4, 1.5 g; Na_2HPO_4, 3.35 g; NH_4Cl, 1.5 g; $MgCl_2 \cdot 6H_2O$, 0.2 g; KCl, 0.1 g; yeast extract, 2 g; resazurin (25 mg mL^{-1}), 0.5 mL; 1x modified Wolfe's mineral solution, 10 mL; 10x modified Wolfe's vitamin elixir, 1 mL.

Modified Wolfe's mineral solution (1x) contained (per liter milliQ water): nitrilotriacetic acid, 1.5 g; $MgSO_4$, 1.47 g; $MnSO_4 \cdot H_2O$, 0.5 g; NaCl, 1.0 g; $FeSO_4 \cdot 7H_2O$, 0.1 g; $CoCl_2 \cdot 6H_2O$, 0.1 g; $CaCl_2 \cdot 2H_2O$, 0.13 g; $ZnSO_4 \cdot 7H_2O$, 0.1 g; $NiCl_2 \cdot 6H_2O$, 0.02 g; $CuSO_4 \cdot 5H_2O$, 0.01 g; $AlK(SO_4)_2 \cdot 12H_2O$, 0.01 g; H_3BO_3, 0.01 g; $Na_2MoO_4 \cdot 2H_2O$, 0.01 g; Na_2SeO_3, 0.01 g; and Na_2WO_4, 0.01 g. Modified Wolfe's vitamin elixir (10x) contained (per liter milliQ water): biotin, 0.02 g; folic acid, 0.02 g; pyridoxine hydrochloride, 0.1 g;

thiamine HCl, 0.05 g; riboflavin, 0.05 g; nicotinic acid, 0.05 g; calcium D(+)-pantothenate, 0.05 g; cobalamin, 0.001 g; *p*-aminobenzoic acid, 0.05 g; and thioctic acid, 0.05 g. Sodium disulfide (Na_2S) at a final concentration of 200mM was used as a reducing agent.

3.3.2 Experimental design

Balch tubes (Bellco Glass Co.) with a total volume of 27 mL were used for all tests. A final working volume of 10 mL was achieved for each experiment by varying the volume of media initially added to each tube, resulting in 8.7, 6.9, and 6.7 mL for experiments i), ii), and iii), respectively. To maintain an anaerobic environment, the tubes containing modified 1191 media were air-sealed with butyl-rubber stoppers, crimped with aluminum seals, and gassed and degassed (1:4 min) for four cycles with 100 % nitrogen (N_2). Sterile Na_2S reducing solution (200 mM) was added (0.1 mL) [127] and each tube was autoclaved.

Anaerobic, filter-sterilized (0.2 μm) cellobiose (100 g L^{-1}) was added to tubes from experiments i) and iii) to a final concentration of 2 g L^{-1}. A 10x stock of fermentation end-products was prepared and contained: formate (81 mM), acetate (79 mM), pyruvate (45 mM), lactate (34 mM), and ethanol (42 mM). The 10x synthetic blend was filter-sterilized, made anaerobic, and 1 mL was added to each tube for experiment ii). For tests containing *G. sulfurreducens* (ii and iii), 1 mL of sterile, anaerobic fumarate (500 mM) was added as a terminal electron acceptor. All tubes were inoculated (10 % v/v) with fresh, mid-late exponential phase cultures that had been serially sub-cultured twice prior to the initiation of the experiment.

Balch tubes containing *C. termitidis* grown on cellobiose were incubated for 48 h. Samples were taken every 8 h based on a cell doubling rate of 8 h [123]. Tubes containing *G. sulfurreducens* grown on the synthetic substrate were incubated for 93 h. Samples were taken every 24 h until growth transitioned from late-log to stationary phase, where sampling occurred every 12 h. Tubes containing both *C. termitidis* and *G. sulfurreducens* on cellobiose were incubated for 57 h. Samples were taken approximately every 12 h until growth stabilized. All batch experiments were incubated at 35^{o}C and three independent replicate samples were taken at each time point.

3.3.3 Analytical procedures

Cell growth and biomass measurements: Cell growth rates were determined spectrophotometrically (Biochrom, Novaspec II) by measuring changes in optical density at 600 nm (OD_{600}). Tubes were inverted three times and values were analyzed within several seconds while cells remained in suspension. All tubes were blanked against an environmental control containing modified 1191 media, substrate, and, if required, fumarate at starting-point concentrations. Protein analysis was determined according to a modified Bradford method [128]. Aliquots (1 mL) of culture were sampled and centrifuged (Legend Micro21R, Sorvall) at 10,000 *g* for 10 min to separate the pellet from the supernatant. The supernatants were transferred to 1.5 mL microcentrifuge tubes (Fisher Scientific) and stored at -20^{o}C for substrate and end-product analysis. The pellets were re-suspended in a 0.9 % (wt/v) aqueous sodium chloride (NaCl) solution then centrifuged at 10,000 *g* for 10 min. The supernatant was decanted and 1 mL of 0.2 N sodium hydroxide (NaOH) was added. The samples were vortexed to re-suspend the pellet then boiled for 10 min in a water bath to solubilize any remaining protein. Each

sample was centrifuged at 10,000 *g* for 5 min and the supernatants were collected for Bradford analysis. Optical densities at 595 nm were measured (Synergy4, BioTek) after kinetic reads stabilized and protein concentrations were calculated based on a protein standard curve (albumin from bovine serum, Sigma-Aldrich) with an R^2 value greater than 98 %. For experiments where *G. sulfurreducens* was grown, the consumption of acetate and formate assimilated into biomass was calculated according to [129, 130]:

$$17C_2H_3O_2^- + 11H_2O = 8C_4H_7O_3 + 2HCO_3^- + 15OH^- \quad \text{acetate assimilation}$$

$$17CHO_2^- + 7H_2O = 2C_4H_7O_3 + 9HCO_3^- + 8OH^- \quad \text{formate assimilation}$$

Substrate and end-product analysis: The supernatants were used to analyze soluble substrate and end-product concentrations. All tests were performed using a high-performance liquid chromatograph (Dionex ICS-3000, Sunnyvale, CA, USA). Acetate, lactate, formate, and pyruvate were separated using an anion-exchange IonPac-AS11 analytical column (4 x 250 mm) and measured using a conductivity detector. Cellobiose was separated using a CarboPac PA1 analytical column (4 x 250 mm) and measured by an electrochemical detector. Fumarate, succinate, and malate were passed through a Bio-Rad Aminex HPX-87H ion exclusion column (7.8 x 300 mm) and measured by a refractive index detector (Shodex, RI-101). Ethanol concentrations were determined using the UV-Test Kit (R-Biopharm AG, Darmstadt, Germany), which spectrophotometrically measured the amount of NADH produced by alcohol dehydrogenase at 340 nm [123, 131].

Gas and pH measurements: The percentage of gas in the headspace (H_2 and CO_2) was measured using a gas chromatograph (SRI Instruments, configuration 8610C), outfitted

with a thermal conductivity detector and argon (Ar) as a carrier gas. A stainless steel (S.S.) molecular sieve 13x packed column (3.2 mm x 1.8 m) was connected in series with a S.S. silica gel packed column (3.2 mm x 1.8 m) to separate H_2 and CO_2 respectively. Gas concentrations were quantified by correcting for temperature, pressure, and volume. Aqueous phase concentrations were estimated according to their solubility in water [132] and the fraction of CO_2 in equilibrium with bicarbonate was calculated [133] (see Appendix B). The pH of each tube was measured using a Sension2 pH ISE meter (Hach) equipped with a ThermoOrion triode probe [123].

3.3.4 Quantitative PCR analysis

Genomic DNA extraction: Population dynamics analysis was performed on co-cultures in experiment iii) only. Aliquots (1 mL) of culture from each time point were dispensed into 1.5 mL microcentrifuge tubes and centrifuged (Legend Micro21R, Sorvall) at 10,000 *g* for 10 min, discarding the supernatants after separation from the pellet. This step was repeated up to five times when necessary to concentrate enough DNA for future analysis. Total genomic DNA was isolated following Promega's protocol for isolating genomic DNA from gram positive and gram negative bacteria (Promega, Wizard Genomic DNA Purification Kit, pp. 16-17). DNA concentration and quality were measured spectrophotometrically at 260 nm (NanoDrop, ND-1000).

Specific primer design: Forward and reverse primers were designed to probe unique *cpn60* sequences belonging to *C. termitidis* and *G. sulfurreducens* [134, 135]. Forward and reverse primer sequences designed specifically for *C. termitids* were 5'- ACC GAC ACC GAG AAA ATG GAA GCA -3' and 5'- ACA GCC ACA CAG GTG AAG GTT

CC -3' respectively, with an amplicon product size of 212 bp. Forward and reverse primer sequences designed specifically for *G. sulfurrerducens* were 5'- CTA CCT GCG CGC CCT TGC TT -3' and 5'- GGG CGG AAC GGG ACA CCT TG -3' respectively, with an amplicon product size of 254 bp. Primer specificity was optimized for PCR amplification (Eppendorf AD, 22331 Hamburg) running 30x cycles at a melting temperature of 67^{o}C. Each PCR reaction contained (per 24 μL total volume): RedTAQ ready mix, 12 μL; forward and reverse primer (1 pmol μL^{-1}), 1 μL each; template DNA (10 nmol μL^{-1}), 1 μL; topped up with milliQ H_2O. Primer specificity and amplicon size were confirmed through gel electrophoresis (agarose, 2 % (w/v); TAE buffer, 1x; template DNA extracted from pure cultures of *C. termitidis* and *G. sulfurreducens* in late-log phase of growth). DNA was extracted and purified following the QIAquick gel extraction kit protocol (QIAGEN, QIAquick Spin Handbook, pp. 25). To increase DNA concentration, only 30 μL of elution buffer was added to each QIAquick column. DNA concentration and quality were measured (NanoDrop, ND-1000).

Standard preparation: Promega's ligation protocol using the pGEM_T vector system was followed (Promega, pp. 4). Approximately 10 ng of PCR product was added to 50 ng of pGEM_T (3.0 kb) to perform a ligation reaction at a 3:1 insert to vector molar ratio. Reactions were incubated overnight to acquire the maximum number of transformants. The pGEM_T vectors with appropriate inserts were transformed into competent DH5α *Escherichia coli* cells prepared using the calcium chloride method and streaked on plates containing: LB broth, 20 g L^{-1}; agar, 1.6 % (w/v); IPTG, 1 mM; X-Gal dissolved in DMSO, 1 mM; and ampicillin, 100 ug mL^{-1}. Plates were incubated for 24 h at 37^{o}C. Only single white colonies were selected and incubated overnight at 37^{o}C in LB broth (20 g L^{-}

^{1}) and ampicillin (100 ug mL^{-1}). Cultures were re-streaked on new plates containing IPTG, X-Gal, and ampicillin to maintain a fresh working stock of culture. Plasmid DNA was extracted from the DH5α *E. coli* cells according to QIAGEN's plasmid DNA purification protocol using the QIAprep spin miniprep kit (QIAprep Miniprep Handbook, pp. 22). Based on the measured plasmid DNA concentration (NanoDrop, ND-1000) and the length of the vector and insert (bp), the exact copy number of specific primer product DNA (molecules μL^{-1}) could be calculated and serially diluted over eight orders of magnitude to create a series of qPCR standards.

qPCR reaction: All samples were measured using Stratagene's Mx3005P quantitative PCR thermocycler. All reactions were exposed to a melting temperature of 67^{o}C and contained (per 24 μL total volume): iTaq's SYBR green fluorescence probe, 12 μL; forward and reverse primer (1 pmol μL^{-1}), 1 μL each; template DNA (10 nmol μL^{-1}), 1 μL; topped up with milliQ H_2O. A standard plot was created relating the threshold cycle (C_t) to the copy number of primer product DNA described above. Three sets of internal controls were added in triplicate to measure process errors associated with varying ratios of *C. termitidis* and *G. sulfurreducens*. Negative controls and no template DNA controls were also administered to determine the fluorescence of any non-specific amplification and background noise.

3.4 Results

3.4.1 Mono-culture of *C. termitidis* grown on 2 g L^{-1} cellobiose in modified 1191 medium

Clostridium termitidis grew in modified 1191 medium as indicated by OD_{600} values and protein concentrations (Fig. 3.1a). Pure cultures of *C. termitidis* containing 2 g L^{-1} cellobiose remained in exponential growth for 32 h with an average doubling time of approximately 11.6 h, based on the average OD_{600} of triplicate measurements taken at individual time points between 0 and 32 h. During this time, cellobiose was completely consumed beyond detectable limits (5 μM) while approximately 1 mM of residual glucose remained unused (Fig. 3.2a). Gas production by *C. termitidis* corresponded to cell growth, characterized by high rates of production in exponential phase that gradually decreased as growth entered the stationary phase (Fig. 3.3a). The ratio of H_2/CO_2 calculated from total gas accumulation displayed a decreasing trend during exponential growth, eventually stabilizing at a 1.1:1 molar ratio by stationary phase. As much as 9.4 and 8.6 mM H_2 and CO_2 were produced respectively on cellobiose, based on the final average (48 h) normalized against initial concentrations (Table 3.1).

Culture pH decreased steadily and significantly throughout the duration of the experiment, stabilizing around 5.8 after 48 h of growth (Fig. 3.3a). This drop in pH correlated with high organic acid synthesis and bicarbonate accumulation (HCO_3^-) due to increased CO_2 partial pressure. Despite a very low final pH value no significant spikes in lactate production were observed in *C. termitidis*' metabolic end-product profile as seen in previous studies [123, 126].

a)

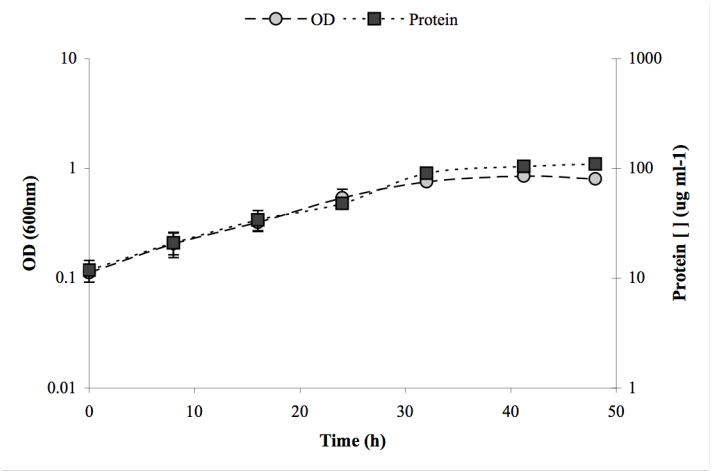

b)

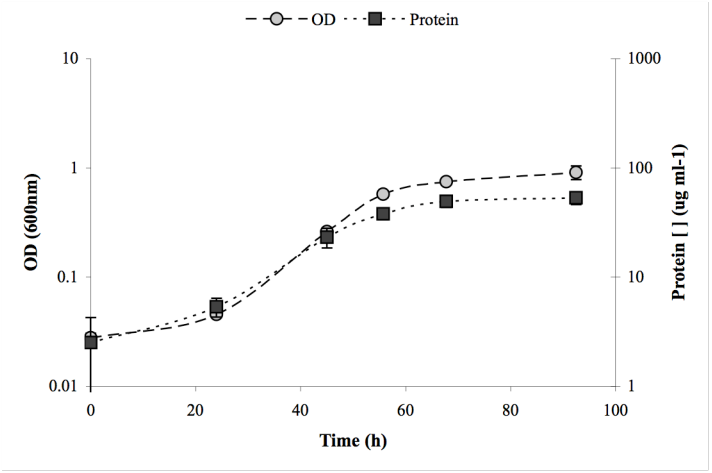

c)

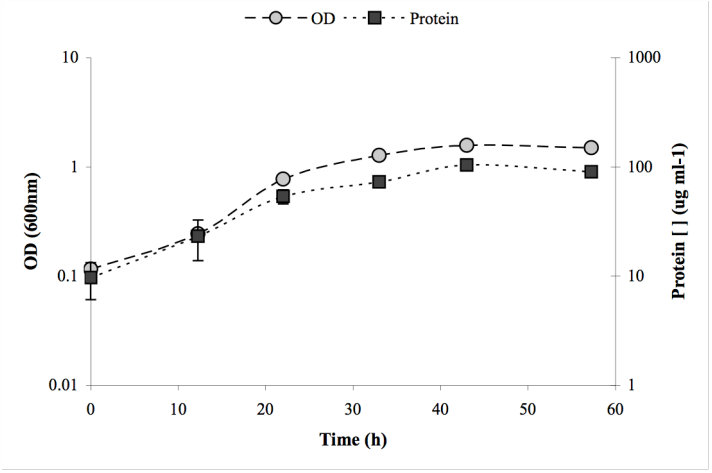

Figure 3.1 Semi-logarithmic plot of optical density (600 nm) and protein production in modified 1191 medium a) mono-culture of *C. termitidis* grown on 2 g L^{-1} cellobiose; b) mono-culture of *G. sulfurreducens* grown on synthetic blend of fermentation end-products; and C) co-culture of *C. termitidis* and *G. sulfurreducens* grown on cellobiose. Data points represent the average of three independent replicates and errors bars represent the standard deviation (SD).

a)

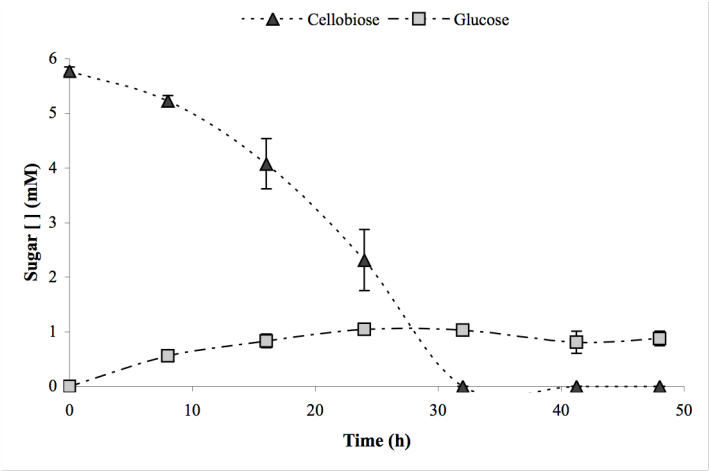

b)

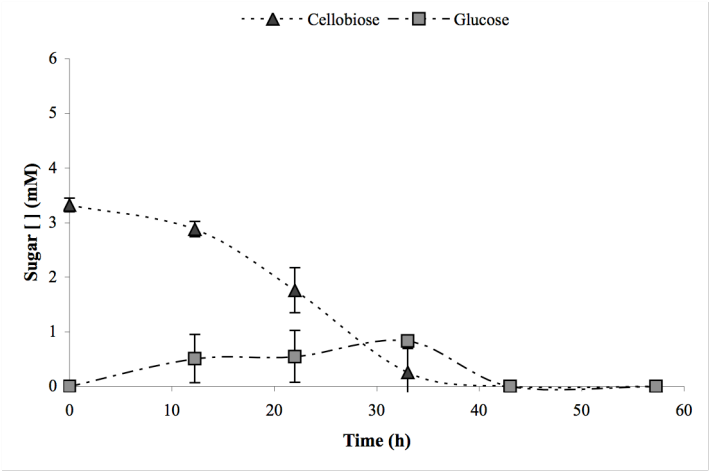

Figure 3.2 Linear plot of cellobiose consumption and residual glucose in modified 1191 medium a) mono-culture of *C. termitidis* grown on 6 mM cellobiose; and b) co-culture of *C. termitidis* and *G. sulfurreducens* grown on 3 mM cellobiose. Despite the difference in starting cellobiose concentrations, both experiments were conducted under carbon excess conditions. Measurable threshold concentration for both glucose and cellobiose was 5 μM. Data points represent the average of three independent replicates and errors bars represent the SD.

a)

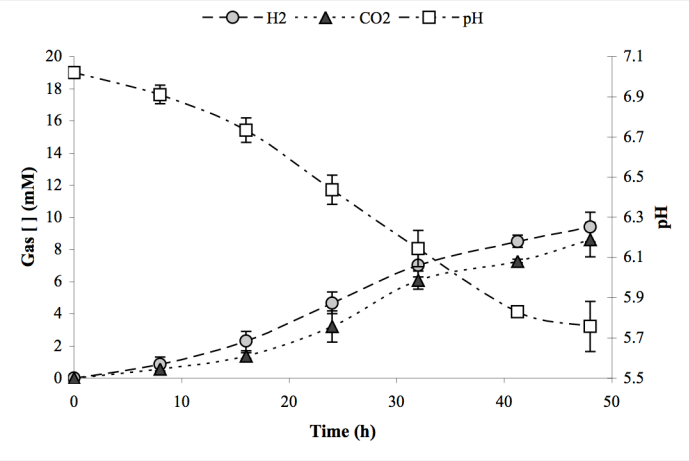

b)

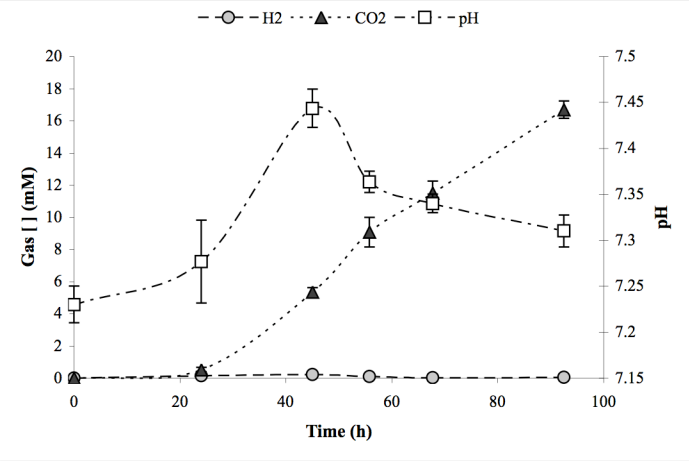

c)

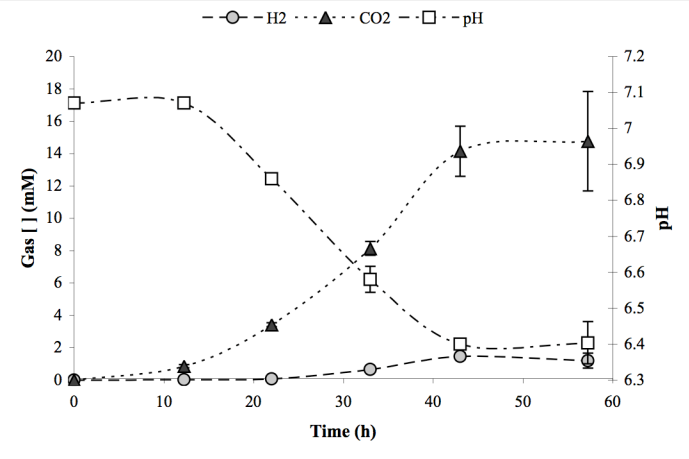

Figure 3.3 Gas production and corresponding changes in pH in modified 1191 medium a) mono-culture of *C. termitidis* grown on 2 g L^{-1} cellobiose; b) mono-culture of *G. sulfurreducens* grown on synthetic blend of fermentation end-products; and c) co-culture of *C. termitidis* and *G. sulfurreducens* grown on 2 g L^{-1} cellobiose. Gas values represent total production, blanked against starting-point concentrations. Data points represent the average of three independent replicates and errors bars represent the SD.

Formate, acetate, lactate, pyruvate, and ethanol were the major soluble fermentation end-products (Fig. 3.4a). Formate and acetate were produced at significantly higher concentrations than ethanol, lactate, and pyruvate. All end-product profiles followed cell growth and concomitant cellobiose utilization with the exception of pyruvate. Pyruvate concentrations were detectable after 16 h of growth only after the pH fell below 6.7. Table 3.1 presents maximum production yields for all end-products synthesized, as well as carbon and electron recoveries at end-point concentrations. A carbon balance of 92.3 % was achieved based on the total amount of carbon produced (biomass via protein analysis, end-products) versus the total amount of carbon consumed (cellobiose, glucose). The electrons recovered in end-products and biomass formation compared well with the amount of electrons available from the oxidation of cellobiose.

3.4.2 Mono-culture of *G. sulfurreducens* grown on a synthetic blend of fermentation end-products in modified 1191 medium

A mono-culture of *G. sulfurreducens* grew using a synthetic blend of fermentation end-products as substrate and fumarate as a terminal electron acceptor (Fig. 3.1b). An average doubling time of 8.7 h was observed, based on the average OD_{600} of triplicate measurements taken at individual time points between 24 and 56 h. Initial substrate concentration was influenced by soluble end-point concentrations synthesized by *C. termitidis* grown on 2 g L^{-1} cellobiose in modified 1191 medium. As much as 10.8 mM of malate accumulated within the medium (Fig. 3.5a). The ratio of fumarate consumed to malate and succinate produced was close to 1 (0.95), indicating fumarate did not contribute to cell growth, serving only as a terminal electron acceptor.

Table 3.1 Total substrate consumption, end-product synthesis, carbon balances, and electron recoveries All values are assumed to be total production, unless noted, and are displayed in mM concentrations.

	$Glucose_{EQ}$ consump. (%)	Protein	CO_2	H_2	Acetate	Formate	Lactate	Pyruvate	Ethanol	Net fumarate consump.	Net succinate prod.	Net malate secreted	Carbon balance (%)[a]	Electron recovery (%)[b]
C. termitidis	92.4	1.9	8.6	9.4	6.9	8.3	2.9	1.6	3.5	-	-	-	92.3	91.5
G. sulfurreducens	-	1.0	16.7	nd	7.2†	7.7†	nd	nd	nd	33.6	24.5	10.8	94.8	89.1
dissimilated[c]					6.1†	3.1†								
Co-culture	100	1.6	14.8	1.5	5.3	nd	nd	0.4	3.0	29.2	20.2	8.7	97.5	113.8

[a] total carbon produced over total carbon consumed
[b] electrons found in reduced end-products compared with the amount of electrons produced from substrate oxidation (in the absence of O_2)
[c] difference between substrate consumed and substrate assimilated into biomass. Calculated from:

$$17C_2H_3O_2^- + 11H_2O \rightarrow 8C_4H_7O_3 + 2HCO_3^- + 15OH^-$$

$$17CHO_2^- + 7H_2O \rightarrow 2C_4H_7O_3 + 9HCO_3^- + 8OH^-$$

† values indicate consumption not production
nd, not detectable

a)

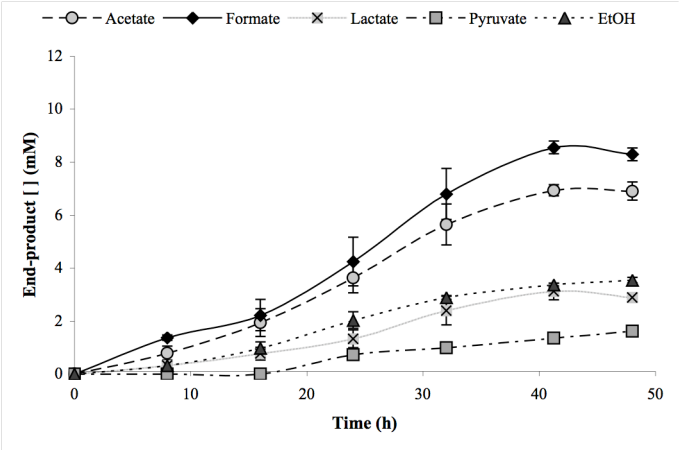

b)

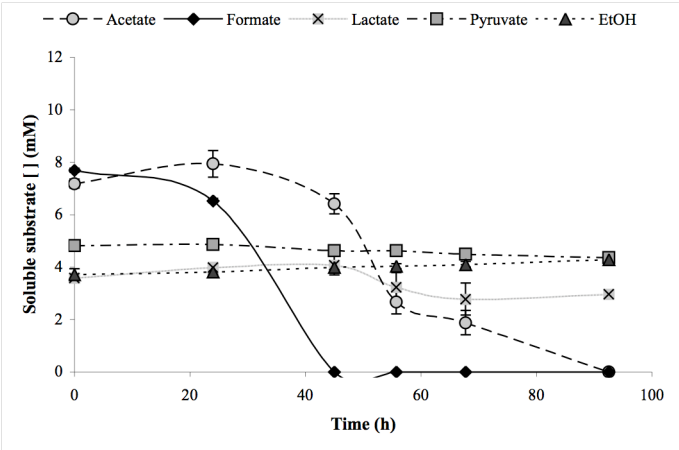

c)

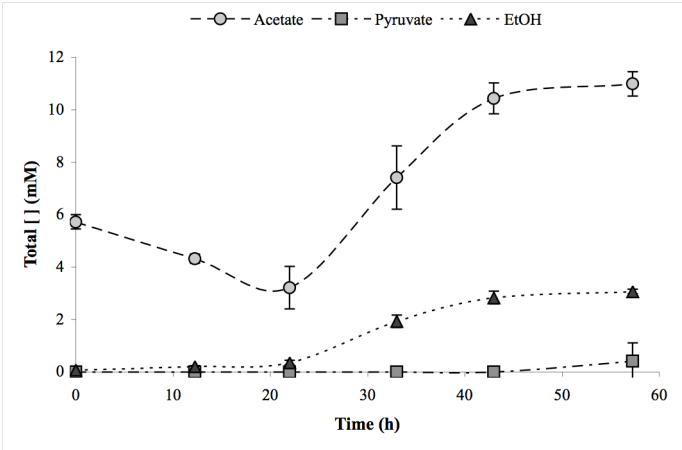

Figure 3.4 Organic acid and ethanol profiles in modified 1191 medium a) Fermentation end-product synthesis patterns by *C. termitidis* grown on 2 g L^{-1} cellobiose; b) soluble substrate consumption by *G. sulfurreducens* – starting values influenced by *C. termitidis* end-point concentrations; and c) organic acid consumption and end-product synthesis by co-culturing *C. termitidis* and *G. sulfurreducens* grown on 2 g L^{-1} cellobiose. Measurable threshold concentration for organic acids was 10 μM. All production values were normalized against an environmental control containing only modified 1191 medium and blanked against starting-point concentrations. Data points represent the average of three independent replicates and errors bars represent the SD.

a)

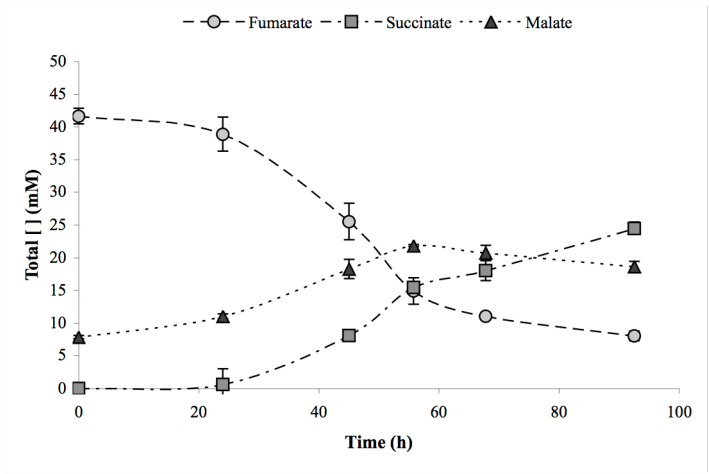

b)

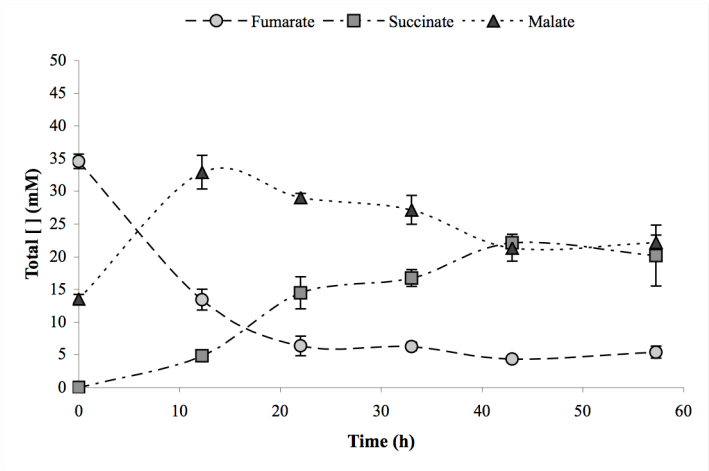

Figure 3.5 Fumarate reduction and subsequent malate and succinate production in modified 1191 medium a) mono-culture of *G. sulfurreducens* grown on synthetic blend of fermentation end-products; and b) co-culture of *C. termitidis* and *G. sulfurreducens* grown on 2 g L^{-1} cellobiose. Measurable threshold concentration was 0.5 mM. Succinate values represent total production and were blanked against starting-point concentrations. Data points represent the average of three independent replicates and errors bars represent the SD.

Organic acid consumption was plotted with respect to time (Fig. 3.4a). Substrate preference was observed with the consumption of formate occurring within the first 45 h followed by the complete oxidation of acetate. Between 45 and 68 h, the average concentration of lactate displayed a decreasing trend. However, this difference was determined statistically insignificant when compared with initial amounts of lactate present at the start of the experiment. No observable changes in pyruvate and ethanol concentrations were detected. The impact of rapid formate removal increased the pH of the medium to 7.4 (Fig. 3.3b), before falling to a final value of 7.3 following high succinate production (24.5 mM).

A carbon recovery of approximately 94.8 % was achieved, directing carbon flow from the consumption of formate and acetate entirely into CO_2 and biomass synthesis. As much as 16.7 mM CO_2 was generated while no H_2 was detected (Fig. 3.3b). The amount of electrons recovered via fumarate reduction was 89.1 % when acetate and formate dissimilation was considered. Approximately 60 % of metabolized formate and 15 % of metabolized acetate was assimilated into biomass.

3.4.3 Co-culture of *C. termitidis* and *G. sulfurreducens* grown on cellobiose in modified 1191 medium

Pure isolates of *C. termitidis* and *G. sulfurreducens* were co-cultured in modified 1191 medium and cellobiose. A maximum OD_{600} of 1.6 was reached after 43 h of growth (Fig. 3.1c), nearly twice the turbidity of individual mono-cultures. Overall CO_2 generation by both organisms totaled 14.8 mM while culture pH dropped only to 6.4 (Fig. 3.3c) with the concomitant production of organic acids and HCO_3^-. At end-point

concentrations, 97.5 % and 113.8 % of carbon and electron consumption were recovered, respectively (Table 3.1).

The growth of *C. termitidis* alone was measured indirectly by cellobiose consumption and end-product synthesis. Major end-products included acetate, ethanol, and trace amounts of pyruvate. By 43 h, cellobiose and glucose was completely consumed (Fig. 3.2b). A starting concentration of 3 mM cellobiose (versus 6 mM in experiment i)) was used to minimize significant drops in pH due to the high accumulation of fermentation end-products within the medium. Both experiments were performed under substrate excess conditions. Small concentrations of H_2 were produced, and were detected only after 22 h (Fig. 3.3c). Growth by *G. sulfurreducens* was measured indirectly by the oxidation of fumarate (Fig. 3.5b), which plateaued after 33 h. A total of 29.2 mM of fumarate was metabolized at end-point concentrations, forming 8.7 mM malate and reducing 20.2 mM succinate (Table 3.1). The ratio of fumarate oxidation to succinate and malate production was 1:1. After 22 h, succinate production was not related to growth but rather to malate consumption due the reversibility of the malate dehydrogenase, converting residual malate into fumarate which was then reduced to succinate [136].

Primer specificity, designed to target unique *cpn*60 regions, was confirmed using gel electrophoresis (Fig. 3.6a). Real-time PCR analysis was used to quantify relative ratios of *G. sulfurreducens* copy numbers to *C. termitidis* copy numbers in the co-cultures (Fig. 3.6b). Samples were taken at every time point up to 43 h, and trends in individual growth were determined. To help visualize the changes in population dynamics, the contribution of protein produced by each bacterium was estimated with respect to total measured

a)

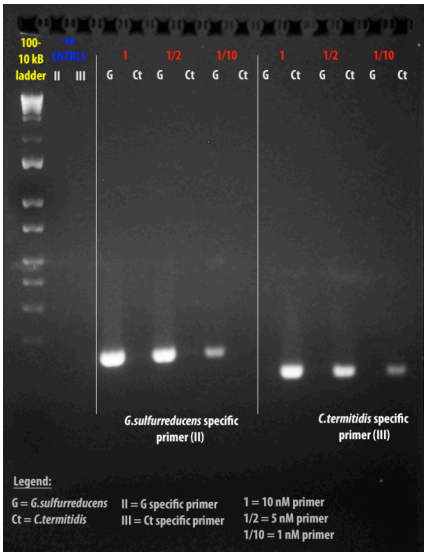

b)

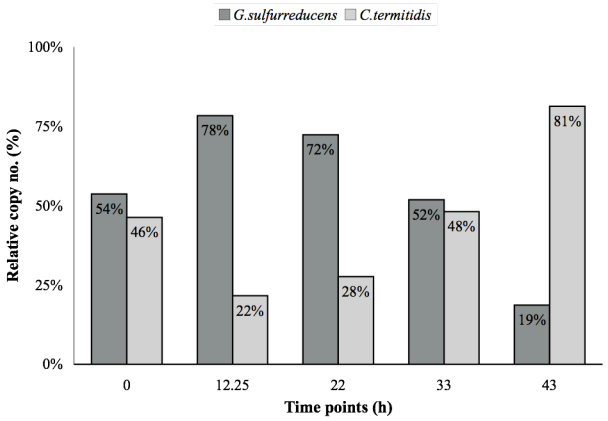

c)

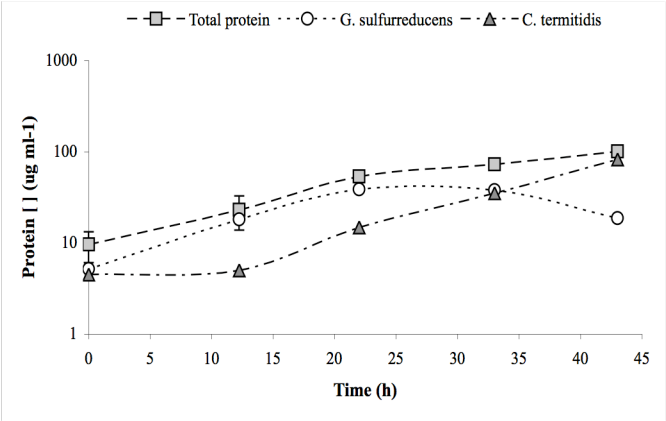

Figure 3.6 qPCR analysis of population dynamics in co-culture experiment iii) a) Confirmation of *G. sulfurreducens* and *C. termitidis* specific primers at concentrations of 10, 5, and 1 pmol μl^{-1}; b) fraction of *C. termitidis* (light bar) and *G. sulfurreducens* (dark bar) copy numbers relative to total combined copy number; and c) semi-logarithmic plot of total protein production versus estimated protein contribution from each organism, assuming equivalent genomic protein content. Total protein data points represent the average of three independent replicates and errors bars represent the SD.

protein (Fig. 3.6c), assuming one genome of biomass of *C. termitidis* is equivalent to one genome of biomass of *G. sulfurreducens*. At 0 h, the culture existed in a 1.2:1 ratio, *G. sulfurreducens* to *C. termitidis* (G:T), consistent with starting inoculation volumes. No initial lag was observed by *G. sulfurreducens*. Cells immediately entered and remained in the exponential phase of growth for the first 22 h, with an average doubling time of 7.6 h, before reaching stationary and subsequent death phase. These findings agree with end-product measurements. Minor cellobiose consumption and limited growth was observed by *C. termitidis* within the first 12 h of the experiment. Between 12 and 33 h, the fraction of *C. termitidis* increased dramatically, from 3.6:1 to 0.2:1 G:T. A doubling time of 8.5 h was observed for *C. termitidis* between 22 to 43 h, entering stationary phase once the carbon source was completely exhausted.

The data suggests both bacteria co-existed at 12, 22, and 33 h, but it is unclear whether growth was independent or syntrophic. A high concentration of acetate (5.7 mM) was present in the medium at 0 h, resulting from parental inoculum carry-over primarily due to *G. sulfurreducens* grown on 50 mM acetate.

3.5 Discussion

3.5.1 Mono-culture growth by *C. termitidis*

The catabolic oxidation of carbohydrates by many fermentative anaerobic bacteria generates a variety of end-products through branched metabolic pathways. Depending on the specific growth environment or the rate of growth by the organism, the metabolic flux will adjust for optimal biomass gain and thermodynamic efficiency [137, 138]. *Clostridium cellulolyticum* is a mesophilic, cellulolytic anaerobe that has been studied extensively. It is known to carry out mixed-product fermentation comparable to *C.*

termitidis [123], whose major end-products from cellulose degradation include CO_2, H_2, acetate, ethanol, lactate, and formate [139]. Verification of gene transcription and subsequent protein activity of critical metabolic enzymes have identified key pathways involved in cellobiose catabolism [22, 140 - 143]. Two branching points in pyruvate catabolism have been determined: i) pyruvate → acetyl-CoA + CO_2 + 2 reduced ferredoxin ($Fd_{(red)}$), or ii) pyruvate → acetyl-CoA + formate. The production of CO_2 and consequent H_2, generated from pools of $Fd_{(red)}$, is regulated by a pyruvate:ferredoxin oxidoreductase (PFO), whereas formate synthesis is mediated by a pyruvate formate-lyase (PFL). It is not uncommon for members belonging to the genus *Clostridium* to simultaneously express genes encoding for PFO and PFL [137, 144]. It is proposed that the central metabolism of *C. termitidis* is closely related to the existing metabolic framework of *C. cellulolyticum,* which will be used to formulate several hypotheses regarding carbon flow and electron flux. The current genome for *C. termitidis* is in draft form and the presence of genes[11] related to pyruvate catabolism and H_2 synthesis are being screened: *pfo* (Cterm_24_0197, 0196, 0098, 0200 for alpha, beta, delta, and gamma subunits respectively), *pfl* (Cterm_77_0373), lactate dehydrogenase (*ldh*) (Cterm_38_0224), and acetaldehyde / alcohol dehydrogenase (*adhE*) (Cterm_108_0137).

Pyruvate catabolism and H_2 synthesis pathways in *C. termitidis*: The 1191 growth medium was modified to support the presence of *G. sulfurreducens*. The increased concentrations of trace vitamins and minerals (in particular Fe^{2+} and Ni^{2+}), and major elements (Mg^{2+}), had considerable effects on mono-culture growth by *C. termitidis* [145]. Despite higher yields in biomass, the specific growth rate by *C. termitidis* was lower in

[11] multiple copies may exist

modified 1191 medium, 0.063 h^{-1}, compared to 1191 medium, 0.099 h^{-1} [123]. The ethanol pathway is responsible for the re-oxidation of reduced coenzyme NADH. It may also be possible to shift electron flow towards an NADH:ferredoxin oxidoreductase and hydrogenase to regenerate its reducing power. However, lower specific rates of ethanol production, relatively equal rates of lactate production, and equimolar concentrations of CO_2 and H_2 production were observed (Table 3.2). It is speculated that slower growth in modified 1191 medium was due to NADH accumulation within the cell, leading to glyceraldehyde-3-phosphate dehydrogenase inhibition during glycolysis [146]. This inhibitory effect was observed in a chemostat culture of *C. cellulolyticum* containing cellobiose [140]. A very high $NADH/NAD^+$ ratio indicated poor control of carbon and electron flow, resulting in limited growth.

The presence of the metabolic intermediate pyruvate suggests PFO and PFL may be metabolic bottlenecks that cannot support high carbon flow from glycolysis [22]. Extracellular pyruvate production is very wasteful, resulting in no cellular ATP gain or reducing equivalent regeneration. Regulatory mechanisms in *C. cellulolyticum* have evolved to control carbon flow entering the cell during cellulose hydrolysis. When cultured on excess cellobiose, rates of carbon consumption are much higher and unregulated. High carbon flux corresponds to lactate production, shifting conventional acetate/ethanol fermentation towards lactate/ethanol fermentation [141]. Lactate was synthesized by *C. termitidis* but greater ethanol production should have been observed. It is possible the concentration of ethanol in solution was underestimated due to its high volatility at room temperature.

Table 3.2 Maximum yields and specific rates by *C. termitidis* grown on 2 g L^{-1} cellobiose in different growth media Yields represent maximum production/consumption. Rates based on the sum of the average individual rates obtained from three consecutive time points obtained during the mid and late exponential phase of growth.

	Consumption			Production				
Media	$Glucose_{EQ}$	H_2	CO_2	Acetate	Lactate	Formate	Pyruvate	Ethanol
Maximum yield				(*mM*)				
1191	8.0	4.6	5.6	5.9	2.0	4.2	nd	3.7
Modified 1191	10.7	9.4	8.6	6.9	2.9	8.3	1.6	3.5
Specific rate				(*mmol g-dry cell*$^{-1}$ *h*$^{-1}$)				
1191[a]	5.1	4.3	5.3	2.7	1.2	1.5	nd	3.0
Modified 1191[b]	4.3	2.6	2.6	2.0	0.9	2.5	0.5	1.0

a. rates calculated from Ramachandran *et.* al. [123], based on yields measured during maximum protein production during log growth (13, 15, 20 h)
b. rates calculated from current experimental data, based on yields measured during maximum protein production during log growth (16, 24, 32 h)
nd, not detectable

Thermodynamically, the anaerobic oxidation of glucose to acetate is the highest H_2 yielding pathway in fermentation, producing a maximum of 4 mol-H_2 mol^{-1}-glucose. In modified 1191 medium, the majority of carbon flow was directed towards acetate, producing 9.4 mM-H_2 (compared to only 4.6 mM-H_2 on 1191 medium). However, when normalizing against substrate consumption, only 0.9 mol-H_2 mol^{-1}-glucose$_{EQ}$ was produced, falling significantly short of experimental and theoretical maximums (as high as 3.2 mol-H_2 mol^{-1}-glucose via dark fermentation [147 - 149]). Greater H_2 formation was directly related to a higher cell density. When accounting for biomass, specific H_2 production rates decreased by 40 % compared to 1191 medium (Table 3.2). Consequently, electrons (and carbon) shifted away from PFO, towards PFL, which saw specific rates of formate production increase by 40 %. According to the metabolic framework of *C. cellulolyticum*, the amount of formate and CO_2 produced should be roughly 1:1 with acetate and ethanol synthesis. *C. termitidis* had an unbalanced ratio of 1.6:1 due to high rates of formate production and low concentrations of ethanol. It is speculated that: i) ethanol concentrations were underestimated. Higher ethanol production would not only improve carbon and electron balances but would also help support extracellular pyruvate production and the shift from ethanol/acetate to ethanol/lactate fermentation; or ii) formate inhibits ethanol production. There is precedence in *Escherichia coli* that the expression of *adhE* reduces PFL activity [150]. The reverse effect may be possible, but further testing is required.

3.5.2 Mono-culture growth of *G. sulfurreducens*

Geobacter sulfurreducens preferred formate consumption above all other fermentation products. According to Fig. 3.4b, *G. sulfurreducens* consumed formate,

followed by acetate, at maximum specific volumetric rates of 7.9 and 7.2 mmol g-dry cell^{-1} h^{-1}, respectively. This finding suggests the complete utilization of both organic acids is possible if grown in the presence of one another. When compared against OD_{600} and protein data (Fig. 3.1b), it appears acetate consumption occurred during the late-log and stationary phases of growth (45 to 93 h). Although acetate was completely utilized, it appears consumption was not growth related. Lactate remained untouched throughout the entire duration of the experiment even though it is a known carbon source for *G. sulfurreducens*.

3.5.3 Co-culture growth by *C. termitidis* and *G. sulfurreducens*

Given the current experimental design, it is difficult to determine the exact nature of the relationship between *C. termitidis* and *G. sulfurreducens*. High initial acetate concentrations present in the medium suggest growth by each organism was independent from one another. Without measuring metabolite flux between *C. termitidis* and *G. sulfurreducens* it is difficult to describe the mechanisms for electron transfer and growth. A synthrophic association is clearly possible given *G. sulfurreducens* is dependent on the fermentation end-products synthesized by *C. termitidis*. However, it appears *C. termitidis* does not require *G. sulfurreducens* for its own survival. An obligate synthrophic relationship requires at least one oxidation step in the conversion of cellobiose to end-products to be energetically taxing, requiring *G. sulfurreducens* to "pull" this reaction forward [151]. Under the tested experimental conditions, a facultative syntrophic association was observed based on: i) increased rate of fumarate reduction, and ii) the lack of formate and H_2.

Increased rate of fumarate reduction: According to Fig. 3.3b, the duration of mono-culture growth by *G. sulfurreducens* was approximately 70 h, based on CO_2 production and an initial lag of 20 h. Net fumarate reduction was 33 mM (Table 3.1). However, the production of CO_2 in the co-culture experiment ceased after only 40 h of growth (Fig. 3.3c) despite 29 mM of fumarate consumed. Maximum volumetric rates of consumption confirm fumarate was reduced more rapidly in mixed (1.7 mM h^{-1}) versus pure cultures (1.0 mM h^{-1}).

No detectable formate and very low H_2 production: The oxidation of substrates by *C. termitidis* requires several electron mediators, including NAD^+ (glyceraldehyde-3-phosphate hydrogenase) and ferredoxin (PFO). The redox couples for $Fd_{(ox)}/Fd_{(red)}$ and NAD^+/NADH are -398 and -320 mV respectively, whereas the redox couple for H^+/H_2 is -414 mV [138, 152]. The redox reactions can be described in terms of changes in Gibbs free energy according to $\Delta G^{\circ\prime} = -nF\Delta E^{o\prime}$, where n is the number of electrons transferred, F is Farraday's constant, and $\Delta E^{o\prime}$ is the potential difference between redox couples:

$$2\ Fd_{(red)} + 2\ H^+ \rightarrow 2\ Fd_{(ox)} + H_2 \qquad (\Delta G^{\circ\prime} + 3.1\ kJ\ mol^{-1})$$

$$NADH + H^+ \rightarrow NAD^+ + H_2 \qquad (\Delta G^{\circ\prime} + 18.1\ kJ\ mol^{-1})$$

The oxidation of $Fd_{(red)}$ is readily coupled to H_2 formation. Unfortunately, the highly positive $\Delta G^{\circ\prime}$ values make the production of H_2 from NADH a thermodynamically unfavorable reaction. Considering free energy values were calculated under standard temperature and pressure (STP) conditions (298 ^oK, pH 7, 1M for solutes, 1 atm for gases), the production of H_2 becomes much more thermodynamically favorable when concentrations and partial pressures are kept very low (ΔG values can be adjusted

according to Eq. 2.8). At a H_2 partial pressure of 10^{-4} atm, the oxidization of NADH to H_2 is thermodynamically possible [151].

When co-culturing *C. termitidis* with *G. sulfurreducens*, two significant metabolic changes were observed: i) no formate was detected despite high concentrations produced during mono-culture growth (Fig. 3.4a); and ii) very low concentrations of H_2 were measured but only after 22 h (Fig. 3.3c), once *G. sulfurreducens* entered the stationary phase of growth (Fig. 3.5b and 3.6c). The latter can be explained by the ability of *G. sulfurreducens* to consume H_2. It has been shown in H_2-dependent growth experiments that *G. sulfurreducens* uses respiratory hydrogenases (*e.g.* Hyb) to oxidize H_2 and reduce fumarate [153]. According to Fig. 3.5b, H_2 production was detectable only after fumarate was no longer reduced. It is also possible that when *C. termitidis* and *G. sulfurreducens* were cultured together, H_2 was being generated at even higher rates than mono-culture studies. High H_2 partial pressure during mono-culture growth by *C. termitidis* makes H_2 production from NADH very unlikely. However, the efficient removal of H_2 by *G. sulfurreducens* may transfer reducing equivalents from NADH to H_2 via ferredoxin [138, 151], providing *C. termitidis* is capable of expressing a NADH:ferredoxin oxidoreductase. Coupling pyruvate to lactate or acetyl-CoA to ethanol can regenerate reducing equivalents in *C. termitidis*. However, co-culture experiments resulted in a reduction in ethanol production and no lactate formation. Calculated carbon balances and electron recoveries (Table 3.1) indicate mass and charge were properly accounted for, yet the decrease in ethanol and lack of lactate indicates a gap in reducing equivalents. Efficient H_2 uptake resulting in low H_2 partial pressures may have thermodynamically driven NADH re-oxidation with concomitant H_2 production.

Similar behavior has been described in chemostat co-cultures of *Ruminococcus albus* and *Wolinella* (*Vibrio) succinogenes* [154]. The fermentation of glucose by mono-cultures of *R. albus* produces ethanol, acetate, CO_2, and H_2. Glycolysis is used in the oxidation of glucose to pyruvate, forming NADH, while the fermentation of pyruvate to acetyl-CoA generates pools of $Fd_{(red)}$. When co-cultured with the H_2-consuming *W. succinogenes*, no ethanol was detected. It was determined H_2 was produced in greater amounts via the oxidation of NADH produced during glycolysis. Ethanol production was no longer required to regenerate reducing equivalents, thus a metabolic shift towards acetate formation resulted in higher ATP gain for *R. albus* [138, 151].

Two possible scenarios can explain the absence of formate. First, formate served as an intermediate and was consumed as fast as it was produced. This is a likely situation given the high desire to produce formate (1.5 mmol g-dry $cell^{-1}$ h^{-1}) by *C. termitidis* and the preferential consumption of formate (7.9 mmol g-dry $cell^{-1}$ h^{-1}) by *G. sulfurreducens*. On the other hand, it is quite possible that *C. termitidis* did not produce any formate at all. The high concentration of acetate initially present in the medium provided *G. sulfurreducens* with enough energy for growth. Increased biomass could lead to high rates of H_2 consumption. Consequently, uptake of H_2 by *G. sulfurreducens* may have enabled the continued flux through PFO, thus negating the use of formate production through PFL.

Chapter 4: Substrate preference by *Geobacter sulfurreducens* and co-culture sustainability with *Clostridium termitidis* in a microbial electrolysis cell

4.1 Summary

Single-chambered MECs were successfully designed to study mono- and co-culture growth of *G. sulfurreducens* and *C. termitidis*. Despite near complete substrate degradation, H_2 production was low compared to other studies. Possible explanations include H_2 recycling, gas leaks at the sampling port, poor H_2 catalysis at the cathode. Mono-culture experiments conducted on a synthetic blend of fermentation end-products revealed preferential substrate degradation by *G. sulfurreducens*: formate and pyruvate were rapidly consumed, followed by acetate then lactate degradation. Although a sustainable co-culture could not be maintained, strategies to overcome the problems encountered are presented in this chapter: i) carbon flux through *C. termitidis* must be minimized by culturing the organism on a complex substrate, ii) neutral pH conditions must be maintained, particularly by avoiding lactate accumulation, and iii) following the successful culturing of methanogenic environments in anaerobic digestion, introduction of acetogenic bacteria may promote syntrophic cooperation and maintain a balance within the microbial MEC community. It has been proposed that online measurements of formate and lactate concentrations could provide researchers with a tool for indirectly monitoring co-culture dynamics in a MEC.

4.2 Introduction

Organic material must be removed from domestic, industrial, and agricultural wastewaters before release into the environment. At the commercial level, aerobic

technologies can effectively treat these pollutants, but unfortunately carry large energy and aeration requirements [155, 156]. It is possible to produce fuels, chemicals, and electricity while simultaneously consuming organics from wastewaters [157]. In particular, anaerobic digestion offers fundamental benefits over conventional aerobic processes because energy can be recovered in the form of biogas [155]. Alternatively, microbial electrohydrogenesis is an emerging bio-electrochemical process capable of near complete oxidation of organic material, while maximizing H_2 production [26, 34]. Electrogenic bacteria catalyze the oxidation of organic substrates in a MEC, transferring electrons to an anode while generating CO_2 and protons. Hydrogen is produced at the cathode by the chemical reduction of H^+ in the presence of a catalyst (typically platinum, Pt).

Microbial electrohydrogenesis is a promising technology that is still in its infancy. Large-scale applications face significant obstacles, including: i) microbiological challenges, such as biofilm pH gradients [158], methanogenesis [109, 111 - 114], and complex substrates [31]; ii) technological challenges, such as ohmic losses [29, 88] and membrane pH gradients [4]; and iii) economical challenges, such as the use of Pt catalyst at the cathode [28, 31, 32, 94, 95] and membrane cost [4]. It can be argued that improvements made to the design of MECs will naturally select for organisms with a greater capacity for substrate degradation, electron flux to the anode, and H_2 production. Most laboratory-scale experiments practice this approach, using mixed cultures enriched from wastewater treatment, activated sludge, or microbial fuel cell (MFC) communities. However, there is considerable value in pure culture studies [159]. Advancements made in understanding microbial interactions with electrodes and associations with other

organisms could significantly influence MEC reactor design, increasing efficiency while reducing cost [160]. In fermentation wastewater recovery (breweries, wineries, etc.), the relationship between fermentative organisms and electricigens is of great importance that warrants further investigation.

Three single-chambered MEC experiments, operated in fed batch mode, were conducted using the cellulolytic, fermentative *Clostridium termitidis* and electrogenic *Geobacter sulfurreducens*: i) a mono-culture of *G. sulfurreducens* was grown on acetate as the sole carbon source to develop a working biofilm along the anode and to evaluate reactor performance; ii) a mono-culture of *G. sulfurreducens* was grown on a synthetic blend of fermentation end-products that mimicked the fermentation end-products generated by *C. termitidis* cultured on cellobiose; and iii) a co-culture of *G. sulfurreducens* and *C. termitidis* was grown together using cellobiose as the sole carbon source. These experiments are a continuation of Chapter 3, where a co-culture of *C. termitidis* and *G. sulfurreducens* was characterized in balch tubes. The purpose of this study is to develop a better understanding of how *G. sulfurreducens* behaves as a mono-culture in a MEC and provide insight into how successful co-cultures with fermentative, cellulolytic bacteria can be achieved.

4.3 Materials and Methods

4.3.1 Microbial source and media (same as section 3.3.1)

4.3.2 Microbial electrolysis cell design and start-up

Three single-chambered MECs were constructed from cast acrylic (tube – ¼" wall; sheet – ½" wall) with a total chamber volume of 180 mL (11 in^3 – 2" diameter x 3 ½" length). Carbon cloth (no wet proofing) was used at the anode and carbon cloth

loaded with 10 % Pt was used at the cathode (Clean Fuel Cell Energy, LLC, Florida, USA). The Pt catalyst layer was prepared (see Appendix A.3) by applying a mixture of the following materials (per 6.5 cm diameter electrode): 10 % (wt) Pt on carbon black (Vulcan CX-72), 166 mg; distilled and deionized H_2O, 138 μL; Nafion binding solution, 1107 μL; and iso-propanol, 641 μL. The catalyst layer was air-dried for 24 h. Each MEC was equipped with one Ag/AgCl reference electrode (BASi Corporate) and one sampling port constructed from Swagelok compression fittings (3/8" tube x ¼" male NPT), nylon ferrules (3/8"), and rubber red replacement septa (7 x 13 mm, New Brunswick Scientific).

Each reactor was loosely assembled then autoclaved, allowing enough space for the acrylic body to expand under the heat. The sterile MECs were tightened and air-sealed within a laminar flow hood (1300 Series A2, Thermo Scientific). To maintain an anaerobic environment, each empty chamber was gassed and degassed (0.5:1 min) for four cycles with 100 % sterile nitrogen (N_2) then leak tested at approximately 103 kPa (15 psi). Sterile, anaerobic, and reduced modified 1191 media was transferred aseptically and each MEC was incubated overnight at 35^{o}C to test for contamination and/or pressure loss.

4.3.3 Operating conditions

All three experiments were tested in three independent MECs operating in fed-batch mode at an applied voltage of 0.6 V (1786B, BK Precision). Each condition was repeated three times to achieve reproducible results. Every run was considered complete once H_2 production stabilized, followed by a chamber exchange in which all gas in the headspace was purged and chamber electrolyte was replaced with fresh modified 1191 medium and substrate. At the start of every batch, fresh medium (40 mL) was

consistently added while maintaining an initial working volume of 80 mL (based on total electrolyte removed).

For experiment i), 25 mM of acetate was added at the beginning of run 1 and 2, then reduced to 12.5 mM for run 3 to minimize the amount of carry-over into experiment ii). A 10 x stock of fermentation end-products was prepared and contained: formate (81 mM), acetate (79 mM), pyruvate (45 mM), lactate (34 mM), and ethanol (42 mM). The 10 x synthetic blend was filter-sterilized, made anaerobic, and 8 mL was added to each reactor for experiment ii). The MECs were incubated at 35^{o}C for experiment i) and ii) and a true phosphate buffer (33 mM) was used to maintain electrolyte pH close to 7.0. For experiment iii), conditions were modified to support co-culture growth. To minimize the effects of low culture pH caused by fermentation end-product accumulation, the buffering capacity of the media was tripled (100 mM) and the starting pH was increased from 7.0 to 7.4. The incubation temperature was lowered to 30^{o}C to reduce the growth rate of *C. termitidis* [145]. Finally, to decrease the total amount of synthesized fermentation end-products, carbon loading was reduced from 2 to 1 g L^{-1} cellobiose.

4.3.4 Analytical procedures

Substrate, gas, and end-product analysis (see section 3.3.3)

Current and pH measurements. The pH of each sample was measured using a Sension2 pH ISE meter (Hach) equipped with an Ag/AgCl pencil electrode (Accumet, Fisher Scientific) [123]. Electron flow was calculated by measuring the voltage drop across a 10 ohm external resistor. Values were logged every 10 min using a data acquisition system (LabJack U12, LabJack Corporation) connected to a PC.

Calculations. Each MEC condition was evaluated in terms of H_2 yields and recoveries, coulombic efficiency, energy contribution from the power source and substrate, and energy recovered as H_2. Many papers and textbooks review these calculations in detail [26, 32]. Sample calculations are included in Appendix B.

4.4 Results

4.4.1 Mono-culture of *G. sulfurreducens* grown on acetate in modified 1191 medium

Growth by *G. sulfurreducens* was indicated by near complete acetate degradation (Fig. 4.1a) and consistent current flux measured at the anode (Fig. 4.1b). An average of 17 mM of acetate was consistently degraded in all three runs, while the duration of run 1 and 2 was much shorter (280 h) when compared to run 3 (530 h). The longer batch was the result of purging the gas in the headspace and allowing operation to continue until H_2 production re-stabilized (see arrow (ii) in Fig. 4.1b). The purpose was to reduce acetate carry-over into experiment ii). The measured current density remained stable at 0.46 A m^{-2}, while the H_2 concentration reached a maximum average of approximately 4.0 ± 0.6 mM across all three reactors. The pH of the media remained at 7.0 (data not shown). Despite a low H_2 recovery of only 44 ± 16 %, 5.3 mol-H_2 mol^{-1}-$glucose_{EQ}$ was produced consistently across three independent reactors (Table 4.1), proof that the MECs constructed were functional.

a)

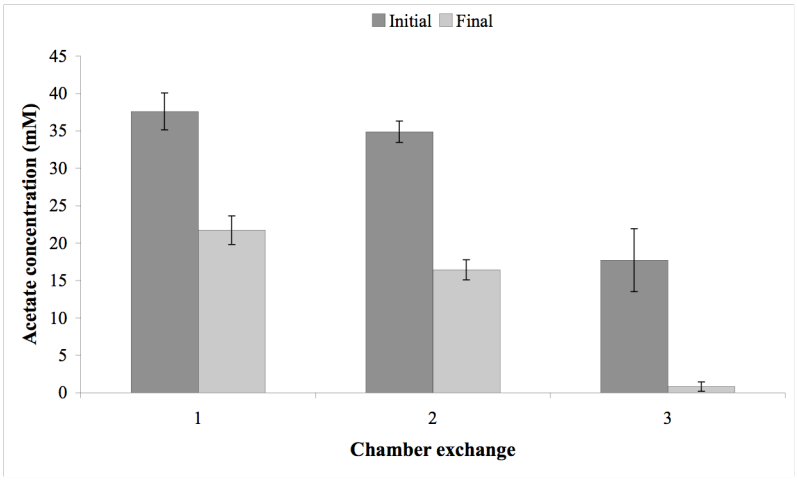

b)

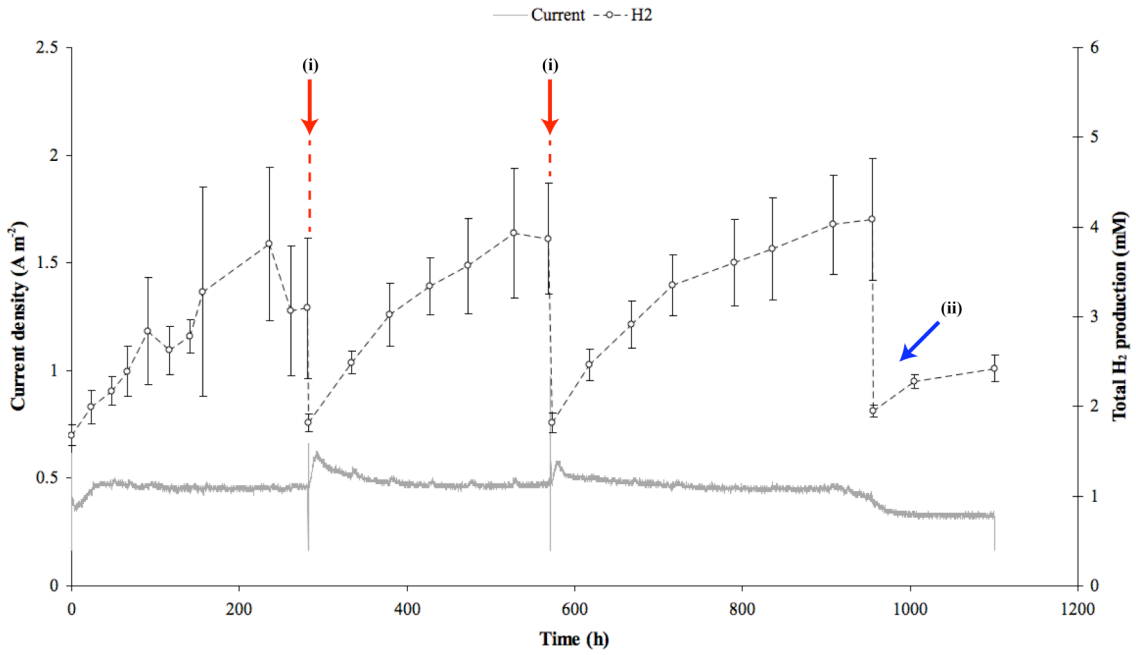

Figure 4.1 Proof of design – *G. sulfurreducens* grown on acetate in a MEC a) Acetate degradation by *G. sulfurreducens* measured before (dark bar) and after (light bar) each chamber exchange; and b) electron flow normalized against working anode surface area and total H_2 production. Arrows (i) indicate chamber exchanges (medium and gas) and substrate addition while arrow (ii) indicates headspace purge (gas only). Data points represent the average of three independent MECs operating in parallel subject to identical growing conditions. Error bars represent the standard deviation (SD).

Table 4.1 MEC performance evaluated in terms of H_2 yields, H_2 recoveries, energy input, and energy recovered Co-culture runs were not reproducible – values were calculated for every run and averaged across three independent reactors. Coulombic efficiency was calculated based on total substrate consumption and did not include biomass assimilation.

				Hydrogen recoveries				Energy recoveries			
		Total H_2 yield		Coulombic		Overall		Electricity input		Electricity + substrate	
Condition		Y_{H2} (mol-H_2 / mol-glucose$_{EQ}$)	(+/-)	C_E (%)	(+/-)	r_{H2} (%)	(+/-)	η_{in} (%)	(+/-)	η_{W+S} (%)	(+/-)
Proof of design[a]		5.3	1.9	101.4[b]	12.9	44.2	16.1	32.0	7.8	28.4	10.5
Synthetic blend[a]		3.5	0.6	92.3	13.3	28.8	5.3	25.8	2.8	20.5	4.1
Co-culture	1	9.7	0.1	65.7[c]	0.8	80.7	11.5	19.7	0.2	62.0	9.0
	2	3.6	0.6	45.4[c]	4.9	29.8	5.1	14.5	1.3	24.3	3.8
	3	2.9	0.6	38.5[c]	3.1	24.5	6.4	12.6	0.8	20.5	5.1

Y_{H2}, H_2 yield per mol glucose$_{EQ}$ consumed; C_E, coulombic efficiency; r_{H2}, total H_2 recovered per total glucose$_{EQ}$ consumed; η_{in}, electrical contribution versus total energy available from electrical and substrate input; η_{W+S}, energy recovered as H_2 versus energy available from electrical and substrate input

[a] values calculated from the average of all three runs carried out in three independent reactors

[b] third run from each reactor was omitted due to inaccurate acetate measurements

[c] total electrons available in substrate included the complete consumption of cellobiose minus the production of end-products by *C. termitidis*

4.4.2 Mono-culture of *G. sulfurreducens* grown on a synthetic blend of fermentation end-products in modified 1191 medium

Consistent growth and substrate utilization was observed in all three runs of each MEC (Fig. 4.2). The duration of runs 1, 2, and 3 gradually increased from 240, 340, to 380 h, respectively. The anodic current density was lower than cultures on acetate alone, eventually stabilizing around 0.37 A m^{-2}, while the total amount of H_2 produced was relatively consistent, plateauing at 3.9 ± 0.7 mM. Complete substrate degradation was observed, and *G. sulfurreducens* preferentially consumed formate and pyruvate before acetate and lactate. The observation that pyruvate was preferentially consumed in a MEC but remained untouched in balch tube (Chapter 3, Fig. 3.4b) may be explained based on differences in metabolic responses of *G. sulfurreducens* towards electron acceptor variations [161]. Culturing *G. sulfurreducens* on an insoluble electron acceptor, such as Fe(III), resulted in pyruvate as the main carbon source for gluconeogenesis. When grown on fumarate, acetate was the primary carbon source.

When the first point at the beginning of each batch was considered, ethanol appeared to be consumed. However, this starting value was an artifact of calculating, rather than measuring, the amount of substrate. Concentration gradients due to the absence of mixing were initially observed when fresh substrate was added to each reactor resulting in inconsistencies between samples. Calculations were based on the measured residual concentrations at the end of each batch (according to $C_1V_1 = C_2V_2$) and totaled with the concentration of fresh substrate added. This was necessary in order to display the consumption of formate and other rapidly degraded substrates. The amount of H_2 recovered was much lower than on acetate alone, at 29 ± 5 % (Table 4.1). Lower

a)

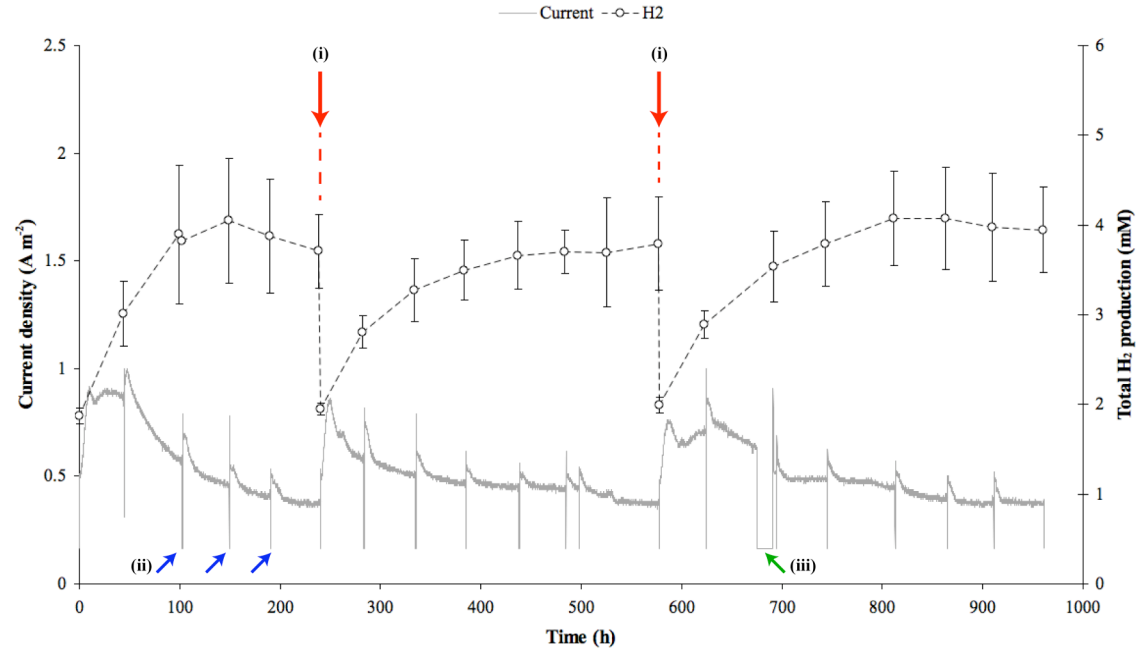

b)

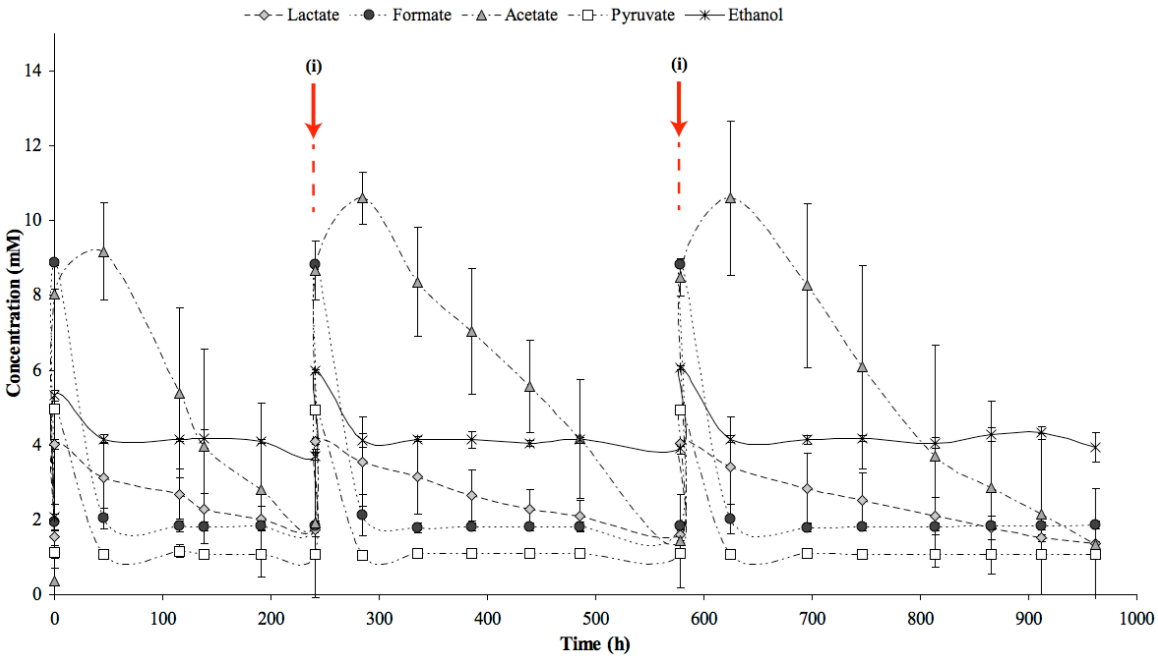

Figure 4.2 Current density, H_2 production, and substrate degradation patterns by *G. sulfurreducens* in MECs grown on a synthetic blend of fermentation end-products a) Electron flow normalized against working anode surface area and total H_2 production; and b) substrate degradation profiles. Substrate addition concentrations were influenced by *C. termitidis* grown on 2 g L^{-1} cellobiose in modified 1191 medium. Arrows (i) indicate chamber exchanges (medium and headspace) and substrate addition, arrows (ii) represent 1 mL samples of reactor medium (MECs were disconnected for aseptic sampling), and arrow (iii) represents a power outage. Initial data points after each chamber exchange were calculated according to $C_1V_1 = C_2V_2$ to determine residual diluted concentrations of remaining substrates. Each data point represents the average of three independent MECs operating in parallel subject to identical growing conditions. Error bars represent the SD.

coulombic efficiencies (92 ± 13 %), and energy recovered as H_2 (21 ± 4 %) were also observed.

4.4.3 Co-culture growth of *G. sulfurreducens* and *C. termitidis* on cellobiose in modified 1191medium

Co-culturing *C. termitidis* with *G. sulfurreducens* was not only difficult to achieve but was not sustainable under the operating conditions tested. The initial growth environment (35^{o}C, 33 mM phosphate buffer, 2 g L^{-1} cellobiose, initial media pH of 7.0) favored growth of *C. termitidis*. Rapid substrate consumption led to high organic acid production and significant drops in culture pH (as low as 5.5). These conditions led to cell death (saponification within media indicative of cell lyses), no current generation, and no chemical H_2 production at the MEC cathode. Parameters were adjusted (see section 4.3.3) to increase the buffering capacity of the media, reduce end-product production, and favor growth of *G. sulfurreducens*. As a result, it appeared growth by both organisms was achieved in run 1. Cellobiose was completely consumed after 25 h (data not shown) by *C. termitidis* and a maximum current density greater than 1 A m^{-2} was produced by *G. sulfurreducens* (Fig. 4.3a). Substrate preference was observed once again with rapid formate consumption within the first 50 h followed by acetate after 95 h (Fig. 4.3b). Lactate degradation was much slower than formate and acetate, consistent with data from experiment ii). Non-significant levels of pyruvate were detected. A very high H_2 recovery was obtained, generating 9.7 ± 0.1 mol-H_2 $mol^{-1}glucose_{EQ}$ from the combined fermentation of cellobiose and bio-electrochemical conversion of its end-products (Table 4.1).

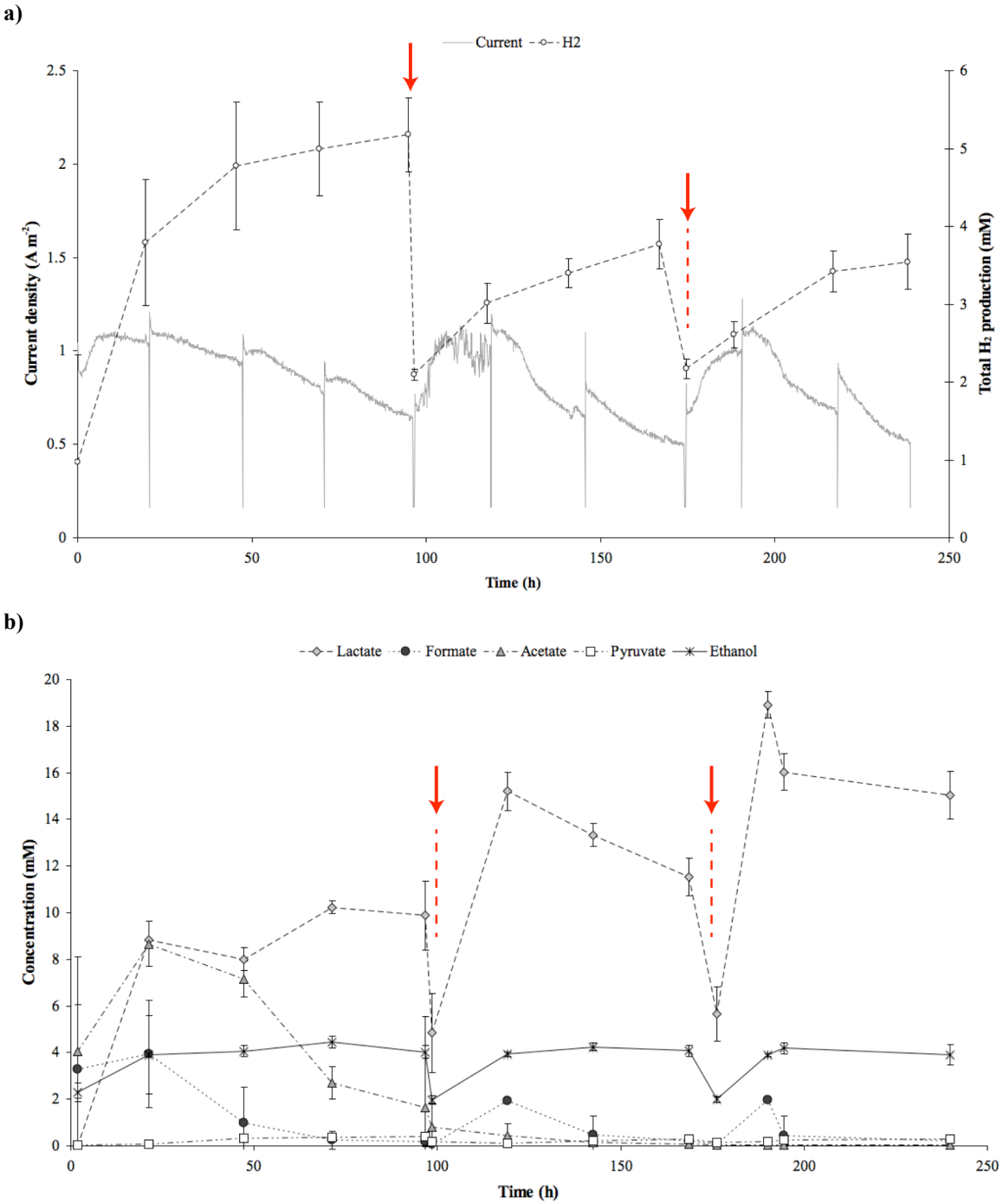

Figure 4.3 Co-culture of *C. termitidis* and *G. sulfurreducens* in a MEC grown on 1 g L^{-1} cellobiose a) Electron flow normalized against working anode surface area and total H_2 production; and b) fermentation end-product production by *C. termitidis* and concomitant substrate degradation by *G. sulfurreducens*. Arrows indicate chamber exchanges (medium and gas) and substrate addition. Data points represent the average of three independent MECs operating in parallel subject to identical growing conditions. Error bars represent the SD.

Unfortunately, these results could not be maintained. A continuous decrease in H_2 recoveries and yields was calculated for run 2 and 3, reaching as low as 25 ± 6 % and 2.9 ± 0.6 mol-H_2 $mol^{-1}glucose_{EQ}$ respectively (Table 4.1). The current density at the anode continued to drop below 0.5 A m^{-2}, suggesting unhealthy conditions impeding growth of *G. sulfurreducens*. It appeared growth by *C. termitidis* continued, characterized by complete cellobiose consumption within the first 25 h of both runs and consistent ethanol production (4 mM). However, the decrease in run length from 79 to 64 h, accumulation of lactate, and gradual decrease in culture pH (from 7.4 to 6.9) suggest *C. termitidis* was being forced into a stationary phase where growth could not be sustained. Contrary to previous experiments reporting substrate preference, formate was detected but acetate was not. It is possible that the presence of a formate dehydrogenase in *G. sulfurreducens* strain PCA (fdnG – selenocysteine-containing major subunit, fdnH – iron-sulfur subunit, GSU0780 – accessory protein fdhD) could produce formate from CO_2 and H_2. However, this statement is purely speculative requiring further investigation to determine the activity of this enzyme under current operating conditions.

4.5 Discussion

4.5.1 Evaluating MEC performance: low H_2 recoveries in pure cultures of *G. sulfurreducens*

Despite near complete acetate removal by run 3 in experiment i) (Fig. 4.1a), only 44 ± 16 % of the theoretical amount of H_2 was recovered (Table 4.1). A H_2 recovery below 100 % suggests H_2 is either being lost or consumed. Previous studies suggest H_2 recycling by *G. sulfurreducens* is possible [32]. It has been previously shown that *G. sulfurreducens* is capable of oxidizing H_2 via uptake hydrogenases [153]. Additionally, a

C_E greater than 100 % (Table 4.1) suggests electrons were being transferred to the anode by some unaccounted source. It is also possible that a small H_2 leak at the septum of the sampling port may have resulted in lower than expected recoveries. The maximum headspace pressure reached in both experiments i) and ii) was 117 kPa (17 psi). Only 4 mM of H_2 was produced, yet more could be generated if the headspace was purged, when the gauge pressure returned to 0 kPa (experiment i), run 3). In experiment iii), the septum of each MEC was re-sealed. As a result, 5.2 mM of H_2 was produced reaching a pressure as high as 165 kPa (24 psi). If H_2 was continuously removed from the headspace, not only would this prevent the accumulation of pressure leading to potential leaks in the system or thermodynamically limiting conditions, but would reduce potential H_2 recycling and microbial consumption of H_2 by scavengers typically found in mixed wastewater populations [109, 111 - 114].

The manual application of the Pt catalyst resulted in slower rates of H_2 production at the cathode. Only 0.13 m^3-H_2 m^{-3} d^{-1} was produced in experiment i), versus 1.00 m^3-H_2 m^{-3} d^{-1} based on previous tests using identical reactors but replacing the existing cathode with a Pt loaded carbon electrode applied via electroplating (BASF Fuel Cell, Inc.). Due to the high cost, this cathode could not be used despite achieving results similar to other MECs reported in literature (Table 4.2).

4.5.2 Strategies for maintaining a sustainable consortium in a microbial electrolysis cell

Syntrophic associations between chemotrophs like *G. sulfurreducens* and *C. termitidis* derive their metabolic energy from Gibbs free energy changes, ΔG, of chemical

Table 4.2 The effect of Pt application on MEC performance, evaluated in terms of H_2 recoveries, energy input, and energy recovered All studies were single-chambered MECs, operated at an applied voltage of 0.6 V, used acetate as the sole carbon source, and had 0.5 mg Pt cm^{-2} catalyst loading at the cathode. Our study was a pure culture of *G. sulfurreducens* while [32] used inoculum from wastewater. Poor MEC performance is attributed to the manual application of the Pt catalyst layer to the cathode versus electroplating.

		Hydrogen recoveries		Energy recoveries	
		Coulombic	Overall	Electricity input	Electricity + substrate
Study	Total liq. volume (mL)	C_E (%)	r_{H2} (%)	η_{in} (%)	η_{W+S} (%)
Proof of design (this study)[a]	80	101	44	32	28
Proof of design (not published)[b]	80	83	92	30	85
Call and Logan (2008) [32]	28	88	92	n/a	80

[a] Pt catalyst was manually applied (see Materials and Methods)
[b] Pt catalyst was applied via electroplating (BASF Fuel Cell, Inc., carbon cloth electrode, ECC, 0.5 mc cm^{-2} TM loading using 10 % Pt (on Vulcan XC-72))
n/a information not available

reactions [151]. Considering the operating environment of a MEC is close to standard temperature and pressure (STP) conditions, it becomes evident that an obligate syntrophic relationship between *G. sulfurreducens* and *C. termitidis* will not exist (Table 4.3). The fate of co-culture experiments was decided by the rate of independent growth by *C. termitidis* and not by the rate of carbon uptake by *G. sulfurreducens*. An unbalanced flux of fermentation end-product formation to consumption was the leading cause of system failure.

To further illustrate this point, consider the microbial interactions between fermentative, acetogenic, and methanogenic organisms typically found in anaerobic digesters. The metabolism of methanogens is restricted to a limited number of substrates, including H_2/CO_2, formate, acetate, and several other alcohols and methylated compounds [162 - 164]. Successful methanogenic environments require fermentative and acetogenic bacteria to oxidize complex organic material into compounds directly useable by methanogens. Most fermentation reactions responsible for the oxidation of complex substrates to reduced organic compounds have negative $\Delta G^{o\prime}$ values and may proceed independently from the microbial population. Conversely, many acetogenic reactions responsible for the further oxidation of these fermentation end-products typically have positive $\Delta G^{o\prime}$ values and are thermodynamically possible only if the products are efficiently removed by methanogens (Table 4.3). Methanogenic bacteria control the process by "pulling" the acetogenic reactions forward. Two strategies have been proposed to maintain stable H_2 production from cellulosic waste in a MEC:

Table 4.3 Common fermentation, acetogenic, methanogenic, and MEC reactions involved in the syntrophic degradation of organic compounds (adapted from [151])[a]

Chemical Reaction	$\Delta G^{o\prime}$ (kJ reaction^{-1})	Reference
Fermentation		
Glucose $\rightarrow$ 2 Pyruvate$^-$ + 2 H^+ + 2 H_2	-112.1	[138]
Glucose + 4 H_2O $\rightarrow$ 2 Acetate$^-$ + 2 HCO_3^- + 4 H^+ + 4 H_2	- 206.3	[138]
Pyruvate$^-$ + H_2 $\rightarrow$ Lactate$^-$	- 43.1	[138]
Pyruvate$^-$ + H_2O + H_2 $\rightarrow$ Ethanol$^-$ + HCO_3^-	- 56.9	[138]
Acetogenic		
Ethanol + H_2O $\rightarrow$ Acetate$^-$ + H^+ +2H_2	+ 9.6	[151]
Lactate$^-$ + 2 H_2O $\rightarrow$ Acetate$^-$ + HCO_3^- + H^+ + 2 H_2	- 4.2	[151]
Acetate$^-$ + 4 H_2O $\rightarrow$ 2 HCO_3^- + H^+ + 4 H_2	+ 104.6	[138, 151]
Methanogenic		
4 H_2 + HCO_3^- + H^+ $\rightarrow$ CH_4 + 3 H_2O	-135.6	[151]
Acetate$^-$ + H_2O $\rightarrow$ CH_4 + HCO_3^-	- 31.0	[c]
Formate$^-$ + H^+ + 3 H_2 $\rightarrow$ CH_4 + 2 H_2O	-134.3	[138]
MEC reactions[b]		
Acetate$^-$ + 4 H_2O $\rightarrow$ 2 HCO_3^- + H^+ + 4 H_2	+ 104.6	[c]
Lactate$^-$ + 6 H_2O $\rightarrow$ 3 HCO_3^- + 2 H^+ + 6 H_2	+ 100.6	[c]
Pyruvate$^-$ + 6 H_2O $\rightarrow$ 3 HCO_3^- + 2 H^+ + 5 H_2	+ 57.4	[c]
Formate$^-$ + H_2O $\rightarrow$ HCO_3^- + H_2	+ 1.3	[c]

[a] changes in Gibbs free energies calculated at 25 ^oC and 1 atm. H_2 and CH_4 in the gaseous state; all other substances in aqueous solutions at concentrations of 1 M.

[b] combination of possible half-reactions at the anode with the reduction of H^+ to form H_2 at the cathode. Example: acetate$^-$ + 4 H_2O $\rightarrow$ 2 HCO_3^- + 9 H^+ + 8 e^- (anode); 2 H^+ + 2 e^- $\rightarrow$ H_2 (cathode)

[c] calculated from Gibbs free energies of formation tables [138], where $\Delta G^o = \sum \Delta f^o$(products) - $\sum \Delta f^o$(reactants) under STP conditions (25^{o}C, 1 M solutes, 1 atm). Values were adjusted to pH 7 (to compensate for physiological conditions) according to $\Delta G^{o\prime} = \Delta G^o + m\Delta G f'(H^+)$, where m is the net number of protons in the reaction and $\Delta G f'(H^+)$ = -39.87 kJ mol^{-1}.

1. Reduce the growth rate of *C. termitidis*. Cellobiose was used as a carbon source to shorten the duration of the experiments and simplify the analysis. It was anticipated the higher rate of growth and product formation by *C. termitidis* could be controlled by *G. sulfurreducens*. Unfortunately, this could not be accomplished despite efforts to manage culture pH, lower incubation temperature to reduce doubling times, and decrease carbon loading to minimize end-product concentrations (Fig. 4.3b). Culturing *C. termitidis* on cellulose, which is a more complex substrate, may be required to successfully co-culture *C. termitidis* with *G. sulfurreducens*.

Batch experiments in modified 1191 medium were conducted using a pure culture of *C. termitidis* on 2 g L^{-1} α-cellulose (not published). Major fermentation end-products included, H_2, CO_2, acetate, formate, and ethanol. An O/R balance of 1.07 was calculated based on the ratio of oxidized products (formate, CO_2) to reduced products (H_2, ethanol), while 98.2 % of the carbon consumed was recovered. Three important differences between growth on α-cellulose versus cellobiose was observed: i) growth was significantly slower, with a doubling time of 54 h versus 12 h; ii) culture pH never dropped below 6.0; and iii) no pyruvate or lactate production was observed. Slow growth on α-cellulose resulted in volumetric rates of acetate and formate production comparable to rates of consumption by *G. sulfurreducens* in a MEC (Table 4.4).

Table 4.4 Comparison of volumetric rates of production of key fermentation end-products by *C. termitidis* in batch with volumetric rates of consumption by *G. sulfurreducens* in a MEC All experiments were conducted in modified 1191 growth medium at 35°C and in triplicates reactors (balch tubes or MEC).

				Volumetric rates of production / consumption			
Organism	**Substrate**	**Doubling time**	**Final pH**	**Acetate**	**Formate**	**Ethanol**	**Lactate**
		h			$\mu M\ h^{-1}$		
C. termitidis	Cellobiose (2 g L^{-1})	12[a]	5.8	231	286	119	101
	Cellulose (2 g L^{-1})	54[b]	6.0	7	28	9	0
G. sulfurreducens[c]	Defined substrates	n/a	7.5-7.6	7	46	0	4

[a] based on OD measured spectrophotometrically at 600nm
[b] based on protein production extracted using the modified Bradford method [128] and measured spectrophotometrically at 540 nm
[c] volumetric rates of consumption were averaged over run 2 and 3 from experiment ii)

The absence of lactate formation is a particularly important result. Lactate was consumed at the slowest rate when in the presence of other fermentation end-products (Fig. 4.2b). Its accumulation within MEC co-cultures is potentially damaging (Fig. 4.3b) if not adequately removed or properly controlled. Previous studies with *C. termitidis* [123] and other members of the genus *Clostridium* have shown that lactate formation is greater under conditions of low pH (*Clostridium thermocellum*) [126, 131] and high substrate flux (*Clostridium cellulolyticum*) [141]. Limiting the amount of carbon available to *C. termitidis* while maintaining culture pH at neutral conditions are highly recommended. Additionally, extracellular pyruvate should not be produced since typically it is only observed under conditions of high carbon flux (see Chapter 3).

2. Addition of acetogenic bacteria to promote syntrophic cooperation and stability to MEC microbial communities. Like electricigens such as *G. sulfurreducens*, methanogens are specialized bacteria limited to a number of substrates [151, 165]. In

typical methanogenic environments, organic material must be degraded by balanced associations with other organisms, in particular fermenting, acetogenic, and other methanogenic bacteria [151]. Countless examples of sustainable methanogenic environments have been achieved in proven wastewater treatment technologies such as Upflow Anaerobic Sludge Bed (UASB) and Expanded Granular Sludge Bed (EGSB) reactors [151, 155]. In such systems, fermentative organisms are not rate limiting and experience short doubling times [166, 167] resulting in an overwhelming presence of up to 90 % of the total microbial population [168]. Yet despite the abundance of fermentative organisms, methanogens are still able to survive. The presence of syntrophic conversion reactions is required to minimize the effect of high concentrations of specific intermediates. This principle can be applied to microbial populations in MECs.

The addition of an acetogenic organism may be an interesting strategy to stabilize the microbial population of the MEC community. Several syntrophic acetogenic candidates include the long-chain fatty acid degrading *Syntrophomonas sapovorans* (C_4-C_{18}) [169] and the alcohol-degrading *Desulfovibrio vulgaris* [170]. In addition to syntrophic relationships with *G. sulfurreducens*, continuous H_2 removal may be necessary to keep partial pressures low to thermodynamically drive acetogenic reactions forward. Thorough investigations into the energetics of syntrophic cooperation in methanogenic degradation, have been reported by Schink (1997) [165].

4.5.3 Using substrate specificity as a tool for online population health measurements

Exploiting preferential substrate degradation by *G. sulfurreducens* may provide engineers and scientists with a tool for indirectly monitoring co-culture health and activity in a MEC. Growth on a synthetic blend of fermentation end-products in batch

using fumarate as a terminal electron acceptor (Chapter 3) and in a MEC (experiment ii)) demonstrate that mono-cultures of *G. sulfurreducens* preferentially consume formate. It was also shown that lactate degradation was rate limiting and accumulation within the reactor was possible (Fig. 4.3b). The accumulation of lactate within the medium indicates environmental pressures (pH, substrate flux) imposed on *C. termitidis* while the accumulation of formate indicates a poor performing or possibly failing culture of *G. sulfurreducens*, providing low H_2 partial pressures are maintained in the headspace. In addition to pH measurements and current flux at the anode, it is proposed that formate and lactate concentrations are monitored because they may serve as useful boundary controls, indicating co-culture sustainability or predicting MEC failure.

Chapter 5: Concluding Remarks

5.1 Strategies for increased, sustainable H_2 production

This purpose of this thesis was to improve our current understanding of the relationship between fermentative and electrogenic bacteria in MECs. The characterization experiments designed to study pure cultures revealed several important conclusions, discussed below. This work lays the foundation for the future design of an MEC capable of generating sustainable amounts of H_2 at increased concentrations from cellulosic waste.

1. Enhanced H_2 production is possible by integrated fermentative microbial electrohydrogenesis. A total of 9.7 mol-H_2 mol^{-1}-glucose$_{EQ}$ was produced at a maximum rate of 1.53 m^3-H_2 m^{-3} day^{-1} (25^{o}C, 1 atm, 0.054 L headspace). Despite a high glucose-to-H_2 conversion efficiency of 81 %, additional H_2 production is possible. A low MEC coulombic efficiency of 65.7 ± 0.8 % and no H_2 production in balch tube co-cultures suggest possible H_2 consumption by *G. sulfurreducens*. It is recommended that H_2 partial pressures are kept to a minimum in combination with a membrane to separate electrode reactions. Low H_2 concentrations in the headspace could thermodynamically favor increased fermentative H_2 production while prevent H_2 consumption by uptake hydrogenases and/or possible formate production (in combination with CO_2). The use of a membrane will eliminate any biological consumption of chemical H_2 production at the cathode.

2. *Geobacter sulfurreducens preferentially consumes formate, followed by acetate and lactate.* Recognizing lactate degradation as rate limiting when in the presence of formate and acetate is an important parameter for engineers to regulate. Lactate is typically produced under conditions of low pH or high carbon flux. Monitoring lactate levels, as well as formate, may be a useful tool for indirectly monitoring co-culture health and activity.

3. *The flux of fermentation intermediates must be balanced to stabilize co-culture dynamics.* High H_2 production within the MEC co-culture could not be maintained. The conversion rate of end-product consumption to electrons was far too slow compared to the fermentation of cellobiose. Slow growth by *G. sulfurreducens* has previously been reported in mixed-culture MFC experiments. Despite the presence of the highly thermodynamically favorable terminal electron acceptor, O_2, relatively slow-growing methanogens are able to compete with electricigens by directing electrons towards methane production and away from electricity generation [160].

Strategies to control the unbalanced flow of intermediates within MEC co-cultures include: i) reducing the growth rate, and ultimately the rate of end-product synthesis, of *C. termitidis* by culturing the bacteria on a much more complex substrate (*e.g.* α-cellulose); and ii) minimize the high concentrations of specific intermediates with the addition of an acetogenic bacteria. Low H_2 partial pressures must be maintained to thermodynamically drive these reactions.

5.2 Limitations of current experiments

The greatest challenge for characterizing co-culture populations in an MEC was accurately sampling, measuring, and differentiating active biomass from anodic biofilm and planktonic cultures. Monitoring a dynamic microbial population in a MEC is a necessary control to maintain process efficiency at maximum operating capacity. Unfortunately, online analysis of planktonic and biofilm dynamics is extremely difficult, elaborate, and time consuming. Precisely measuring MEC biomass is an area that requires further investigation and development. Additionally, future studies should be directed towards the characterization of *C. termitidis* with special emphasis on pyruvate catabolism and carbon distribution. The flux of metabolites between *C. termitidis* and *G. sulfurreducens* must be explored in greater detail to identify key mechanisms of carbon and electron flow between organisms. Continuous chemostat experiments are recommended in order to maintain constant rates of growth, production, and consumption, at defined dilution rates and substrate loading concentrations.

5.3 Future engineering design considerations

Continuous removal of contaminants and replacement of nutrients and salts is necessary for the sustained operation of any system. Numerous complications may arise when operating in batch and fed-batch mode, the most prominent including the accumulation of undesired products (catalyst fouling, sluggish kinetics, lowered pH), the consumption of buffer (large fluctuations in solution pH), and the utilization of substrate (carbon limiting conditions for microorganisms). In continuous MEC operation, low H_2 and CO_2 partial pressures can be maintained, while ethanol can be efficiently removed to

avoid accumulation and contamination. The build-up of lactate can also be avoided, and possibly recycled, minimizing the effects of low medium pH.

It appears that small electrical resistances at the laboratory scale may become enormous energy sinks during the scale-up of MEC reactors. The distance electrons travel between electrodes must be kept to a minimum in addition to using highly conductive materials. Another important design consideration is as current densities improve at the anode, H_2 production at the cathode becomes rate limiting [29, 41, 160]. In light of new electrode materials and catalysts, increasing the surface area of the cathode relative to the anode will help minimize cathodic reactions from limiting electron transfer rates to the anode [160].

Finally, future reactor designs should incorporate concepts employed by wastewater technologies since MEC co-culture dynamics closely resemble microbial communities typically found in anaerobic digestion. In particular, the Upflow Anaerobic Sludge Bed (UASB) reactor serves as an appropriate model. The construction, design, and mode of operation favors i) high activated sludge retention and ii) sufficient contact between viable biomass and medium [155]. A continuous MEC (Fig. 5.1) could retain cells by two means: i) brush anodes inserted down the center of a tubular frame will not only increase anodic surface area up to 300x greater [32], but will allow *G. sulfurreducens* to form thick, healthy biofilms; and ii) *C. termitidis* is known to adhere directly to insoluble substrates during hydrolysis (Fig. 5.2a). When cultured on α-cellulose, cells and substrate group together forming clumps with satisfactory settling properties (Fig. 5.2b and 5.2c). As substrate is consumed, cells would be carried to the

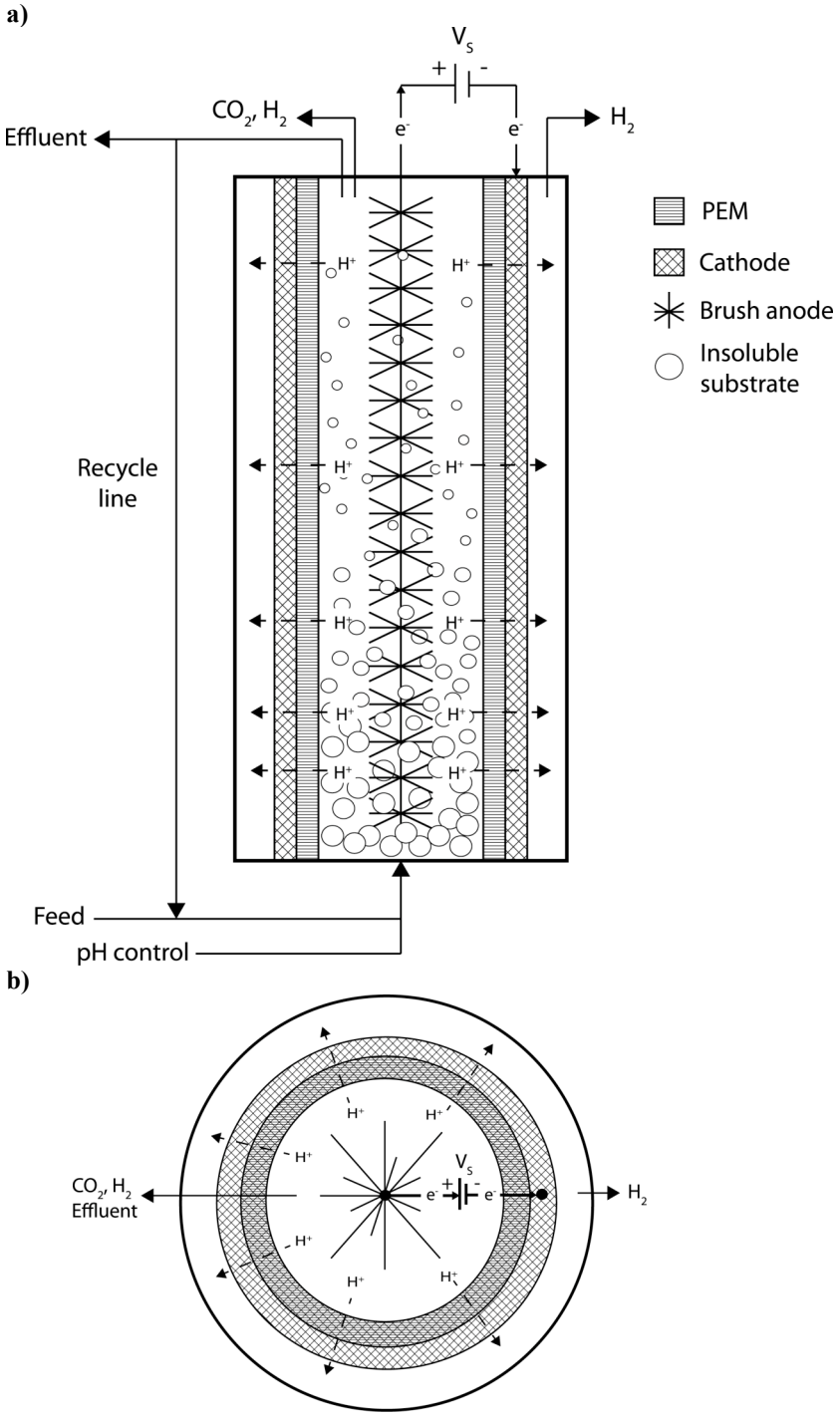

Figure 5.1 Potential UASB-MEC reactor configuration for enhanced H_2 production The proposed drawing addresses several of the problems the existing design currently faces. a) Cross-sectional view and b) top view of the tubular reactor architecture. Continuous operation will provide more control over environmental conditions. Mass transfer could potentially be improved with heightened biomass-to-medium contact. A brush anode and circular cathode/PEM will increase electrode surface areas and electron flux.

surface of the reactor and removed from the system. Sufficient contact between cells and medium could be achieved from biogas production and an even upflow velocity from the feed line placed at the bottom of the reactor. Mixing would be kept to a minimum because the biofilms formed by *G. sulfurreducens* on the anode and *C. termitidis* on the substrate are vulnerable to heavy agitation. A proton exchange membrane (PEM), heat pressed directly against a Pt coated cathode, would encircle the brush anode. Not only would this create a liquid/solid/gas barrier separating H_2 production from the microbial community, but the circular design would significantly increase the surface area of the cathode.

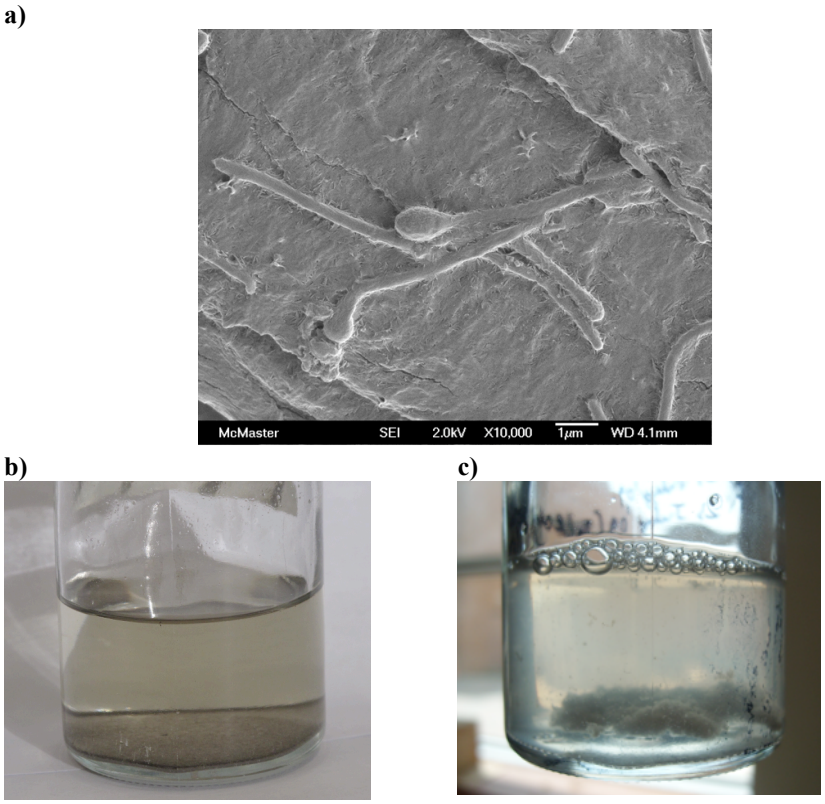

Figure 5.2 Advantageous growth characteristics of *C. termitidis* on insoluble substrates a) Scanning electron microscopy images display small appendages protruding from the body of *C. termitidis*, demonstrating the organism's ability to attach directly to the surface of its carbon source. A serum bottle containing 2 g L^{-1} α-cellulose and b) no culture (negative control) versus c) a pure culture of *C. termitidis* is illustrated. Growth on cellulose clumps substrate with biomass, providing good settling properties desirable in a USAB-MEC type reactor. Gas bubbles and medium turbidity indicate cell growth.

References

1. Logan, B.E. 2004. Extracting hydrogen and electricity from renewable resources. Environ Sci Technol. 38(9): 160A-167A.

2. Lattin, W.C. and V.P. Utgikar. 2007. Transition to hydrogen economy in the United States: a 2006 status report. Int. J. Hydrogen Energy. 32: 3230-3237.

3. Ramachandran, R. and R.K. Menon. 1998. An overview of industrial uses of hydrogen. Int. J. Hydrogen Energy. 23(7): 593-598.

4. Rozendal, R.A. 2007. Hydrogen Production through Biocatalyzed Electrolysis. Department of Environmental Technology, Wageningen University. PhD.

5. "Canadian fuel cell commercialization roadmap update." 2008. from www.ic.gc.ca/hydrogen.

6. Agarwal, A.K. 2007. Biofuels (alcohols and biodiesel) applications as fuels for internal combustion engines. Progress in Energy and Combustion Science. 33(3): 233-271.

7. IEA 2005 International Energy Agency - Resources to Reserves: Oil & Gas Technologies for the Energy Markets of the Future. International Energy Agency, Head of Publications Service

8. Petrus, L. and M.A. Noordermeer. 2006. Biomass to biofuels, a chemical perspective. Green Chem. 8: 861-867.

9. Holladay, J.D., J. Hu, D.L. King and Y. Wang. 2009. An overview of hydrogen producing technologies. Catalysis Today. 139: 244-260.

10. Levin, D.B., L. Pitt and M. Love. 2004. Biohydrogen production: prospects and limitations to practical application. Int. J. Hydrogen Energy. 29: 173-185.

11. McKendry, P. 2002. Energy production from biomass (part 1): overview of biomass. Bioresource Technology. 83: 37-46.

12. Demain, A.L., M. Newcomb and J.H. Wu. 2005. Cellulase, clostridia, and ethanol. Microbiol Mol Biol Rev. 69(1): 124-154.

13. Ragauskas, A.J., C.K. Williams, B.H. Davison, G. Britovsek, J. Cairney, C.A. Eckert, W.J. Frederick Jr., J.P. Hallett, D.J. Leak, C.L. Liotta, J.R. Mielenz, R. Murphy, R. Templer and T. Tschaplinsky. 2006. The path forward for biofuels and biomaterials. Science. 311: 484-489.

14. Ni, M., D.Y.C. Leung, M.K.H. Leung and K. Sumathy. 2006. An overview of hydrogen production from biomass. Fuel Processing Technology. 87(5): 461-472.

15. Hawkes, F.R., R. Dinsdale, D.L. Hawkes and I. Hussy. 2002. Sustainable fermentative hydrogen production: challenges for process optimization. Int. J. Hydrogen Energy. 27: 1339-1347.

16. Leshine, S.B. 1995. Cellulose degradation in anaerobic environments. Annu. Rev. Microbiol. 49: 399-426.

17. Debabov, V.G. 2008. Electricity from microorganisms. Mikrobiologiia. 77(2): 149-157.

18. Monserrate, E., S.B. Leschine and E. Canale-Parola. 2001. *Clostridium hungatei* sp nov., a mesophilic, N_2-fixing cellulolytic bacterium isolated from soil. International Journal of Systematic and Evolutionary Microbiology. 51: 123-132.

19. Lynd, L.R., P.J. Weimer, W.H. van Zyl and I.S. Pretorius. 2002. Microbial cellulose utilization: Fundamentals and biotechnology. Microbiology and Molecular Biology Reviews. 66(3): 506.

20. Campbell, N.A. and J.B. Reece. 2002. Biology. Ed. 6. Benjamin Cummings, Toronto.

21. Prescott, L.M., J.P. Harley and D.A. Klein. 2005. Microbiology. Ed. 6. McGraw-Hill, Toronto.

22. Desvaux, M. 2005. *Clostridium cellulolyticum*: model organism of mesophilic cellulolytic clostridia. Fems Microbiology Reviews. 29(4): 741-764.

23. Lynd, L.R., P.J. Weimer, G. Wolfaardt and Y.P. Zhang. 2006. Cellulose hydrolysis by *Clostridium thermocellum*: A microbial perspective in: (Eds.). Molecular Anatomy and Physiology of Proteins. Nova Science Publishers.

24. Ren, Z., T.E. Ward, B.E. Logan and J.M. Regan. 2007. Characterization of the cellulolytic and hydrogen-producing activities of six mesophilic *Clostridium* species. Journal of Applied Microbiology. 103(6): 2258-2266.

25. Lee, H.S., M.B. Salerno and B.E. Rittmann. 2008. Thermodynamic evaluation on H_2 production in glucose fermentation. Environmental Science & Technology. 42(7): 2401-2407.

26. Logan, B.E. 2008. Microbial Fuel Cells. John Wiley & Sons, Inc., New Jersey.

27. Li, C.L. and H.H.P. Fang. 2007. Fermentative hydrogen production from wastewater and solid wastes by mixed cultures. Critical Reviews in Environmental Science and Technology. 37(1): 1-39.

28. Liu, H., S. Grot and B.E. Logan. 2005. Electrochemically assisted microbial production of hydrogen from acetate. Environ Sci Technol. 39(11): 4317-4320.

29. Rozendal, R.A., H.V. Hamelers and C.J. Buisman. 2006. Effects of membrane cation transport on pH and microbial fuel cell performance. Environ Sci Technol. 40(17): 5206-5211.

30. Rozendal, R.A., H.V. Hamelers, R.J. Molenkamp and C.J. Buisman. 2007. Performance of single chamber biocatalyzed electrolysis with different types of ion exchange membranes. Water Res. 41(9): 1984-1994.

31. Cheng, S. and B.E. Logan. 2007. Sustainable and efficient biohydrogen production via electrohydrogenesis. Proc Natl Acad Sci U S A. 104(47): 18871-18873.

32. Call, D. and B.E. Logan. 2008. Hydrogen production in a single chamber microbial electrolysis cell lacking a membrane. Environ Sci Technol. 42(9): 3401-3406.

33. Tartakovsky, B., M.F. Manuel, H. Wang and S.R. Guiot. 2009. High rate memrane-less microbial electrolysis cell for continuous hydrogen production. Int. J. Hydrogen Energy. 34: 672-677.

34. Logan, B.E., D. Call, S. Cheng, H.V. Hamelers, T.H. Sleutels, A.W. Jeremiasse and R.A. Rozendal. 2008. Microbial electrolysis cells for high yield hydrogen gas production from organic matter. Environ Sci Technol. 42(23): 8630-8640.

35. Spath, P.L. and M.K. Mann. 2001. Life cycle assessment of hydrogen production via natural gas steam reforming. 33.

36. Jameel, H., D.R. Keshwani, S.F. Carter and T.H. Treasure. 2010. Thermochemical conversion of biomass to power and fuels in: J. Cheng (Eds.). Biomass to Renewable Energy Processes. CRC Press - Taylor & Francis Group, Boca Raton, FL, USA: pp**.** 437-489.

37. Ciferno, J.P. and J.J. Marano. 2002. Benchmarking biomass gasification technologies for fuels, chemical, and hydrogen production. National Energy Technology Laboratory, US Department of Energy.

38. Sigurvinsson, J. and F. Werkoff. 2005. On the cost of the hydrogen produced by alkaline electrolysis. International Hydrogen Energy Congress and Exhibition (IHEC), Istanbul, Turkey.

39. Ivy, J. 2004. Summary of electrolytic hydrogen production. National Renewable Energy Laboratory, Colorado. pp. 27.

40. Barbir, F. 2005. PEM electrolysis for production of hydrogen from renewable energy sources. Solar Energy. 78: 661-669.

41. Lee, H.-S. and B. Rittmann. 2010. Characterization of energy losses in an upflow single-chamber microbial electrolysis cell. International Journal of Hydrogen Energy. 35: 920-927.

42. Clauwaert, P., P. Aelterman, T.H. Pham, L. De Schamphelaire, M. Carballa, K. Rabaey and W. Verstraete. 2008. Minimizing losses in bio-electrochemical systems: the road to applications. Appl Microbiol Biotechnol. 79(6): 901-913.

43. Bullen, R.A., T.C. Arnot, J.B. Lakeman and F.C. Walsh. 2006. Biofuel cells and their development. Biosensors and Bioelectronics. 21(11): 2015-2045.

44. Kipnis, N. 1987. Luigi Galvani and the debate on animal electricity, 1971-1800. Annals of Science. 44: 107-142.

45. Grove, W.R. 1839. Philosophy Magazine Series. 3(14): 127.

46. Potter, M.C. 1911. Electrical effects accompanying the decomposition of organic compounds. Proceedings of the Royal Society of London. Series B. 84(571): 260-276.

47. He, Z. and L.T. Angenent. 2006. Application of bacterial biocathodes in microbial fuel cells. Electroanalysis. 18(19-20): 2009-2015.

48. Rabaey, K., J. Rodriguez, L.L. Blackall, J. Keller, P. Gross, D. Batstone, W. Verstraete and K.H. Nealson. 2007. Microbial ecology meets electrochemistry: electricity-driven and driving communities. ISME J. 1(1): 9-18.

49. Berk, R.S. and J.H. Canfield. 1964. Bioelectrochemical Energy Conversion. Appl Microbiol. 12: 10-12.

50. Cohen, B. 1931. The bacterial culture as an electrical half-cell. Journal of Bacteriology. 21(1): 18-19.

51. Shukla, A.K., P. Suresh, S. Berchmans and A. Rajendran. 2004. Biological fuel cells and their applications. Current Science. 87(4): 455 - 468.

52. Lewis, K. 1966. Symposium on bioelectrochemistry of microorganisms. IV. Biochemical fuel cells. Bacteriol Rev. 30(1): 101-113.

53. Lovley, D.R. and K.P. Nevin. 2008. Electricity production with electricigens in: J.D. Wall, C.S. Harwood and A. Demain (Eds.). Bioenergy. ASM Press, Washington, D.C.: pp. 295-306.

54. Allen, R.M. and H.P. Bennetto. 1993. Microbial fuel-cells: electricity production from carbohydrates. Applied Biochemistry and Biotechnology. 39/40(1): 27-40.

55. Bond, D.R., D.E. Holmes, L.M. Tender and D.R. Lovley. 2002. Electrode-reducing microorganisms that harvest energy from marine sediments. Science. 295(5554): 483-485.

56. Jung, S. and J.M. Regan. 2007. Comparison of anode bacterial communities and performance in microbial fuel cells with different electron donors. Appl Microbiol Biotechnol. 77(2): 393-402.

57. Chae, K.J., M.J. Choi, J.W. Lee, K.Y. Kim and I.S. Kim. 2009. Effect of different substrates on the performance, bacterial diversity, and bacterial viability in microbial fuel cells. Bioresour Technol. 100(14): 3518-3525.

58. Logan, B.E. and J.M. Regan. 2006. Electricity-producing bacterial communities in microbial fuel cells. Trends Microbiol. 14(12): 512-518.

59. Aelterman, P., K. Rabaey, L.D. Schamphelaire, P. Clauwaert, N. Boon and W. Verstraete. 2008. Microbial fuel cells as an engineered ecosystem in: J.D. Wall, C.S. Harwood and A.L. Demain (Eds.). Bioenergy. ASM Press, Washington, D.C.: pp. 307-322.

60. Lovley, D.R. 2008. The microbe electric: conversion of organic matter to electricity. Curr Opin Biotechnol. 19(6): 564-571.

61. Heidelberg, J.F., I.T. Paulsen, K.E. Nelson, E.J. Gaidos, W.C. Nelson, T.D. Read, J.A. Eisen, R. Seshadri, N. Ward, B. Methe, R.A. Clayton, T. Meyer, A. Tsapin, J. Scott, M. Beanan, L. Brinkac, S. Daugherty, R.T. DeBoy, R.J. Dodson, A.S. Durkin, D.H. Haft, J.F. Kolonay, R. Madupu, J.D. Peterson, L.A. Umayam, O. White, A.M. Wolf, J. Vamathevan, J. Weidman, M. Impraim, K. Lee, K. Berry, C. Lee, J. Mueller, H. Khouri, J. Gill, T.R. Utterback, L.A. McDonald, T.V. Feldblyum, H.O. Smith, J.C. Venter, K.H. Nealson and C.M. Fraser. 2002. Genome sequence of the dissimilatory metal ion-reducing bacterium *Shewanella oneidensis*. Nat Biotechnol. 20(11): 1118-1123.

62. Methe, B.A., K.E. Nelson, J.A. Eisen, I.T. Paulsen, W. Nelson, J.F. Heidelberg, D. Wu, M. Wu, N. Ward, M.J. Beanan, R.J. Dodson, R. Madupu, L.M. Brinkac, S.C. Daugherty, R.T. DeBoy, A.S. Durkin, M. Gwinn, J.F. Kolonay, S.A. Sullivan, D.H. Haft, J. Selengut, T.M. Davidsen, N. Zafar, O. White, B. Tran, C. Romero, H.A. Forberger, J. Weidman, H. Khouri, T.V. Feldblyum, T.R. Utterback, S.E. Van Aken, D.R. Lovley and C.M. Fraser. 2003. Genome of *Geobacter sulfurreducens*: metal reduction in subsurface environments. Science. 302(5652): 1967-1969.

63. Newman, D.K. and R. Kolter. 2000. A role for excreted quinones in extracellular electron transfer. Nature. 405(6782): 94-97.

64. Lanthier, M., K.B. Gregory and D.R. Lovley. 2008. Growth with high planktonic biomass in *Shewanella oneidensis* fuel cells. FEMS Microbiol Lett. 278(1): 29-35.

65. Marsili, E., D.B. Baron, I.D. Shikhare, D. Coursolle, J.A. Gralnick and D.R. Bond. 2008. *Shewanella* secretes flavins that mediate extracellular electron transfer. Proc Natl Acad Sci U S A. 105(10): 3968-3973.

66. von Canstein, H., J. Ogawa, S. Shimizu and J.R. Lloyd. 2008. Secretion of flavins by *Shewanella* species and their role in extracellular electron transfer. Appl Environ Microbiol. 74(3): 615-623.

67. Bond, D.R. and D.R. Lovley. 2005. Evidence for involvement of an electron shuttle in electricity generation by *Geothrix fermentans*. Appl Environ Microbiol. 71(4): 2186-2189.

68. Mahadevan, R., D.R. Bond, J.E. Butler, A. Esteve-Nunez, M.V. Coppi, B.O. Palsson, C.H. Schilling and D.R. Lovley. 2006. Characterization of metabolism in the Fe(III)-reducing organism *Geobacter sulfurreducens* by constraint-based modeling. Appl Environ Microbiol. 72(2): 1558-1568.

69. Lies, D.P., M.E. Hernandez, A. Kappler, R.E. Mielke, J.A. Gralnick and D.K. Newman. 2005. *Shewanella oneidensis* MR-1 uses overlapping pathways for iron reduction at a distance and by direct contact under conditions relevant for Biofilms. Appl Environ Microbiol. 71(8): 4414-4426.

70. Holmes, D.E., S.K. Chaudhuri, K.P. Nevin, T. Mehta, B.A. Methe, A. Liu, J.E. Ward, T.L. Woodard, J. Webster and D.R. Lovley. 2006. Microarray and genetic analysis of electron transfer to electrodes in *Geobacter sulfurreducens*. Environ Microbiol. 8(10): 1805-1815.

71. Lovley, D.R., E.J. Phillips, D.J. Lonergan and P.K. Widman. 1995. Fe(III) and S0 reduction by *Pelobacter carbinolicus*. Appl Environ Microbiol. 61(6): 2132-2138.

72. Lovley, D.R. 2008. Extracellular electron transfer: wires, capacitors, iron lungs, and more. Geobiology. 6(3): 225-231.

73. Bond, D.R. and D.R. Lovley. 2003. Electricity production by *Geobacter sulfurreducens* attached to electrodes. Appl Environ Microbiol. 69(3): 1548-1555.

74. Reguera, G., K.P. Nevin, J.S. Nicoll, S.F. Covalla, T.L. Woodard and D.R. Lovley. 2006. Biofilm and nanowire production leads to increased current in *Geobacter sulfurreducens* fuel cells. Appl Environ Microbiol. 72(11): 7345-7348.

75. Nevin, K.P., H. Richter, S.F. Covalla, J.P. Johnson, T.L. Woodard, A.L. Orloff, H. Jia, M. Zhang and D.R. Lovley. 2008. Power output and coulombic efficiencies from biofilms of *Geobacter sulfurreducens* comparable to mixed community microbial fuel cells. Environ Microbiol. 10(10): 2505-2514.

76. Reguera, G., K.D. McCarthy, T. Mehta, J.S. Nicoll, M.T. Tuominen and D.R. Lovley. 2005. Extracellular electron transfer via microbial nanowires. Nature. 435(7045): 1098-1101.

77. Reguera, G. 2009. Are microbial conversations being lost in translation? Microbe. **4:** 506-512.

78. Lucas, C.E., E. Brown and B.S. Fields. 2006. Type IV pili and type II secreation play a limited role in *Legionella pneumophila* biofilm colonization and retention. Microbiology. 152: 3569-3573.

79. Reguera, G., R.B. Pollina, J.S. Nicoll and D.R. Lovley. 2007. Possible nonconductive role of *Geobacter sulfurreducens* pilus nanowires in biofilm formation. J Bacteriol. 189(5): 2125-2127.

80. Bard, A.J. and L.R. Faulkner. 2001. Electrochemical methods : fundamentals and applications. Ed. 2nd. Wiley, New York.

81. Newman, J.S. and K.E. Thomas-Alyea. 2004. Electrochemical systems. Ed. 3rd. Wiley-Interscience, Hoboken, N.J.

82. Bagotsky, V.S. 2005. Fundamentals of Electrochemistry. Ed. 2. John Wiley & Sons, Inc., New Jersey.

83. Alberty, R.A. 2001. Use of legendre transforms in chemical thermodynamics. Pure and Applied Chemistry. 73(8): 1349-1380.

84. Thauer, R.K., K. Jungermann and K. Decker. 1977. Energy conservation in chemotrophic anaerobic bacteria. Bacteriol Rev. 41(1): 100-180.

85. Logan, B.E., B. Hamelers, R. Rozendal, U. Schroder, J. Keller, S. Freguia, P. Aelterman, W. Verstraete and K. Rabaey. 2006. Microbial fuel cells: methodology and technology. Environ Sci Technol. 40(17): 5181-5192.

86. Hamelers, H.V., A. Ter Heijne, T.H. Sleutels, A.W. Jeremiasse, D.P. Strik and C.J. Buisman. 2010. New applications and performance of bioelectrochemical systems. Appl Microbiol Biotechnol. 85(6): 1673-1685.

87. Torres, C.I., A.K. Marcus and B.E. Rittmann. 2007. Kinetics of consumption of fermentation products by anode-respiring bacteria. Appl Microbiol Biotechnol. 77(3): 689-697.

88. Sleutels, T.H.J.A., H.V.M. Hamelers, R.A. Rozendal and C.J.N. Buisman. 2009. Ion transport resistance in Microbial Electrolysis Cells with anion and cation exchange membranes. Int. J. Hydrogen Energy. 34(9): 3612-3620.

89. Ter Heijne, A., H.V. Hamelers, V. De Wilde, R.A. Rozendal and C.J. Buisman. 2006. A bipolar membrane combined with ferric iron reduction as an efficient cathode system in microbial fuel cells. Environ Sci Technol. 40(17): 5200-5205.

90. Prausnitz, J.M., R.N. Lichtenthaler and E.G. de Azevedo. 1998. Molecular thermodynamics of fluid-phase equilibria. Ed. 3rd. Prentice Hall.

91. Jeremiasse, A.W., H.V. Hamelers, J.M. Kleijn and C.J. Buisman. 2009. Use of biocompatible buffers to reduce the concentration overpotential for hydrogen evolution. Environ Sci Technol. 43(17): 6882-6887.

92. Rabaey, K., G. Lissenns and W. Verstraete. 2005. Microbial fuel cells: performances and perspectives in: P. Lens, P. Westermann, M. Haberbauer and A. Moreno (Eds.). Biofuels for Fuel Cells: Renewable Energy from Biomass Fermentation. IWA Publishing, London: pp**.** 377-399.

93. Freguia, S., K. Rabaey, Z. Yuan and J. Keller. 2008. Sequential anode-cathode configuration improves cathodic oxygen reduction and effluent quality of microbial fuel cells. Water Res. 42(6-7): 1387-1396.

94. Ditzig, J., H. Liu and B.E. Logan. 2007. Production of hydrogen from domestic wastewater using a bioelectrochemically assisted microbial reactor (BEAMR). J. Hydrogen Energy. 32: 2296-2304.

95. Hu, H., Y. Fan and H. Liu. 2008. Hydrogen production using single-chamber membrane-free microbial electrolysis cells. Water Res. 42(15): 4172-4178.

96. Couper, A.M., D. Pletcher and F.C. Walsh. 1990. Electrode materials for electrosynthesis. Chem. Rev. 90(5): 837-865.

97. Selembo, P.A., M.D. Merrill and B.E. Logan. 2010. Hydrogen production with nickel powder cathode catalysts in microbial electrolysis cells. Int. J. Hydrogen Energy. 35: 428-437.

98. Call, D.F., M.D. Merrill and B.E. Logan. 2009. High surface area stainless steel brushes as cathodes in microbial electrolysis cells. Environ Sci Technol. 43(6): 2179-2183.

99. Selembo, P.A., M.D. Merrill and B.E. Logan. 2009. The use of stainless steel and nickel alloys as low-cost cathodes in microbial electrolysis cells. Journal of Power Sources. 190(2): 271-278.

100. Rozendal, R.A., A.W. Jeremiasse, H.V. Hamelers and C.J. Buisman. 2008. Hydrogen production with a microbial biocathode. Environ Sci Technol. 42(2): 629-634.

101. Jeremiasse, A.W., H.V. Hamelers and C.J. Buisman. 2009. Microbial electrolysis cell with a microbial biocathode. Bioelectrochemistry.

102. Sleutels, T.H.J.A., R. Lodder, H.V.M. Hamelers and C.J.N. Busiman. 2009. Improved performance of porous bio-anodes in microbial electrolysis cells by enhanced mass and charge transport. Int. J. Hydrogen Energy. 34: 9655-9661.

103. Lee, H.S., W.F. Vermaas and B.E. Rittmann. 2010. Biological hydrogen production: prospectives and challenges. Trends Biotechnol.

104. Torres, C.I., A.K. Marcus, H.S. Lee, P. Parameswaran, R. Krajmalnik-Brown and B.E. Rittmann. 2010. A kinetic perspective on extracellular electron transfer by anode-respiring bacteria. FEMS Microbiol Rev. 34(1): 3-17.

105. Rittmann, B.E. and P.L. McCarty. 2001. Environmental biotechnology : principles and applications. McGraw-Hill, Boston.

106. Monod, J. 1942. Resherches sur la croissance des cultures bacteriennes. Hermann, Paris.

107. Esteve-Nunez, A., M. Rothermich, M. Sharma and D. Lovley. 2005. Growth of *Geobacter sulfurreducens* under nutrient-limiting conditions in continuous culture. Environ Microbiol. 7(5): 641-648.

108. Lee, H.S., C.I. Torres and B.E. Rittmann. 2009. Effects of substrate diffusion and anode potential on kinetic parameters for anode-respiring bacteria. Environ Sci Technol. 43(19): 7571-7577.

109. Lee, H.S. and B.E. Rittmann. 2010. Significance of biological hydrogen oxidation in a continuous single-chamber microbial electrolysis cell. Environ Sci Technol. 44(3): 948-954.

110. Kato Marcus, A., C.I. Torres and B.E. Rittmann. 2007. Conduction-based modeling of the biofilm anode of a microbial fuel cell. Biotechnol Bioeng. 98(6): 1171-1182.

111. Clauwaert, P. and W. Verstraete. 2009. Methanogenesis in membraneless microbial electrolysis cells. Appl Microbiol Biotechnol. 82(5): 829-836.

112. Lee, H.S., C.I. Torres, P. Parameswaran and B.E. Rittmann. 2009. Fate of H_2 in an upflow single-chamber microbial electrolysis cell using a metal-catalyst-free cathode. Environ Sci Technol. 43(20): 7971-7976.

113. Cheng, S., D. Xing, D.F. Call and B.E. Logan. 2009. Direct biological conversion of electrical current into methane by electromethanogenesis. Environ Sci Technol. 43(10): 3953-3958.

114. Wagner, R.C., J.M. Regan, S.E. Oh, Y. Zuo and B.E. Logan. 2009. Hydrogen and methane production from swine wastewater using microbial electrolysis cells. Water Res. 43(5): 1480-1488.

115. Yi, H., K.P. Nevin, B.C. Kim, A.E. Franks, A. Klimes, L.M. Tender and D.R. Lovley. 2009. Selection of a variant of *Geobacter sulfurreducens* with enhanced capacity for current production in microbial fuel cells. Biosens Bioelectron. 24(12): 3498-3503.

116. Logan, B.E. 2010. Scaling up microbial fuel cells and other bioelectrochemical systems. Appl Microbiol Biotechnol. 85(6): 1665-1671.

117. Bond, D.R. and D.R. Lovley. 2003. Electricity production by *Geobacter sulfurreducens* attached to electrodes. Applied and Environmental Microbiology. 69(3): 1548-1555.

118. Chaudhuri, S.K. and D.R. Lovley. 2003. Electricity generation by direct oxidation of glucose in mediatorless microbial fuel cells. Nature Biotechnology. 21(10): 1229-1232.

119. Lovley, D.R. 2006. Bug juice: harvesting electricity with microorganisms. Nature Reviews Microbiology. 4(7): 497-508.

120. Ren, Z.Y., T.E. Ward and J.M. Regan. 2007. Electricity production from cellulose in a microbial fuel cell using a defined binary culture. Environmental Science & Technology. 41(13): 4781-4786.

121. Mcinerney, M.J. and P.S. Beaty. 1988. Anaerobic community structure from a nonequilibrium thermodynamic perspective. Canadian Journal of Microbiology. 34(4): 487-493.

122. Lovley, D.R. and E.J.P. Phillips. 1989. Requirement for a microbial consortium to completely oxidize glucose in Fe(III)-reducing sediments. Applied and Environmental Microbiology. 55(12): 3234-3236.

123. Ramachandran, U., N. Wrana, N. Cicek, R. Sparling and D.B. Levin. 2008. Hydrogen production and end-product synthesis patterns by *Clostridium termitidis* strain CT1112 in batch fermentation with cellobiose or a-cellulose. Int. J. Hydrogen Energy. 33: 7006-7012.

124. Lovley, D.R., D.E. Holmes and K.P. Nevin. 2004. Dissimilatory Fe(III) and Mn(IV) reduction. Advances in Microbial Physiology, Vol. 49. 49: 219-286.

125. Yang, T.H., M.V. Coppi, D.R. Lovley and J. Sun. 2010. Metabolic response of *Geobacter sulfurreducens* towards electron donor/acceptor variation. Microb Cell Fact. 9(90): 1-15.

126. Islam, R. 2005. Effect of substrate loading on metabolic flux of *Clostridium thermocellum* during fermentative hydrogen production using cellulosic substrates, University of Manitoba, Fall 2005.

127. Daniels, L., N. Belay and B.S. Rajagopal. 1986. Assimilatory reduction of sulfate and sulfite by methanogenic bacteria. Applied and Environmental Microbiology. 51(4): 703-709.

128. Bradford, M.M. 1976. A rapid and sensitive method for the quantitation of microgram quantities of protein utilizing the principle of protein-dye binding. Anal Biochem. 72: 248-254.

129. Esteve-Nunez, A., M. Rothermich, M. Sharma and D. Lovley. 2005. Growth of *Geobacter sulfurreducens* under nutrient-limiting conditions in continuous culture. Environmental Microbiology. 7(5): 641-648.

130. Galushko, A.S. and B. Schink. 2000. Oxidation of acetate through reactions of the citric acid cycle by *Geobacter sulfurreducens* in pure culture and in syntrophic coculture. Archives of Microbiology. 174(5): 314-321.

131. Magnusson, L., R. Islam, R. Sparling, D. Levin and N. Cicek. 2008. Direct hydrogen production from cellulosic waste materials with a single-step dark fermentation process. Int. J. Hydrogen Energy. 33(20): 5398-5403.

132. Sander, R. 1999. Compilation of Henry's law constants for inorganic and organic species of potential importance in environmental chemistry. Air Chemistry Department. Mainz, Germany, Max-Planck Institute of Chemistry.

133. Darrett, R.H. and C.M. Drisham. 1995. Biochemistry. Saunders College Publishing, New York, NY.

134. "National Center for Biotechnology Information." Retrieved September, 2010, from http://www.ncbi.nlm.nih.gov.

135. "cpnDB - A Chaperonin Database." Retrieved September, 2010, from http://cpndb.cbr.nrc.ca.

136. Mahadevan, R., D.R. Bond, J.E. Butler, A. Esteve-Nunez, M.V. Coppi, B.O. Palsson, C.H. Schilling and D.R. Lovley. 2006. Characterization of metabolism in the Fe(III)-reducing organism *Geobacter sulfurreducens* by constraint-based modeling. Applied and Environmental Microbiology. 72(2): 1558-1568.

137. Sparling, R., R. Islam, N. Cicek, C. Carere, H. Chow and D.B. Levin. 2006. Formate synthesis by *Clostridium thermocellum* during anaerobic fermentation. Canadian Journal of Microbiology. 52(7): 681-688.

138. Thauer, R.K., K. Jungermann and K. Decker. 1977. Energy-conservation in chemotropic anaerobic bacteria. Bacteriological Reviews. 41(1): 100-180.

139. Petitdemange, E., F. Caillet, J. Giallo and C. Gaudin. 1984. *Clostridium cellulolyticum* sp nov., a cellulolytic, mesophilic species from decayed grass. International Journal of Systematic Bacteriology. 34(2): 155-159.

140. Payot, S., E. Guedon, C. Cailliez, E. Gelhaye and H. Petitdemange. 1998. Metabolism of cellobiose by *Clostridium cellulolyticum* growing in continuous culture: evidence for decreased NADH reoxidation as a factor limiting growth. Microbiology-Sgm. 144: 375-384.

141. Guedon, E., S. Payot, M. Desvaux and H. Petitdemange. 1999. Carbon and electron flow in *Clostridium cellulolyticum* grown in chemostat culture on synthetic medium. Journal of Bacteriology. 181(10): 3262-3269.

142. Desvaux, M. 2004. Mapping of carbon flow distribution in the central metabolic pathways of *Clostridium cellulolyticum*: Direct comparison of bacterial metabolism with a soluble versus an insoluble carbon source. Journal of Microbiology and Biotechnology. 14(6): 1200-1210.

143. Carere, C.R., V. Kalia, R. Sparling, N. Cicek and D.B. Levin. 2008. Pyruvate catabolism and hydrogen synthesis pathway genes of *Clostridium thermocellum* ATCC 27405. Indian Journal of Microbiology. 48(2): 252-266.

144. Sridhar, J., M.A. Eiteman and J.W. Wiegel. 2000. Elucidation of enzymes in fermentation pathways used by *Clostridium thermosuccinogenes* growing on inulin. Applied and Environmental Microbiology. 66(1): 246-251.

145. Hethener, P., A. Brauman and J.L. Garcia. 1992. *Clostridium termitidis* sp nov., a cellulolytic bacterium from the gut of the wood-feeding termite, *Nasutitermes lujae*. Systematic and Applied Microbiology. 15(1): 52-58.

146. Lovitt, R.W., G.J. Shen and J.G. Zeikus. 1988. Ethanol production by thermophilic bacteria - biochemical basis for ethanol and hydrogen tolerance in *Clostridium thermohydrosulfuricum*. Journal of Bacteriology. 170(6): 2809-2815.

147. Levin, D.B. and R. Chahine. 2010. Challenges for renewable hydrogen production from biomass. Int. J. Hydrogen Energy. 35(10): 4962-4969.

148. Levin, D.B., L. Pitt and M. Love. 2004. Biohydrogen production: prospects and limitations to practical application. Int. J. Hydrogen Energy. 29(2): 173-185.

149. Turner, J., G. Sverdrup, M.K. Mann, P.C. Maness, B. Kroposki, M. Ghirardi, R.J. Evans and D. Blake. 2008. Renewable hydrogen production. International Journal of Energy Research. 32(5): 379-407.

150. Kessler, D., I. Leibrecht and J. Knappe. 1991. Pyruvate-formate-lyase-deactivase and acetyl-CoA reductase activities of *Escherichia coli* reside on a polymeric protein particle encoded by adhE. FEBS Lett. 281(1-2): 59-63.

151. Alfons, J.M.S. 1994. Metabolic interactions between anaerobic bacteria in methanogenic environments. Antonnie van Leeuwenhoek. 66: 271-294.

152. Jungermann, K., R.K. Thauer, G. Leimenstoll and K. Decker. 1973. Function of reduced pyridine nucleotide-ferredoxin oxidoreductase in saccharolytic Clostridia. Biochimica et Biophysica Acta. 305: 268-280.

153. Coppi, M.V., R.A. O'Neil and D.R. Lovley. 2004. Identification of an uptake hydrogenase required for hydrogen-dependent reduction of Fe(III) and other electron acceptors by *Geobacter sulfurreducens*. Journal of Bacteriology. 186(10): 3022-3028.

154. Iannotti, E.L., D. Kafkewitz, M.J. Wolin and M.P. Bryant. 1973. Glucose fermentation products of *Ruminococcus albus* grown in continuous culure with *Vibrio succinogenes*: changes caused by interspecies transfer of H_2. J. Bacteriol. 114: 1231-1240.

155. Lettinga, G. 1995. Anaerobic digestions and wastewater treatment systems. Antoine van Leeuwenhoek. 67: 3-28.

156. Rozendal, R.A., H.V. Hamelers, K. Rabaey, J. Keller and C.J. Buisman. 2008. Towards practical implementation of bioelectrochemical wastewater treatment. Trends Biotechnol. 26(8): 450-459.

157. Angenent, L.T., K. Karim, M.H. Al-Dahhan, B.A. Wrenn and R. Domiguez-Espinosa. 2004. Production of bioenergy and biochemicals from industrial and agricultural wastewater. Trends in Biotechnology. 22(9): 477-485.

158. Franks, A.E., K.P. Nevin, R.H. Glaven and D.R. Lovely. 2010. Microtoming coupled to microarray analysis to evaluate the spatial metabolic status of *Geobacter sulfurreducens* biofilms. The ISME Journal. 4: 509-519.

159. Call, D.F., R.C. Wagner and B.E. Logan. 2009. Hydrogen production by *Geobacter* species and a mixed consortium in a microbial electrolysis cell. Appl Environ Microbiol. 75(24): 7579-7587.

160. Lovley, D.R. 2009. Future shock from the microbe electric. Microbial Biotechnology. 2: 139-141.

161. Yang, T.H., M.V. Coppi, D.R. Lovley and J. Sun. 2010. Metabolic response of *Geobacter sulfurreducens* towards electron donor/acceptor variation. Microbial Cell Factories. 9(90): 1-15.

162. Jones, W.J. 1991. Diversity and physiology of methanogens in: J.E. Roger and W.B. Whitman (Eds.). Microbial production and consumption of greenhouse gases: methane, nitrogen oxides, and halomethanes. American Society for Microbiology, Washigton: pp**.** 39-55.

163. Vogels, G.D., J.T. Keltjens and C. van der Drift. 1988. Biochemistry of methane formation in: A.J.B. Zehnder (Eds.). Biology of anaerobic microorganisms. John Wiley & Sons, New York: pp**.** 707-770.

164. Whitman, W.B., T.L. Bowen and D.R. Boone. 1992. The methanogenic bacteria in: A. Balows, H.G. Truper, M. Dworkin, W. Harder and K.H. Schleifer (Eds.). The Prokaryotes. Springer Verlag, New York: pp**.** 719-768.

165. Schink, B. 1997. Energetics of syntrophic cooperation in methanogenic degradation. Microbiology and Molecular Biology Reviews. 61(2): 262.

166. Gujer, W. and A.J.B. Zhender. 1983. Conversion processes in anaerobic digestion. Water SCi. Technol. 15: 127-167.

167. Mosey, F.E. 1983. Mathematical modelling of the anaerobic digestion process: regulatory mechanisms for the formation of short-chain volatile acids from glucose. Water Sci. Technol. 15: 209-232.

168. Pereira, M.A. 2003. Anaerobic biodegradation of long chain fatty acids: biomethanisation of biomass-associated LCFA as a challenge for the anaerobic treatment of effluents with high lipid/LCFA content. Portugal, Minho University. PhD.

169. Roy, F., E. Samain, H.C. Dubourguier and G. Albagnac. 1986. *Synthrophomonas sapovorans* sp nov., a new obligately proton reducing anaerobe oxidizing saturated and unsaturated long-chain fatty-acids. Archives of Microbiology. 145(2): 142-147.

170. Bryant, M.P., L.L. Campbell, C.A. Reddy and M.R. Crabill. 1977. Growth of *Desulfovibrio* in lactate or ethanol media low in sulfate in association with H_2-utilizing methanogenic bacteria. Applied and Environmental Microbiology. 33(5): 1162-1169.

Appendix A: The Microbial Electrolysis Cell

Contained in this appendix: A.1 CAD drawings of the MECs detailing how the reactor body can be constructed from cast acrylic. A complete list of materials used in the assembly and operation of each reactor is also provided, including part numbers and cost; A.2 a standard operating protocol (SOP) for reactor start-up; and A.3 a procedure on how to make a catalyst layer for a carbon cloth cathode.

A.1 MEC fabrication

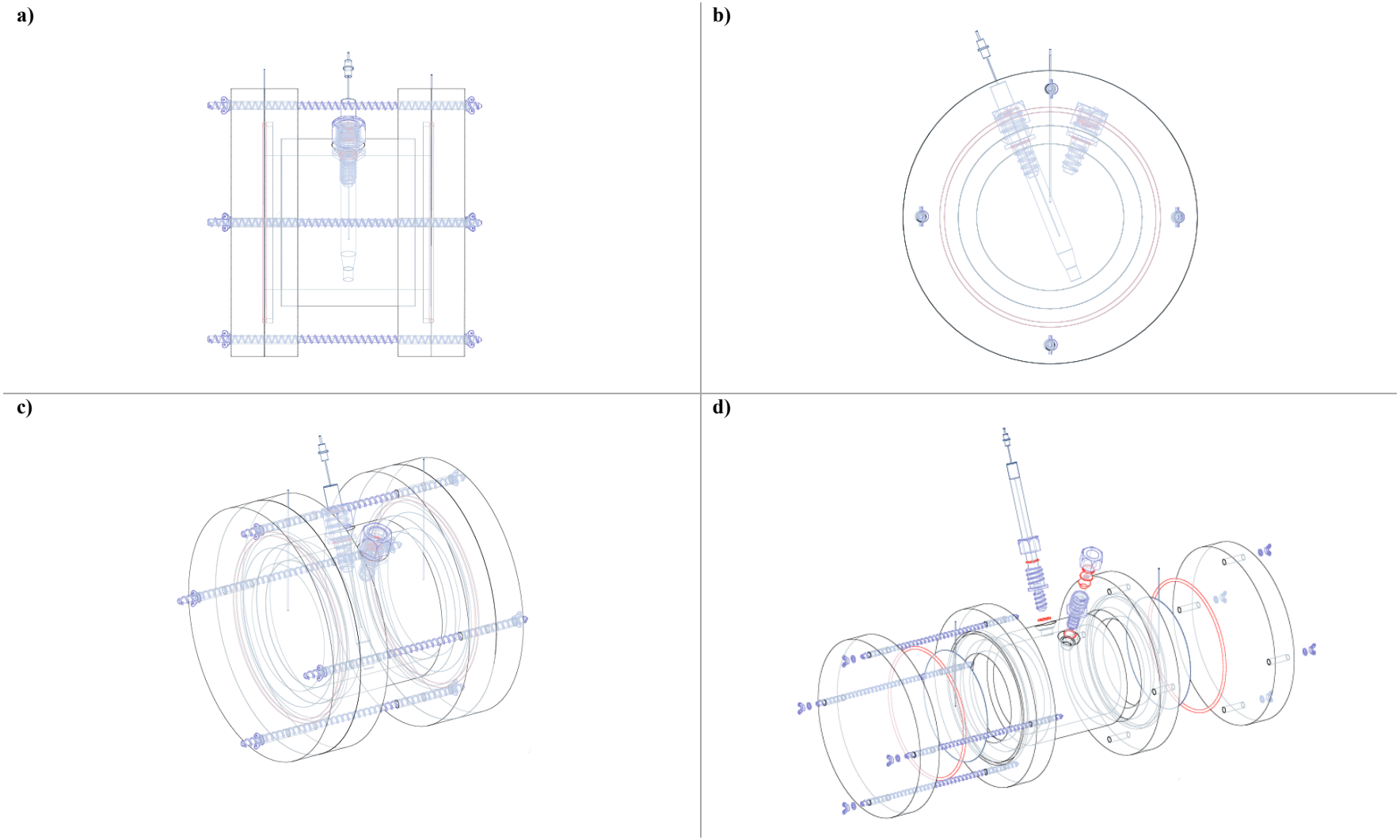

Figure A.1.1 Drawings of the fabricated microbial electrolysis cell a) Right view, b) front view, and c) trimetric view of the assembled reactor. Exploded view represented in d). All drawings were composed using Ashlar Vellum, Xenon v.7 SP2. Drawings are not to scale.

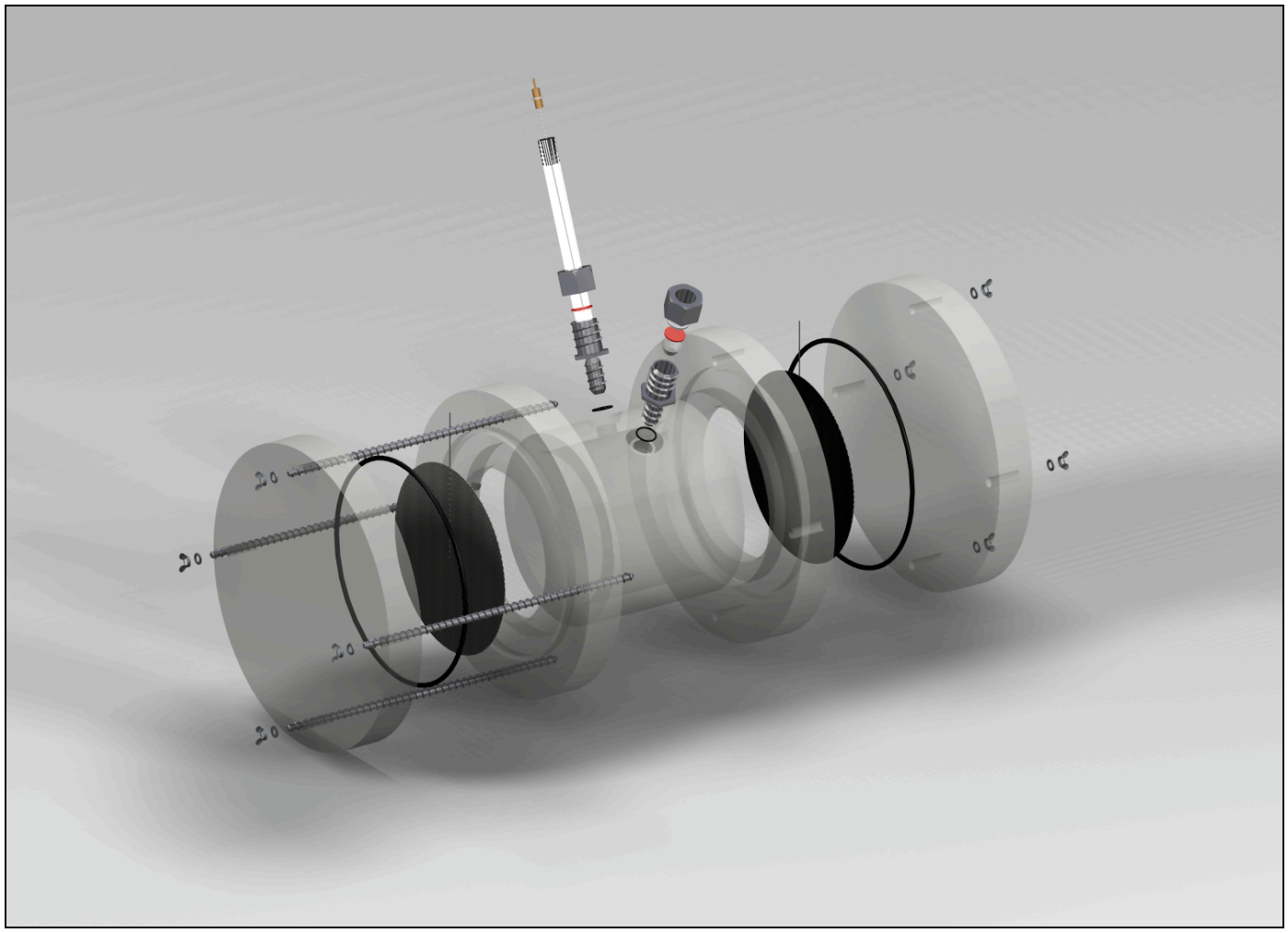

Figure A.1.2 Conceptual model of the microbial electrolysis cell Note threaded rods (4x) seen in drawing were replaced with threaded bolts (8x) in order to effectively seal the chamber.

a)

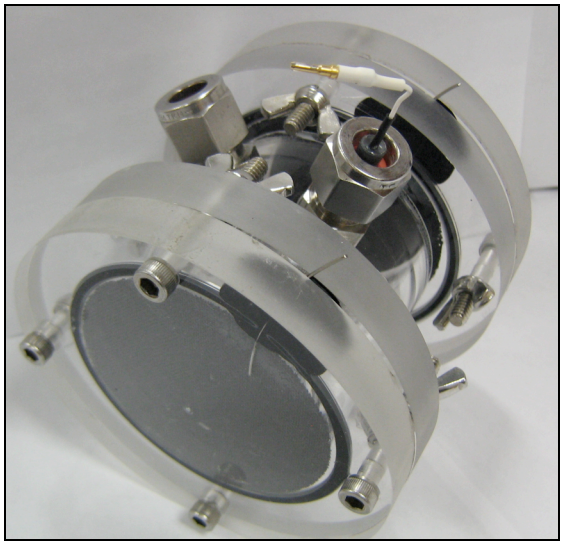

b)

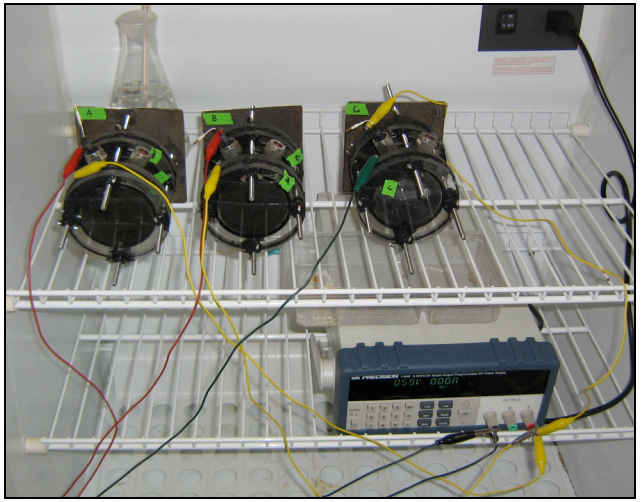

c)

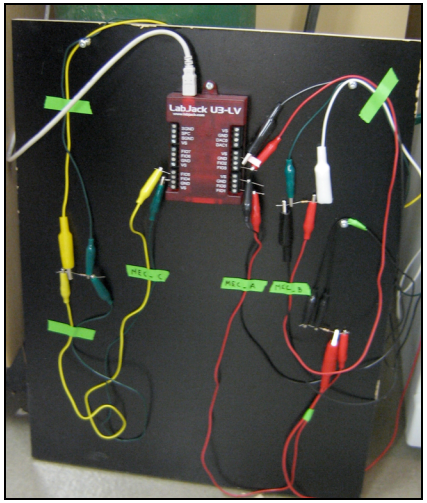

Figure A.1.3 Constructed MECs in operation a) Close-up of reactor without a Ag/AgCl reference probe. b) 3 x MEC experimental set-up with rectifier inside the incubator, next to the c) LabJack data acquisition system.

A.2 MEC start-up procedure

Materials

[A] Reactor

2	Endplates – cast acrylic
1	Cell chamber – cast acrylic
2	S.S. 3/8” compression fitting to ¼” Male NPT w/ tapered neck - reduction fitting
2	S.S. 3/8” nuts for compression fittings
2	Nylon ferrule set
2	3/8” inner diameter nitrile rubber o-ring
2	2 ¾” inner diameter nitrile rubber o-ring
1	½” Septa Puresep T
1	New Brunswick fermentor septa with hole bored out in middle
1	Ag/AgCl reference electrode, 11 mm diameter, BASi
1	Carbon cloth electrode
1	Carbon cloth electrode loaded with 0.5 mg Pt/C catalyst
2	20 G S.S. wire pieces – approx. 1 ½” long
4	S.S. ¼” threaded rods – approx. 7” long
8	S.S. lock washers
8	S.S. wing nuts

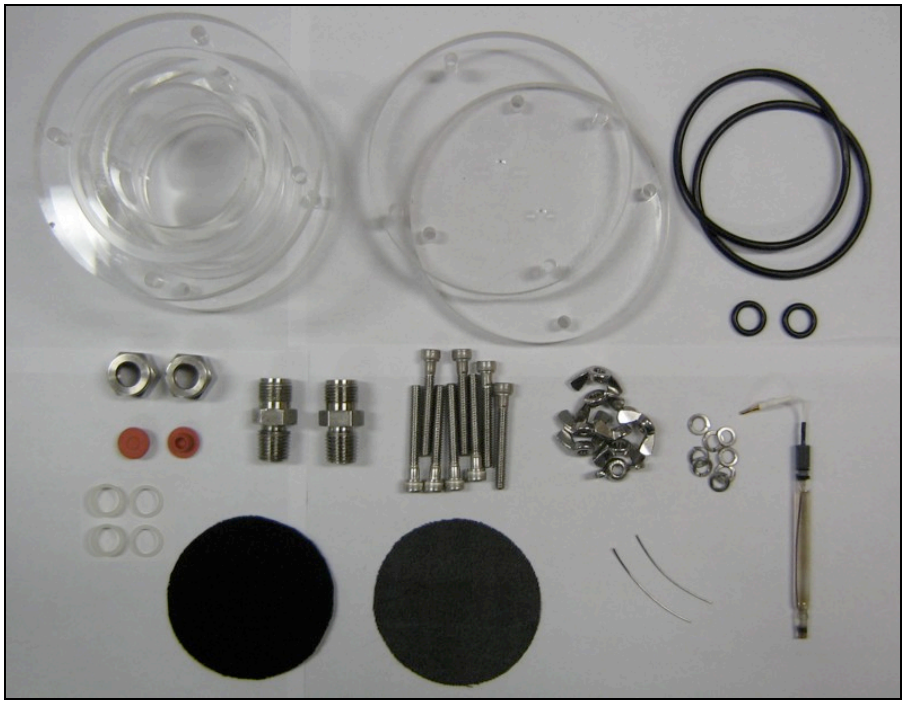

[B] Assembly Tools

1 Tin foil
1 5/8” crescent wrench
1 4 mm Allen key
1 Loctite 5905 Flange sealant
4 Sterile 22G1 needles
1 Sterile filter – 0.2 μm
1 60 ml syringe
1 Pair of examination gloves
1 70% ethanol

Procedure

1. Place new 3/8” nitrile o-rings into the circular grooves located at the end of the cell chamber. Ensure o-ring sits properly in groove – thoroughly inspect for any imperfections in the rubber and remove any debris that may interfere with the seal.

2. Cut a carbon cloth electrode to size and center within the o-ring. Trim any loose ends – any fibers that lay across the o-ring will prevent a gas-tight seal.

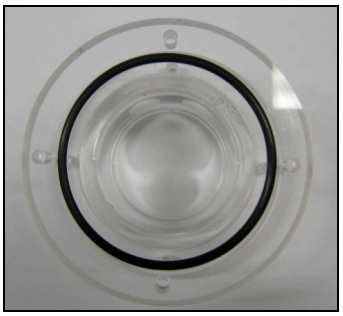
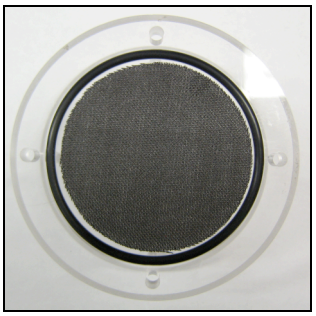

3. Lay a 20G S.S. wire across the electrode, o-ring, and cell chamber, allowing a slight overhang over the edge of the chamber. Ensure the wire is pointing in the same direction as the S.S. fittings. To prevent any leaks, place a bead of silicone onto the tip of a 22G1 needle and spread evenly across the S.S. wire and o-ring.

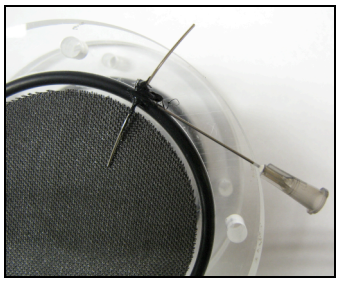

4. Lower the end cap into place, being careful not to disturb the S.S. wire. Use the 1 ½ in hex bolts to properly align the end cap with the chamber. Place a lock washer and wing nut at the end of each bolt and gently squeeze the end cap into place. Wing nuts should be screwed no more than FINGER TIGHT.

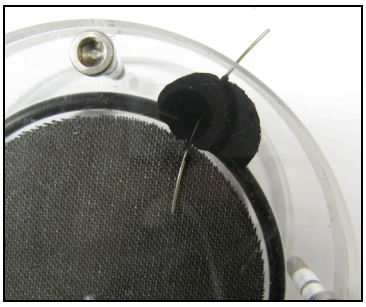
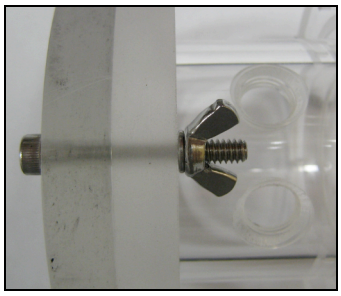

5. Repeat steps 1 to 4 for the other side of the chamber, using the carbon cloth electrode loaded with 0.5 mg Pt/C catalyst. Make sure the electrode face with the Pt catalyst is facing inwards.

6. Place a 2 ¾" nitrile o-ring around the tapered neck of two S.S. fasteners. Thread the NPT end of both fasteners into the chamber until finger tight.

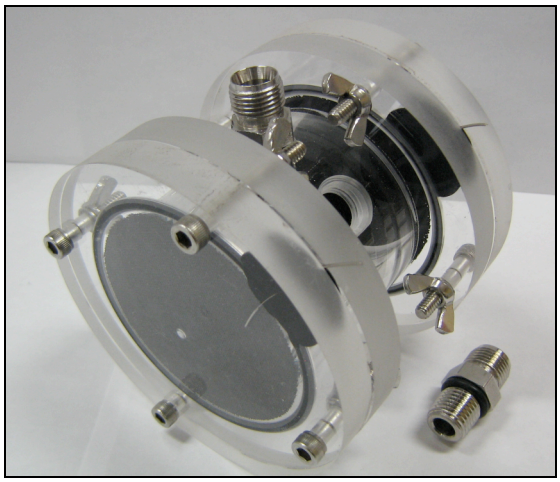

7. Loosen wing nuts without separating end cap from chamber. The cast acrylic needs room to breath when inside the autoclave. If this is not followed, the plastic will warp at the pressure points.

8. Assemble the sampling port. Sandwich a septum between a set of nylon ferrules. Place assembly inside a 3/8" compression nut.

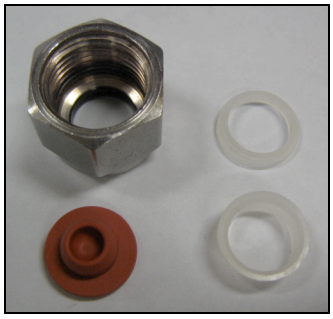

9. Place the reactor inside a beaker and cover with tin foil. Group the septum assembly and second compression nut with nylon ferrules and wrap in tin foil as well. Disconnect one gas manifold hose, cover the ends with tin foil, and place

inside a metal hose container. Paper napkins, a 5/8" crescent wrench, and 4mm allen key must also be wrapped in tin foil. **Note: The only pieces that will not be autoclaved are the reference electrode and the septum with a hole bored through the middle.**

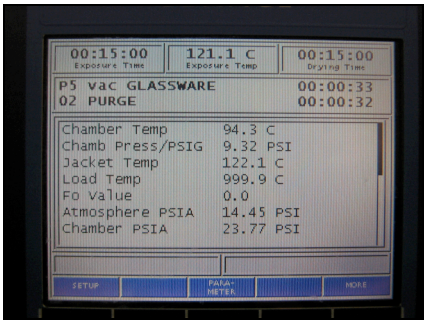

10. Place all pieces in the autoclave and set for a 15 min exposure and 15 min drying time.

Laminar Flow Hood Preparation Procedure:

Note: Anything entering the flow hood must be wiped down with 70% EtOH (including your examination gloves) to avoid the introduction of possible contaminants

1. Wearing examination gloves, wipe down all surfaces (walls and bench) with 70% EtOH.
2. Place inside the flow hood: i) alcohol burner, ii) lighter, iii) bottle of 70% EtOH, and iv) paper towel
3. Lower the sache to the bottom position and turn the UV light ON.
4. After 1 hour, turn UV light OFF, raise sache into the upper position, and allow air to flow for 15 min.
5. Wipe down working surface with 70% EtOH and ignite alcohol burner.

---

11. Remove items from the autoclave and place inside the laminar flow hood. Remove all tin foil from hood. Place the reactor within relatively close proximity to the flame and allow to cool for 30 min. The flame from an alcohol burner should sterilize the air around it but should not be hot enough to heat up and melt the plastic reactor.

12. Using the 4 mm Allen key, carefully tighten all wing nuts one side at a time in a criss-cross pattern until both reactor ends are sealed. **Use caution: over-tightening may cause the acrylic body to crack.**

13. Using the 5/8” crescent wrench, securely tighten both fasteners making sure the o-ring makes a tight and even seal all the way around. **Use caution: fastener may bite into the seal when tightening. If this occurs, the seal is compromised and must be replaced. Over tightening may also strip the threads and/or crack the acrylic chamber.**

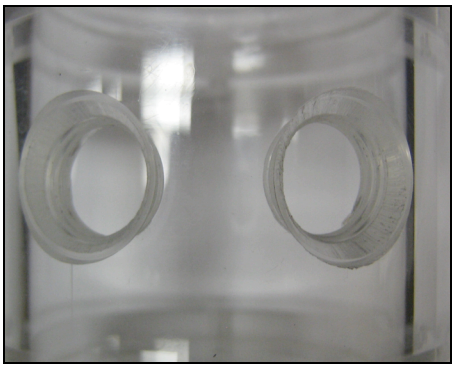
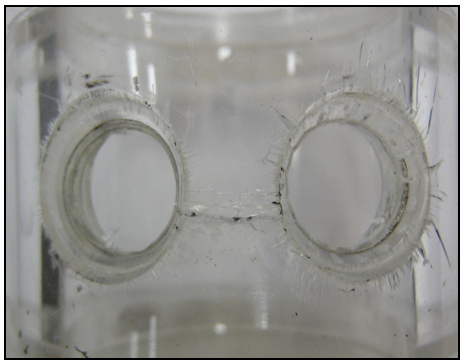

14. Screw the septum assembly with compression nut onto one of the open ports. Build the reference electrode assembly using the same procedure as in step 8 (except this time there will be an electrode through the middle of the septum) and screw the compression nut onto the second open port.

Note: Because the reference electrode cannot be autoclaved, soak the electrode (with the septum) in 15% bleach for 10 min. Place in laminar flow and soak with 70% EtOH. Air dry.

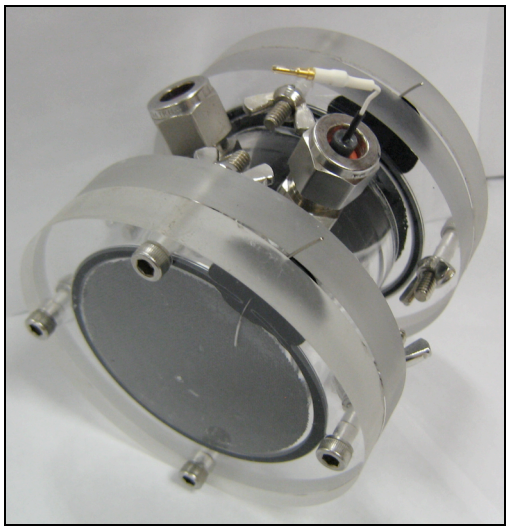

15. **Check for leaks:**
    i. Spray 70% EtOH on the reactor sampling port
    ii. Reconnect the sterilized hose to the gas manifold
    iii. With the N_2 tank regulator set to 25 psi, allow gas to flow through the manifold. Attach a sterile filter tip (0.2 um) and sterile 22G1 needle to the

end of the hose and stab the septum. Allow the pressure within the reactor chamber to equilibriate (30 sec to 1 min).

iv. With the chamber now pressurized, use Snoop, soapy water, or some other leak detection solution and look for any bubbles than may develop. **Pay special attention to the fastener seals and both S.S. wires at each end.**

Any leaks must be plugged with silicone. All leaks should be addressed within the laminar flow hood. Allow fresh silicone to cure for AT LEAST 8 hours before continuing.

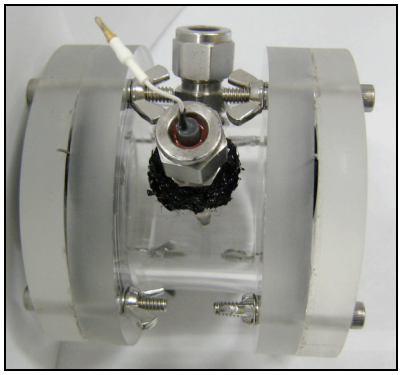

16. With an air-tight seal, all O_2 must be removed from the reactor chamber. This is performed by toggling between gas:vaccum cycles using 100% N_2 for 1:1.5 min respectively, 5 times with the N_2 regulator pressure set to 12-14 psi. **Reminder: to ensure N_2 is sterile, attach a 0.2 µm filter to gas manifold and spray sampling port with alcohol prior to injection.**

17. Using aseptic techniques, under the flame transfer 45 ml of sterile, anaerobic medium to the reactor chamber using a 60 ml syringe. User should experience significant resistance during this step. If no backpressure exists, check reactor for leaks.

18. Using aseptic techniques, under the flame add 2 ml of filter sterilized acetate (1M) and fumarate (1 M) to the reactor.

19. Aseptically check the pressure of the chamber and incubate the reactor at 35°C. **After 24 hrs of incubation:**
    i. The medium should remain clear. If not, the reactor is contaminated and the entire process must be repeated from **step 1**.
    ii. The pressure should hold. If there is any pressure drop, there is a leak in your system that must be detected and corrected with silicone. Repeat **steps 15, 16, and 19** until the problem is solved.

20. Using aseptic techniques, under the flame inoculate the reactor with 31 ml of a pure culture of *G. sulfurreducens* (in log phase). This brings the working volume of the reactor to 80 ml.

21. Incubate the reactor at 35°C for 2 days. Aseptically take a 1 ml GC gas sample. There should be **NO H_2 PRODUCTION**. *Geobacter sulfurreducens* does not produce any H_2 gas during growth on acetate and fumarate. A peak here means the reactor is contaminated and the entire process must be repeated from **step 1**. If no H_2 is detected, the experiment is ready to go.

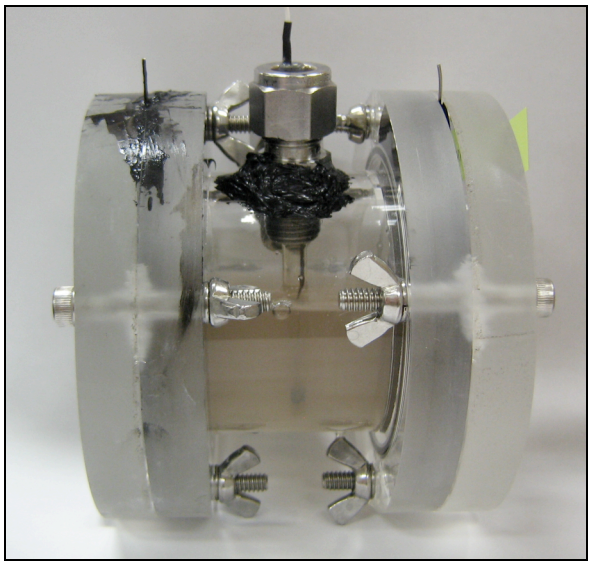

A.3 Making a Pt/C Catalyst Layer[1]

[1] Middaugh, J. (2006). How to make cathodes with a diffusion layer for single-chamber microbial fuel cell.

Electrode Dimension

Diameter (ϕ) = 6.5 cm
Radius (r) = 3.25 cm
Area ($A_{electrode}$) = $\pi \cdot r^2$
= 33.18 cm^2

Procedure

1. 10% Pt/C needed for 0.5 mg Pt loading per cm^2:
   - 0.5 mg/cm^2 * 33.18 cm^2 = 16.59 mg Pt catalyst
   - for powder containing only10% Pt
     16.59 mg / 0.1 = **165.92 mg of 10% Pt/C**

2. Add 0.83 µl DI water per mg Pt/C:
   - 0.83 µl/mg Pt/C * 165.92 mg Pt/C = **137.71 µl DI water**

3. Vortex mixture in capped container with 6-8 glass beads

4. Add Nafion Binding Solution:
   - 6.67 µl/mg Pt/C * 165.92 mg Pt/C = **1,106.66 µl Nafion Solution**

5. Add iso-propanol:
   - 3.33 µl/mg Pt/C * 165.92 mg Pt/C = **640.76 µl iso-propanol**

6. Vortex mixture. Evenly coat electrode using a thin paintbrush, being as homogenous and careful as possible. Allow coating to air-dry for at least **24h**.

Figure A.3.1 Freshly prepared cathodes curing for 24 h in laminar flow-hood used to clear any particulates from sticking to electrode surface.

Pictures

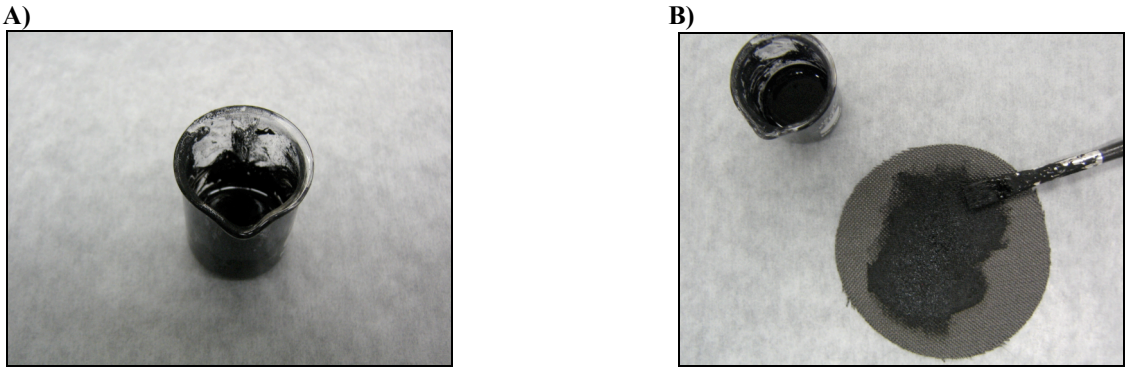

Figure A.3.2 Preparing and applying the catalyst layer Catalyst mixture should have the same consistency as wall paint A). Gently and evenly apply the mixture with a fine tip paintbrush. Catalyst should be homogenously spread across entire electrode surface B).

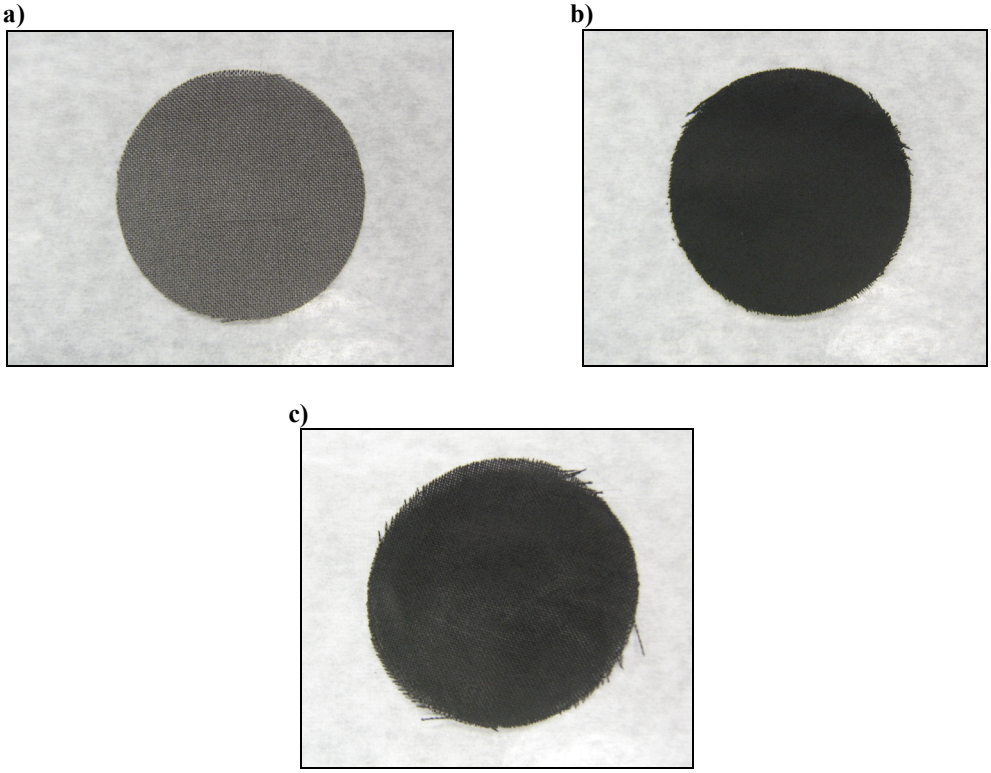

Figure A.3.3 Carbon cloth electrodes a) Carbon cloth electrode before the catalyst layer is applied and b) after a 0.5 mg Pt/Catalyst layer is applied. c) An uneven, non-homogenous catalyst layer.

Appendix B: Calculations

List of Symbols

B	= number of cells at the beginning		
b	= number of cells at the end		
b_{es}	= mole of e- for each substrate generated from half reactions		[mol-e^-]
C	= van't Hoff constant		[K]
$C_{g,(aq)}$	= molar amount of aqueous gas		[mol L^{-1}]
Δc_s	= total substrate consumption		[mol L^{-1}]
E_{ps}	= power source voltage		[V]
F	= Farraday's constant,	96,485	[C mol^{-1}-e^-]
g	= cell doubling time		[time / generations]
ΔH_{H2}	= heat of combustion of H_2		[kJ mol^{-1}]
ΔH_s	= heat of combustion of substrate		[kJ mol^{-1}]
I	= measured current		[A]
$\int_{t_i}^{t_f} Idt$	= total amount of electrons recovered as current		[C]
k	= cell growth rate		[generations / time]
k_H	= Henry's constant		[mol L^{-1} atm^{-1}]
n	= number of generations		
n_{H2}	= mol H_2 produced		[mol]
n_s	= mol substrate consumed		[mol]
P	= absolute pressure		[mmHg]
p_g	= partial pressure of gas = P · (% gas)		[atm]
R	= universal gas constant,	62.3637	[L mmHg mol^{-1} K^{-1}]
R_{ex}	= external resistor		[Ω]
T	= incubation temperature		[K]
T^{Θ}	= standard temperature,	298.15	[K]
Δt	= change in time		[h]
V_g	= volume of gas in headpsace		

	= ($V_{\text{headspace}}$) · (% gas)	[L]
v_L	= volume of liquid in anode chamber	[L]
W_{in}	= total energy added to cell	[kW·h]
W_{ps}	= energy added by power source	[kW·h]
W_{Rex}	= energy lost from external resistance	[kW·h]

List of values

C_{H2}	= 500	[K]
C_{CO2}	= 2400	[K]
$k_{H,H_2}\big\vert_{T^\theta}$	= 7.9 x 10^{-4}	[mol L^{-1} atm^{-1}]
$k_{H,CO_2}\big\vert_{T^\theta}$	= 3.4 x 10^{-2}	[mol L^{-1} atm^{-1}]

1. Growth rate and doubling time

General equation:

$$b = B \cdot 2^n \quad \ldots \quad \text{(A2.1)}$$

Solving for n:

$$n = \frac{\log b - \log B}{\log 2} \quad \ldots \quad \text{(A2.2)}$$

Expressed as a growth rate:

$$k = \frac{n}{\Delta t} = \frac{\log b - \log B}{0.301(t_b - t_B)} \quad \ldots \quad \text{(A2.3)}$$

Expressed as a doubling time:

$$g = \frac{1}{k} \quad \ldots \quad \text{(A2.4)}$$

2. Gas production

i) Express the % gas sampled from the headspace (GC analysis) in molar quantities, n, assuming ideal gas behavior:

$$PV_g = nRT \quad \ldots \quad \text{(A2.5)}$$

ii) Determine the soluble fraction of gas in the medium according to Henry's Law. Assume water is the medium.

$$C_{g,(aq)} = p_g k_H \quad \ldots \quad \text{(A2.6)}$$

Note: The temperature dependence of k_H can be corrected according to the van't Hoff equation:

$$k_H\big|_T = k_H\big|_{T^\theta} \exp\left[-C\left(\frac{1}{T} - \frac{1}{T^\theta}\right)\right] \quad \ldots \quad \text{(A2.7)}$$

iii) For CO_2, determine the amount of carbon expressed in the bicarbonate, HCO_3^-, fraction.

Carbonate equilibrium reactions:

$CO_{2,(g)} \Leftrightarrow CO_{2,(aq)} + H_2O \Leftrightarrow H_2CO_3 \Leftrightarrow HCO_3^- + H^+$

Consider the equilibrium reaction between the weak acid, $CO_{2,(aq)}$, and its conjugate base, HCO_3^-. H_2CO_3 is an intermediate, which is produced as fast as it is consumed, therefore the acid dissociation constant becomes:

$$k_a = \frac{\left[HCO_3^-\right]\left[H^+\right]}{[CO_{2,(aq)}]} = 4.21 \times 10^{-7} \quad \ldots \quad \text{(A2.8)}$$

$$pk_a = -\log_{10} k_a \quad \ldots \quad \text{(A2.9)}$$

Use the Henderson-Hasselbalch equation to solve for $[HCO_3^-]$:

$$pH = pk_a + \log_{10} \frac{[HCO_3^-]}{[CO_{2,(aq)}]} \quad \ldots \quad \text{(A2.10)}$$

3. Redox balance and electron recovery

An oxidation/reduction ratio for balch tube experiments was calculated for *C. termitidis* according to:

$$\frac{oxidized\ species}{reduced\ species} = \frac{(mol\ pyruvate) + 2(mol\ CO_2) + (mol\ formate)}{2(mol\ EtOH) + (mol\ H_2)}$$

where redox values of -0.5, 1, and 0 for H, O, and C respectively were assigned to each end-product.

e.g. Ethanol, C_2H_6O $= (2\cdot 0) + (6\cdot\text{-}0.5) + (1\cdot 1) = -2$

Electron recovery is the amount of electrons recovered in measured end-products and biomass versus the amount of electrons produced from the substrate consumed:

$$\%\ e^-_{recovery} = \frac{e^- - mol\ produced\ in\ end-products}{e^- - mol\ available\ from\ substrate\ consumption} \quad \text{(A2.11)}$$

Example A2.1: mono-culture of *G. sulfurreducens* grown on acetate and fumarate as the terminal e^- acceptor

i) complete oxidation of acetate in the absence of O_2 generates 8 e^-:
$Acetate^- + 4\ H_2O \rightarrow 2\ HCO_3^- + 9\ H^+ + 8\ e^-$

ii) the reduction of fumarate to succinate requires 2 e^-:
$C_4H_4O_4 + 2\ H^+ + 2\ e^- \rightarrow C_4H_6O_4$

iii) acetate assimilation into biomass follows:
$17\ C_2H_3O_2^- + 11\ H_2O = 8\ C_4H_7O_3 + 2\ HCO_3^- + 15\ OH^-$

By measuring the amount of protein in the culture, the fraction of acetate used for biomass assimilation is determined from iii). The remaining dissimilated acetate is used to reduce fumarate, producing succinate:

$$\%\, e^-_{\text{recovered}} = \frac{(mol\ succinate)(2e^-)}{(mol\ dissimilated\ acetate)(8e^-)}$$

---

4. Hydrogen yield

The H_2 yield represents overall H_2 production based on the amount of substrate consumed

$$Y_{H_2} = \frac{n_{H_2}}{v_L \Delta c_s} \qquad \ldots \qquad \text{(A2.12)}$$

5. Coulombic efficiency

Coulombic efficiency, C_E, is defined as the number of electrons recovered as a current versus the amount of electrons available in the substrate

$$C_E = \frac{\int_{t_i}^{t_f} Idt}{F b_{es} v_L \Delta c_s} \qquad \ldots \qquad \text{(A2.13)}$$

Formula break down:

$$C_E = \frac{Coulombs\ recovered}{Theoretical\ coulombs\ in\ substrate} = \frac{n_{CE}}{n_{th}} \qquad \ldots \qquad \text{(A2.14)}$$

where,

$$n_{CE} = \frac{\int_{t=0}^{t} Idt}{F} \qquad \ldots \qquad \text{(A2.15)}$$

$$n_{th} = b_{es} v_L \Delta c_s \qquad \ldots \qquad \text{(A2.16)}$$

Example A2.2:

Substrate	=	Acetate		
b_{es}	=	8 mol-e^-	$\Rightarrow$	$Acetate^- + 4\ H_2O \rightarrow 2\ HCO_3^- + 9\ H^+ + 8\ e^-$
v_L	=	0.08 L		
Δc_s	=	0.0503 mol L^{-1}		

To determine C_E, must i) import experimental data into MatLAB, ii) assign a line of best fit, and iii) calculate the area under the curve:

i) MatLAB commands

data = [];	% creates an open matrix named 'data'
openvardata;	% opens variable editor workspace named 'data' to input experimental values. Only load one column vector per array.
cftool;	% opens the curve fitting toolbox

ii) Assigning line of best fit

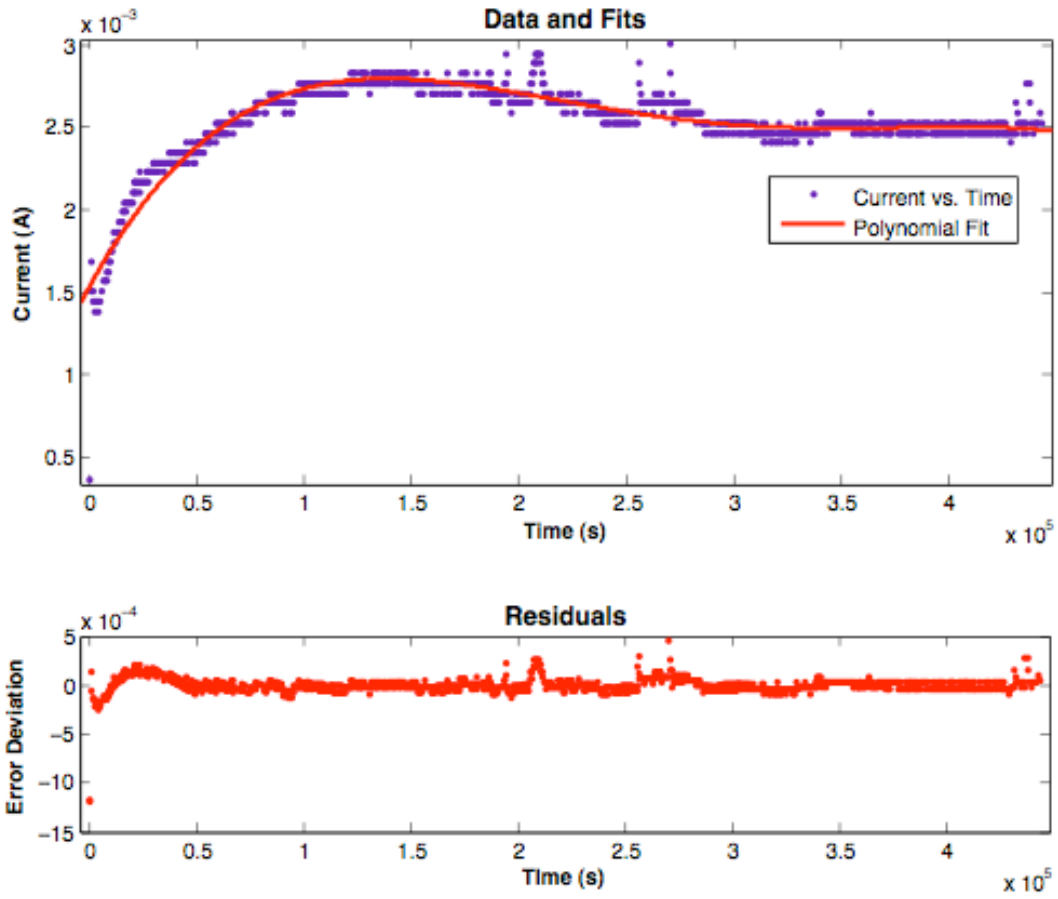

Linear model Poly4:

f(x) = p1*x^4 + p2*x^3 + p3*x^2 + p4*x + p5

where x is normalized by mean 2.199e+05 and std 1.271e+05

Coefficients (with 95% confidence bounds):

p1 = -7.724e-05 (-8.295e-05, -7.152e-05)

p2 = 0.0001905 (0.0001855, 0.0001955)

p3 = 1.491e-05 (-4.508e-07, 3.027e-05)

p4 = -0.0002966 (-0.0003064, -0.0002867)

p5 = 0.002662 (0.002655, 0.00267)

Goodness of fit:

SSE: 8.649e-06

R-square: 0.9018

iii) Integrate the curve

Xi	Integral
0	0
44352.6	87.3863
88705.2	199.591
133058	321.891
177410	445.317
221763	565.445
266116	681.166
310468	793.479
354821	904.262
399173	1015.06
443526	**1125.87**

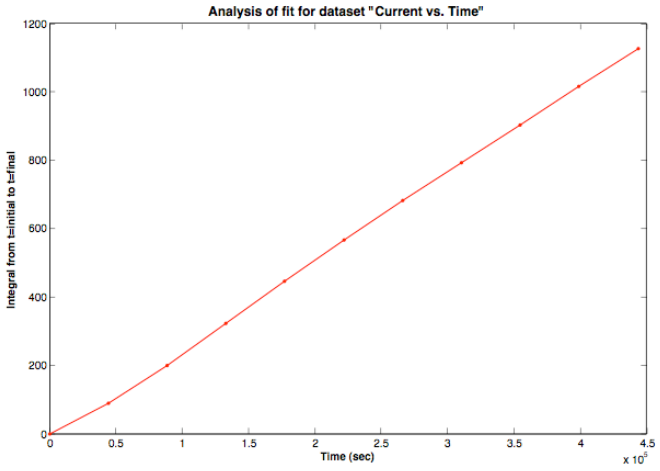

Calculate, C_E:

$$C_E = \frac{1125.87}{(96485)\cdot(8)\cdot(0.08)\cdot(0.0503)} = 36.26\,\%$$

---

6. Overall H_2 recovery

Total amount of H_2 produced versus theoretical amount of H_2 that could be produced

$$r_{H_2} = \frac{n_{H_2}}{n_{th}} \qquad \ldots \qquad (A2.17)$$

7. Energy recovery based on electrical input

Energy contribution of power source versus total energy input (electrical and substrate)

$$\eta_{in} = \frac{W_{in}}{W_{in} + W_s} \quad \ldots \quad \text{(A2.18)}$$

where,

$$W_{in} = W_{ps} - W_{R_{ex}} = \int_{t=0}^{t} (IE_{ps} - I^2 R_{ex}) \quad \ldots \quad \text{(A2.19)}$$

$$W_s = n_s \Delta H_s \quad \ldots \quad \text{(A2.20)}$$

Note: 3600 kJ mol^{-1}

8. Energy recovery based on substrate and electrical input

Overall energy recovery based on the energy within the substrate and contribution of input voltage

$$\eta_{W+S} = \frac{W_{H_2}}{W_{in} + W_s} \quad \ldots \quad \text{(A2.21)}$$

where,

$$W_{H_2} = n_{H_2} \Delta H_{H_2} \quad \ldots \quad \text{(A2.22)}$$